

Fall 2008

Dual microcapsule system for autonomous self-healing coatings

Jonathan K. Nguyen

University of New Hampshire, Durham

Follow this and additional works at: <https://scholars.unh.edu/thesis>

Recommended Citation

Nguyen, Jonathan K., "Dual microcapsule system for autonomous self-healing coatings" (2008). *Master's Theses and Capstones*. 393.
<https://scholars.unh.edu/thesis/393>

This Thesis is brought to you for free and open access by the Student Scholarship at University of New Hampshire Scholars' Repository. It has been accepted for inclusion in Master's Theses and Capstones by an authorized administrator of University of New Hampshire Scholars' Repository. For more information, please contact nicole.hentz@unh.edu.

DUAL MICROCAPSULE SYSTEM FOR AUTONOMOUS
SELF-HEALING COATINGS

BY

JONATHAN K. NGUYEN

B.S. Chemical Engineering, University of New Hampshire, 2006

THESIS

Submitted to the University of New Hampshire

in Partial Fulfillment of

the Requirements for the Degree of

Master of Science

in

Materials Science

September, 2008

UMI Number: 1459509

INFORMATION TO USERS

The quality of this reproduction is dependent upon the quality of the copy submitted. Broken or indistinct print, colored or poor quality illustrations and photographs, print bleed-through, substandard margins, and improper alignment can adversely affect reproduction.

In the unlikely event that the author did not send a complete manuscript and there are missing pages, these will be noted. Also, if unauthorized copyright material had to be removed, a note will indicate the deletion.

UMI[®]

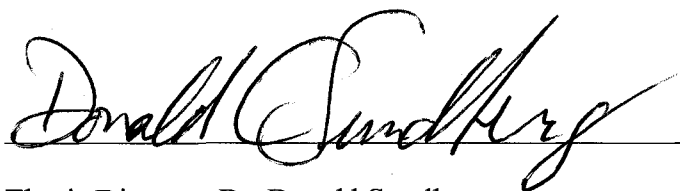
UMI Microform 1459509

Copyright 2008 by ProQuest LLC.

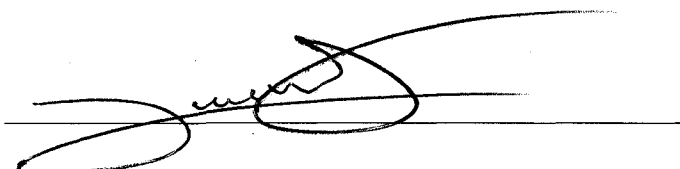
All rights reserved. This microform edition is protected against unauthorized copying under Title 17, United States Code.

ProQuest LLC
789 E. Eisenhower Parkway
PO Box 1346
Ann Arbor, MI 48106-1346

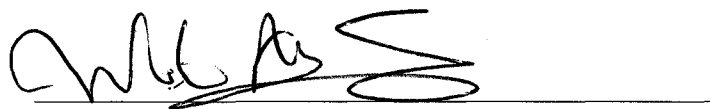
This thesis has been examined and approved.

A handwritten signature in black ink, appearing to read "Donald Sundberg", written over a horizontal line.

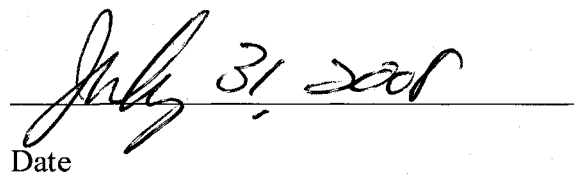
Thesis Director, Dr. Donald Sundberg
Professor of Materials Science

A handwritten signature in black ink, appearing to read "Yvon Durant", written over a horizontal line.

Dr. Yvon Durant
Research Associate Professor of Materials Science

A handwritten signature in black ink, appearing to read "Weihua Ming", written over a horizontal line.

Dr. Weihua Ming
Research Associate Professor of Materials Science

A handwritten date "July 31, 2008" written over a horizontal line.

Date

TABLE OF CONTENTS

LIST OF TABLES	vi
LIST OF FIGURES.....	vii
ABSTRACT	xiv
I. INTRODUCTION	1
Background on Self-Healing.....	2
Thermally Self-healing Materials.....	3
Autonomous Self-healing.....	6
Microvascular Networks.....	6
Hollow Fibers.....	8
Microcapsules.....	10
Background on Microencapsulation.....	13
Encapsulation Techniques.....	14
Background on Fracture Toughness.....	17
II. ONE PART AUTONOMOUS SELF HEALING SYSTEM.....	20
Feasibility of Self Healing System.....	21
Encapsulation of DCPD.....	24
Fracture Testing.....	29
III. A TWO MICROCAPSULE AUTONOMOUS SELF HEALING SYSTEM.....	35
Feasibility of Self Healing System	37
Capillary Flow.....	37
Diffusional Mixing.....	40
Epoxy Curing Kinetics.....	44
Encapsulation of Resin Capsules.....	46
Encapsulation of Epoxy Resin Using the Concentrate Route.....	46
Encapsulation of Epoxy Resin Using Urea Formaldehyde.....	48
Amine Adduct.....	50
Desired Properties of the Amine Adduct.....	50
Amine Adduct Synthesis.....	51
Addition of Inert Component.....	53
Addition of a Reactive Component.....	54
Analysis of Various Adducts.....	55
Isophorone Diamine Adduct.....	57
Isophorone Diamine/Epoxyoctane (IDEO) Adduct Synthesis.....	58
IDEO Adduct Characterization.....	61
Encapsulation of Amines.....	70

Interfacial Polymerization.....	70
Complex Coacervation.....	73
In-situ Polymerization.....	75
Second Cropping.....	85
Aqueous Radical Scavenger.....	86
Amine Capsule Properties.....	88
Microcapsule Payload.....	88
IDEO Adduct Density.....	90
Sonication and Homogenization.....	91
Polymer Shell Properties.....	92
Amine Capsule Titration.....	94
Encapsulation Using V-65 Initiator.....	96
Characterization of JN4-72 Microcapsules.....	104
Scanning Electron Microscopy (SEM).....	105
Fourier Transform Infrared Spectroscopy (FTIR).....	106
Encapsulated Adduct Reactivity.....	107
Microcapsule Payload.....	109
Reproduction of JN4-72 Microcapsules.....	112
IV. CONCLUSIONS AND RECOMENDATIONS.....	114
Conclusions.....	114
Recommendations.....	115
LIST OF REFERENCES	118
APPENDICES.....	121
APPENDIX A.....	121
Hydrodynamic Flow Calculations for a One Part Autonomous Self Healing System...	121
APPENDIX B.....	129
Dicyclopentadiene Microcapsule DSC and Payload Data.....	129
APPENDIX C.....	133
Hydrodynamic Flow Calculations for a Two Part Autonomous Self Healing System...	133
APPENDIX D.....	146
Amine Adducts.....	146

APPENDIX E.....	149
NMR Data of IDEO Adduct and Starting Components.....	149
APPENDIX F.....	164
Calculation of the Extent of Reaction vs. Time from DSC Analysis.....	164
APPENDIX G.....	168
Characterization of PMMA/PBMA Copolymer from IDEO Amine Adduct.....	168
APPENDIX H.....	171
IDEO Amine Adduct Encapsulation Experiments.....	171

LIST OF TABLES

Table 3-1.	Bulk polymerization experiments (JN4-53).....	98
Table 3-2.	Bulk polymerization experiments (JN4-54).....	98

LIST OF FIGURES

Figure 1-1.	Diels-Alder reaction to make prepare polymeric material ¹⁰	3
Figure 1-2.	Fracture toughness specimens of 3M4F. Sample (A) is cracked. Sample (B) is thermally healed ¹¹	4
Figure 1-3.	Load vs. Displacement curve for virgin and healed samples of 3M4F ¹⁰ ...	4
Figure 1-4.	Diagrams of microvascular networks. Human Skin (left), Epoxy coating (right) ¹²	7
Figure 1-5.	Cracked and healed structure with 2.5% catalyst loading ¹²	8
Figure 1-6.	Various Systems using hollow fibers ¹⁴	9
Figure 1-7.	Crack propagation in a self healing composite ⁵	10
Figure 1-8.	SEM picture of DCPD capsules manufactured using Urea formaldehyde process ⁸	11
Figure 1-9.	Cross section of a microcapsule ²⁰	13
Figure 1-10.	TCBD geometry. Dimensions in mm ⁵	17
Figure 1-11.	Load vs. displacement curve of an in-situ sample ⁵	19
Figure 2-1.	Epoxy matrix with DCPD microcapsules and Grubb's catalyst with a crack filled with healing agent	20
Figure 2-2.	Plot of time required to fill various crack lengths and crack radii with a contact angle of 30°	22
Figure 2-3.	Plot of time required to fill a 10μm crack varying crack radii and contact angles	23

Figure 2-4.	ROMP of DCPD and Grubb's catalyst ²⁸	23
Figure 2-5.	Predictions for degree of curing at isothermal conditions (30°C) at low, medium and high catalyst concentrations ²⁸	24
Figure 2-6.	Polymerization mechanism for urea-formaldehyde resin.....	25
Figure 2-7.	Proposed mechanism for UF shell formation ²⁹	26
Figure 2-8.	Experimental set up for encapsulation of DCPD.....	27
Figure 2-9.	Light Microscope (left) and SEM (right) Images of DCPD Microcapsules ²⁵	28
Figure 2-10.	Molding process used to make epoxy TDCB specimens.....	30
Figure 2-11	Load vs. displacement data for fracture of a microcapsule filled epoxy TDCB specimen ²⁵	31
Figure 2-12.	Close-up image of pre-cracked region in TDCB specimen.....	12
Figure 2-13.	SEM picture of a fracture surfaces from an epoxy matrix filled with DCPD microcapsules ²⁵ (left) and fracture surface of neat epoxy (right).....	33
Figure 2-14.	Load vs. Displacement curve of a healed sample.....	34
Figure 3-1.	Epoxy matrix filled with resin and amine capsules, showing a crack filled with each healing agent.....	35
Figure 3-2.	Fracture of microcapsules within a matrix.....	37
Figure 3-3.	Time required to a fill crack with epoxy resin, varying crack lengths and crack radii with a contact angle of 48°.....	38
Figure 3-4	Contact angle of EPON 815C on an epoxy matrix.....	39

Figure 3-5.	Time required to fill a crack with amine hardener, varying crack lengths and crack radii with a contact angle of 43°	39
Figure 3-6	Contact angle for amine hardener(IDEO adduct) on an epoxy surface....	40
Figure 3-6.	Diffusion model of resin and hardener between microcapsules. The colored regions indicate areas that the liquid core materials occupy the crack plane. The circles are the embedded microcapsules.....	41
Figure 3-7.	Concentration profile of hardener in a 100 μ m length.....	43
Figure 3-8.	Degree of mixing in a crack vs. time.....	43
Figure 3-9.	Epoxy reaction sequence ³⁵	44
Figure 3-4.	Light microscope (left) and SEM (right) photos of Epon® 815C Resin capsules using UF process (YD3-56).....	49
Figure 3-5.	One mole DETA plus two moles of 1, 2' Epoxyhexane.....	52
Figure 3-6.	One mole 4, 4 Diaminodicyclohexylmethane plus two moles of 1,2 Epoxyhexane.....	52
Figure 3-7.	One mole DETA plus two moles Benzaldehyde.....	54
Figure 3-8.	One mole Ethylene Diamine plus two moles of Benzaldehyde.....	54
Figure 3-9.	Structure of Isophorone Diamine.....	57
Figure 3-10.	FTIR Spectra of Acetone Mixed with 1,2-Epoxyhexane (left) and Isophorone Diamine (right) ³⁹	58
Figure 3-11.	FTIR Spectra of Ethanol Mixed with Isophorone Diamine (left) and 1,2-Epoxyhexane (right) ³⁹	59
Figure 3-12.	Diagram of Isophoronediamine and 1,2-epoxyoctane.....	60

Figure 3-20.	Various configurations of the IDEO adduct.....	63
Figure 3-21.	Proton NMR of 1,2-epoxyoctane. Prediction (left), actual spectra (right).....	64
Figure 3-22.	Carbon NMR of 1,2-epoxyoctane. Prediction (left), actual spectra (right).....	65
Figure 3-23.	Proton NMR of isophorone diamine. Prediction (left), actual spectra (right).....	66
Figure 3-24	Carbon NMR of isophorone diamine. Prediction (left), actual spectra (right).....	67
Figure 3-25	Extent of reaction vs. Time for EPON815C/IDEO adduct curing at 25°C.....	69
Figure 3-26.	Drop-wise interfacial polymerization process.....	71
Figure 3-27.	Experimental set-up of the ultra-turrax homogenizer.....	72
Figure 3-28.	Complex Coacervation of Toluene as a Model System (JN3-59) ³⁸	75
Figure 3-29.	Initiators used for in-sit polymerization encapsulation process ^{41,42}	77
Figure 3-30.	First Attempt at Free-Radical Polymerization Based Encapsulation of the IDEH adduct by a p(MMA-MA) Shell (JN3-80) ³⁹	78
Figure 3-31.	Clusters of JN3-82 Amine Adduct Capsules Encapsulated by pMMA/MA (left), Capsules after Being Crushed and Amine Adduct Liquid Content Released (right).....	79
Figure 3-32.	Close-up optical microscope image of broken JN3-82 capsule releasing IDEH amine adduct liquid.....	80

Figure 3-33.	Optical microscopy of JN3-84 capsules from free-radical polymerization based encapsulation of the IDEH adduct by a p(MMA-MA) shell with AIBN initiator.....	81
Figure 3-34.	Clusters of JN3-84 IDEH amine adduct capsules encapsulated by p(MMA-MA) (left), capsules after being crushed and amine adduct liquid content released (right).....	81
Figure 3-35.	Adduct of Isophorone Diamine and 1,2 Epoxyhexane (top), Adduct of Isophorone Diamine and 1,2 Epoxyoctane (bottom).....	82
Figure 3-36	Optical microscopy of JN3-85 capsules from free-radical polymerization based encapsulation of the IDEO Adduct by a p(MMA-MA) shell with AIBN initiator.....	83
Figure 3-37.	Clusters of JN3-85 amine adduct capsules encapsulated by pMMA/MA (left), capsules after being crushed and IDEO amine adduct liquid content released (right).....	83
Figure 3-38.	Light microscope images of JN4-11 wet (left) and dried (right, polarized lens).....	84
Figure 3-39.	Conversion curve of MMA batch polymerization with AIBN. A charge of radical scavenger was place at t=30 Min.....	86
Figure 3-40.	Conversion curve of Styrene batch polymerization with AIBN. A charge of radical scavenger was place at t=30 Min.....	87
Figure 3-41.	Graph of theoretical payload and shell thickness of a 100 μ m diameter microcapsule.....	90

Figure 3-42.	Titration curves of adduct, water, and JN4-11 microcapsules with the specified acid fed at a rate of 5ml per hour.....	94
Figure 3-43.	Light microscope images of JN4-11 in pH 2 after seven days Light microscope(left), Light microscope with polarized lens (right).....	95
Figure 3-44.	Chemical structures of V-65(left) and AIBN (right) ^{41,42}	96
Figure 3-45	Solution polymerization of MMA/BMA/IDEO adduct. 20ml vial (left) Broken halves (right).....	99
Figure 3-46.	Light microscope images of washed and dried JN4-64 microcapsules. Whole capsules (left) and crushed capsules (right).....	100
Figure 3-47.	Paper test of dried and washed JN4-64 microcapsules. Whole Capsules (left) and crushed capsules (right).....	100
Figure 3-48.	Titration curve of JN4-64 capsules, water, and IDEO adduct in water...101	
Figure 3-49.	JN4-72 capsules in dispersion (left) and dried crushed capsules (right).102	
Figure 3-50.	Paper test of JN4-72 capsules. Whole capsules (left) and crushed capsules (right).....	103
Figure 3-51.	Experimental set-up of encapsulation process used in JN4-72.....	104
Figure 3-52.	Dynamic light scattering data (Microtrac S3500) of JN4-72 dispersion.....	104
Figure 3-53.	SEM Images of JN4-72 capsules. Whole capsules (left). Crushed capsules (right).....	105
Figure 3-54.	SEM Images of JN4-72 capsule (left) and a section of its shell (right)...	106

Figure 3-55. FTIR Spectra of IDEO Adduct, MMA/BMA copolymer, and JN4-72 microcapsules.....	107
Figure 3-56. Image of crushed JN2-32 Resin Capsules and JN4-72 IDEO adduct capsules between two glass slides.....	108
Figure 3-57. DSC trace of JN4-63 IDEO adduct.....	109
Figure 3-58. DSC trace of JN4-68 MMA/BMA polymer.....	110
Figure 3-59. DSC trace of JN4-72 IDEO amine adduct capsules.....	110

ABSTRACT

DUAL MICROCAPSULE SYSTEM FOR AUTONOMOUS SELF-HEALING COATINGS

by

Jonathan K. Nguyen

University of New Hampshire, September 2008

Polymer coatings are vulnerable to external and internal damage. Formation of microcracks can occur because of an impact event or through oscillatory stresses such as thermal expansion and contraction. Self-healing offers a solution to respond to internal damage and repair the polymeric structure.

This work utilizes a dual microcapsule system as the autonomous self-healing mechanism for use in an epoxy coating. The system is comprised of an epoxy resin microcapsule and an amine adduct capsule embedded in an epoxy matrix. Encapsulation of the epoxy resin was achieved, however encapsulation of the amine adduct is very challenging, and was the main focus of this work. The amine adduct has been successfully encapsulated, resulting in a satisfactory microcapsule payload and size, but reproducibility has proven to be difficult. Though reproducibility is an issue, the adhesive properties of amine adduct and epoxy capsules have been successful by adhering two pieces of epoxy together.

CHAPTER I

INTRODUCTION

Polymers along with other materials are vulnerable to external and internal damage¹⁻⁴. Internal growths of microcracks occur within the material because of an external act such as an impact event¹. External force typically damages the material on the surface and can be seen visually and be repaired accordingly. Internal damage is often very difficult to detect. Internal damages can be formed through oscillatory stresses such as vibrations or thermal expansion and contraction within the material. Techniques such as ultrasonics and radiography are used as non-destructive tests to detect internal damage, but leave a lot of the damage undetected¹. Self-healing offers a solution to internal damage by autonomously responding and repairing damage within the polymeric structure¹.

Self-healing systems are able to detect the signs of internal failure and react to repair the material. The term smart (stimuli responsive) material comes from the system's ability to react on its own without any external input. The use of self-healing systems may prolong the life of many polymeric structures.

For many self-healing polymers, the mechanism of self-healing is initiated when damage occurs. Sources of damage can originate from fatigue or impact. Fatigue cracks form by oscillatory stresses within the material. The event of impact can form cracks within or on the surface of the material. Crazing leads to microcrack formation, and this

in turn grows into a macrocrack. A self-healing system within the material would react to the damage at the microscale and accordingly results in healing of the crack prior to macrocrack formation. Ideally, the self-healing mechanism would recover the material's original mechanical properties (i.e. fracture toughness, modulus, etc.). Current systems only recover a fraction of their original strength⁵. The best system to date has shown a sample with a healing efficiency up to 90% of the original virgin material fracture strength⁽⁶⁻⁹⁾.

Background on Self-Healing

Thermal self-healing materials and autonomous self-healing materials are investigated mechanisms for self-healing research. Thermally self-healing polymers require a source of heat to initiate repair^{5,10-12}. Autonomous self-healing systems require no external input to initiate the healing process³. In the following sections, examples of thermally healing and autonomous self-healing systems will be discussed.

Thermally Self-Healing Materials

Frank Wudl et al. have developed a thermally self-healing material, in which the material mechanical properties equal properties of other commercial resins¹⁰. The system utilizes the thermally reversible Diels-Alder reaction (DA), for crosslinking linear polymers.

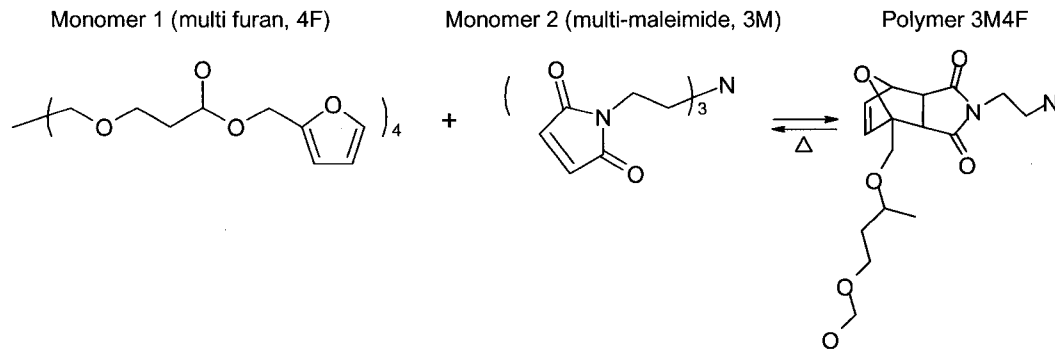


Figure 1-1: Diels-Alder reaction to make prepare polymeric material¹⁰.

Two monomers, multifuran (4F) and multi-maleimide (3M) are synthesized to produce the bulk copolymer (3M4F). The 3M4F polymeric material is tough and solid at room temperature. At a temperature of around 120°C, 30% of covalent intermolecular linkages are detached and upon cooling the detached linkages are reconnected¹¹. Reconnecting broken crosslinks, under thermo cycling allows healing of the material across the fracture

region. In addition, the 3M4F polymer material heals without additional ingredients such as catalyst, additional monomer, or surface treatment ¹¹.

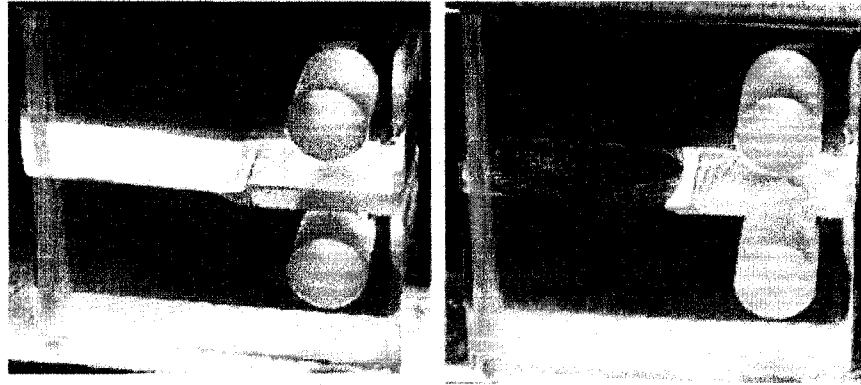


Figure 1-2: Fracture toughness specimens of 3M4F. Sample (A) is cracked. Sample (B) is thermally healed ¹¹.

Figure 1-2 is a fracture toughness sample of 3M4F polymer broken under tensile stress and thermally healed at 150 °C. Load vs. displacement curves have shown a 57% recovery of the original fracture load as shown in Figure 1-3. During the test, the samples were broken into two separate pieces making it difficult to place them together perfectly for healing¹⁰. The lower healing efficiencies are partially due to the fact the two pieces are not assembled perfectly together¹⁰.

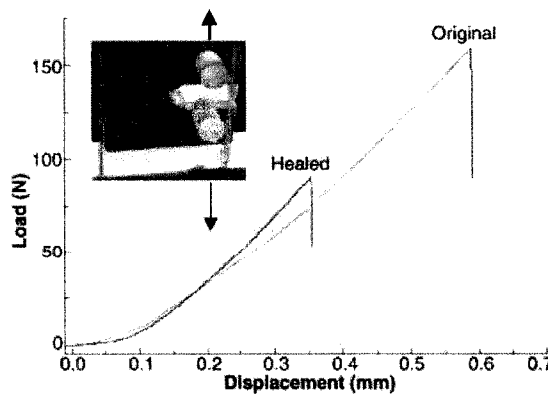


Figure 1-3: Load vs. Displacement curve for virgin and healed samples of 3M4F¹⁰.

The critical fracture load or force in which the sample would break, for a third consecutive crack has been shown to be 80% of the previous critical fracture load, which suggests that the polymeric material can be healed multiple times¹⁰.

An advantage of auto-mending material is that it does not have any long-term problems such as a critical shelf life. The healing system uses existing material in the sample, and can heal multiple times without the use of additional material^{10,11}. A disadvantage though, is that auto-mending material requires an external source of energy to promote healing¹². The external source of energy essentially makes the thermally self-healing material not “self” healing.

Autonomous Self-Healing

Approaches to autonomous self-healing have ranged from the use of microvascular networks, hollow glass fibers, or incorporating microcapsules to the material^{3-9,12-14}. Autonomous systems do not require any external input to repair¹⁵. Many approaches to autonomous self-healing use liquid reactants embedded in the material, eliminating the need of additional material to repair the damage. Autonomous systems require a means of responding to any mechanical damage and heal the corresponding region.

Microvascular Networks

Microvascular networks are designed to mimic the architecture of human skin¹². The outer epidermal layer is composed of multiple sub layers that work in conjunction to rebuild the surface of the skin. As can be seen Figure 1-4, the dermal layer underneath supplies the nutrients required in repairing the above epidermal layer¹². Microvascular networks have been designed to deliver necessary components to “heal” the area of damage^{12,16}. This allows the healing fluid to reach all crack sites that occur throughout the material. A network of channels is fabricated into the material and filled with a healing agent. After damage occurs the healing agent flows from the microchannels to the microcrack through capillary action¹².

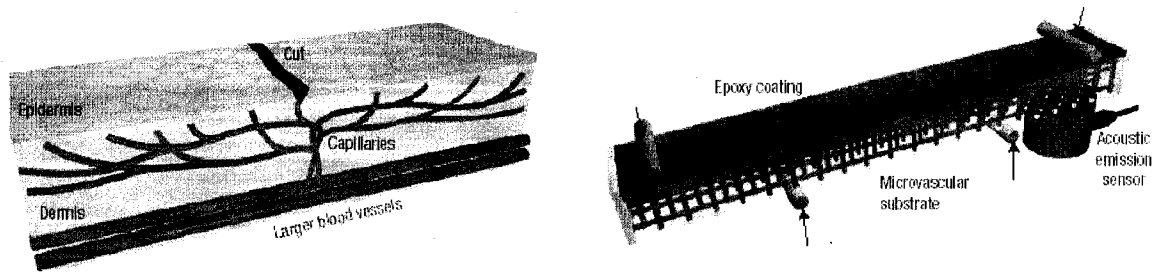


Figure 1-4: Diagrams of microvascular networks. Human Skin (left), Epoxy coating (right) ¹².

The microvascular system consists of an epoxy coating that is deposited on a ductile structure that contains a three-dimensional network¹². Networks are made using a direct-write assembly made from 16-layer structures and microchannels that are interconnected¹⁷. The direct-write assembly would produce a three-dimensional scaffold with a fugitive ink, which is solid at room temperature and can liquefy around 60°C¹⁷. Once the scaffolding is produced the structure is impregnated with resin and hardened to form a complete matrix. The matrix is then warmed to liquefy the fugitive ink and is removed leaving a matrix with an intricate network within¹⁷. An epoxy coating with Bis-tricyclohexylphosphine benzylidene ruthenium (IV) dichloride, also known as Grubb's catalyst is deposited on top of the matrix and the microchannels are filled with dicyclopentadiene (DCPD) monomer as the healing agent¹². The reaction mechanism used to polymerize the DCPD monomer is ring-opening metathesis polymerization (ROMP)⁷.

White et al.¹² tested microvascular specimens under a four point bending test. In Figure 1-5, the excess monomer flowing out of the cracks after a four point bend test is evident. The sample was cracked and healed numerous times with an average healing efficiency of 50%. Results of further testing revealed healing halted after a seventh loading test, due to loss of catalyst in the cracked area¹².

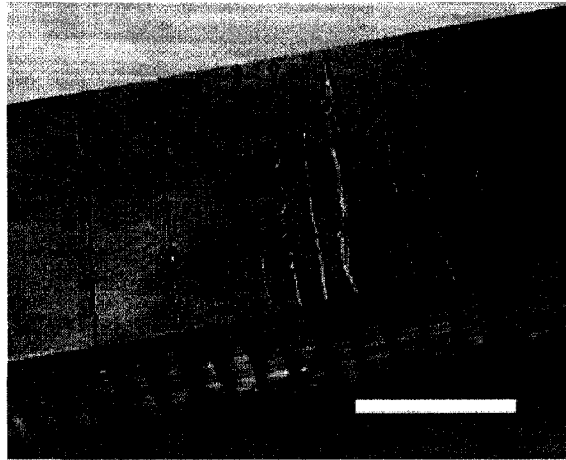


Figure 1-5: Cracked and healed structure with 2.5% catalyst loading¹².

The microvascular system has a lot of potential in some structural systems, but implementing vascular networks in coatings is difficult to achieve. The system uses a 700 μm coating but requires a 16-layer system of 200 μm diameter channels to operate¹², where coating thicknesses are generally in the hundreds of microns.

Hollow Fibers

It has been found that advanced composite materials are susceptible to impact loading, cracks or delaminations that form within the structure^{3,4,13}. Hollow fibers have been used as another type of self-healing system. Hollow fibers can detect by breaking the hollow fiber and deliver the necessary materials to a damaged area. Various composites with hollow fibers have been filled with healing agent(s)^{1-4, 13, 14}. Flexural strength results have indicated a 16% reduction in strength when incorporating hollow fibers, but has been shown to have an 87% recovery after the sample was broken and healed¹⁴.

Like any autonomous system, a means of responding to any mechanical damage is required. In the case of the hollow fibers the cracking of the material will break the hollow fibers and release the healing agent to the damaged region¹.

Upon cracking, the hollow fibers are broken releasing its contents into the crack that has broken the hollow fibers initially. In Figure 1-6, hollowed fibers can be used in various configurations. An example system uses two types of hollow fibers utilizing a two part healing system where one fiber is filled with a reactive resin while the other is filled with a reactive hardener. When a crack occurs the two reactive materials flow into the crack plane, diffuse, and react to heal the damaged area.

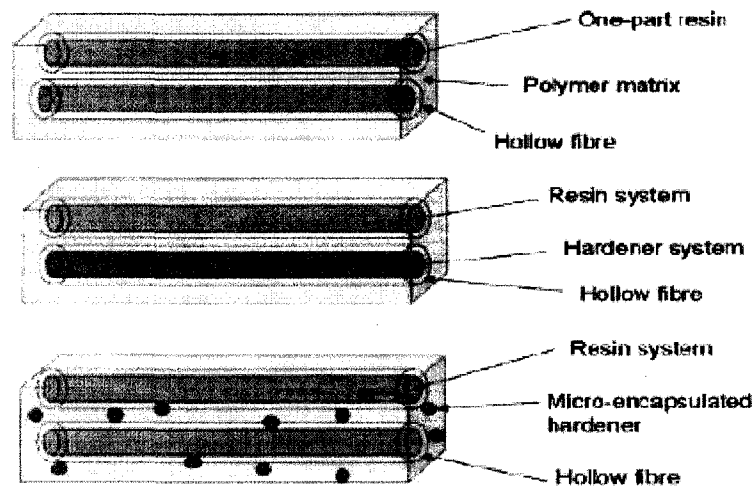


Figure 1-6: Various Systems using hollow fibers¹⁴.

Bond et al.² have implemented a “bleeding” system where one part would be the autonomous healing system and the other is to use a fluorescent dye that can reveal areas that underwent some catastrophic mechanical load and healed overtime . Eighteen piles of hollow fibers (stacked to a height of 2mm) were manufactured using a hand lay-up

process. Four point bending flexural tests of this system have shown a healing efficiency of 97% using an epoxy matrix embedded with resin and hardener filled hollow fibers².

The use of hollow fibers has shown excellent healing efficiencies, but requires a substantial amount of labor to produce the composites². For the use in coatings, hollow fibers cannot be plausible due to the amount of fibers stacked to a height of approximately 2mm to achieve a 97% efficiency². The large thickness, can be problematic in a coating that is 250-500 μ m.

Microcapsules

Another example of an autonomous self-healing material uses microcapsules and catalyst embedded in an epoxy matrix. The system is an epoxy resin matrix that has microcapsules of a monomer along with catalyst dispersed within the material^{5,6,8,9,18}. The system uses encapsulated DCPD and embedded Grubbs catalyst, as the self-healing materials⁶.

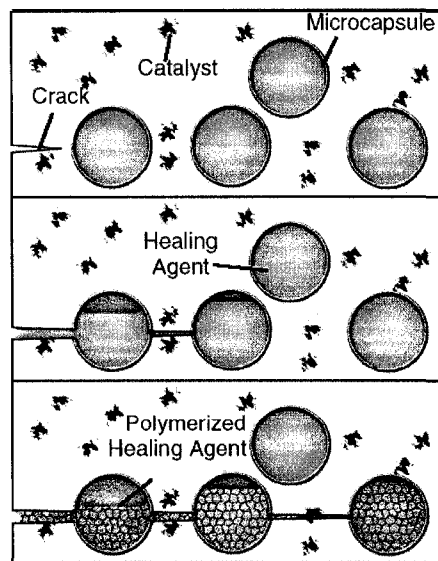


Figure 1-7: Crack propagation in a self healing composite⁵

As shown in Figure 1-7, as a microcrack propagates through a matrix material, the microcapsules break releasing their contents. The liquid monomer is released into the crack plane by capillary action, filling the crack volume^{5-7,18}. During the filling process the monomer flows and makes contact with the catalyst, dissolving the catalyst. The dissolved catalyst polymerizes the monomer repairing the crack by bonding the crack faces together⁷. The crack becomes filled with a cured monomer and a large fraction (e.g. 90%⁵) of the virgin mechanical strength is reported to be recovered^{5-7,18}

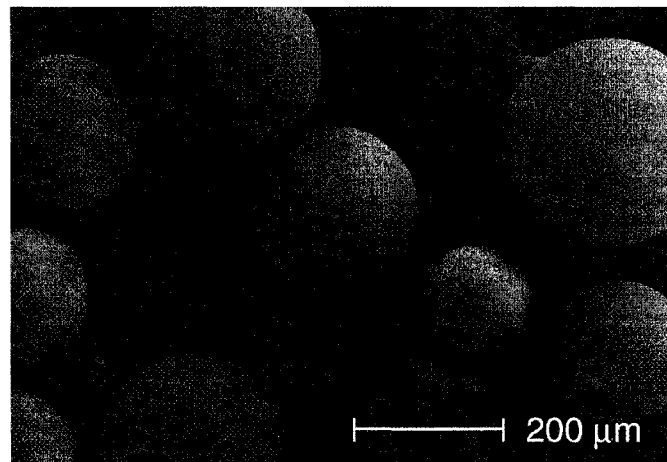


Figure 1-8: SEM picture of DCPD capsules manufactured using Urea formaldehyde process⁸.

The microcapsules in Figure 1-8 have been made using an in-situ polymerization process as an oil in water emulsion¹⁹. The microcapsules were made of a DCPD core with a urea formaldehyde shell, with sizes ranging from 10-1000 μm ¹⁹. The microcapsules had sufficient strength to remain intact during polymerization and subsequent recovery and drying, but rupture within the epoxy matrix when microcracks form.

The system performed well with a large (2.5wt%) catalyst loading but, attempts to reduce the catalyst loading resulted in very low healing efficiencies¹⁸. The Grubbs

catalyst did not disperse well as a powder within the epoxy matrix and the amine hardener used to make the epoxy matrix can deactivate the Grubbs catalyst significantly reducing its activity¹⁸. A method of first encapsulating the catalyst with wax was performed to protect the catalyst from the amine hardener as a solution to the deactivation of the catalyst. Results have shown that the wax protection saved 69% of the catalysts activity prior to healing; with no protection the activity was zero¹⁸.

The microcapsule approach is the most viable system to use for self healing of composite coatings. Documented healing efficiencies of 90% were demonstrated using DCPD and wax coated Grubbs catalyst system^{9,10}. With a high healing efficiency, prolonging the life of the coating may be realized. It is important to note that this is not a perfect solution. The method only can be used once in the same location, due to the limited chemical resources in a specific area, however the small capsule sizes may allow application to coatings of certain thicknesses. The Grubbs catalyst automatically makes this process quite expensive, but it can be used as a model system to provide comparisons to other systems under investigation.

Background on Microencapsulation

Microencapsulation is a process of enclosing micron sized material, either a solid or liquid, with an inert shell²⁰. Microencapsulation technology is used for various purposes, to have controlled release, protection from the environment, or allow for mixing between incompatible material²⁰. The product of a microencapsulation process is a particle known as the microcapsule. Microcapsules are usually made up of two parts, the core and the shell as depicted in Figure 1-9.

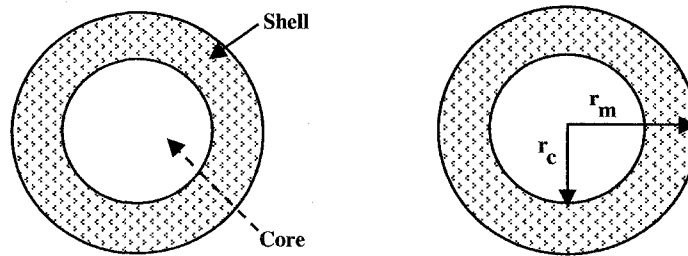


Figure 1-9: Cross section of a microcapsule²⁰

Core material can be encapsulated in the form of a liquid, solid or gas. Efficiency of microencapsulation depends on the compatibility of the core and shell material. A variety of materials such as monomers, fragrances, dyes, and catalysts have been encapsulated. A wide variety (and combinations) of polymers can be used for a shell that can be engineered to be permeable, semi-permeable, or impermeable²⁰.

Separation of the reactive components via microencapsulation is an important characteristic for use in a smart self-healing coating. The chemical reaction can then be initiated by crushing the microcapsules, releasing their contents and exposing each reactant to each other²¹. Importantly microcapsules can be obtained as a free flowing powder and be applied to a coating formulation²¹.

Encapsulation Techniques

There are numerous techniques that can be used to encapsulate core materials. The techniques can be categorized into two groups, chemical and physical methods. Chemical processes such as in-situ polymerization, complex coacervation, along with interfacial polycondensation are commonly used. Examples of physical methods include spray drying, fluid bed coating and extrusion. The following are examples of common encapsulation methods used or discussed throughout this thesis^{20,21}.

Encapsulation techniques can be performed in an aqueous or organic medium depending on the polarity of the encapsulate. Complex coacervation is a technique that utilizes phase separation from an aqueous solution. The technique uses two oppositely charged colloids that are mixed together and then a phase separation occurs from an electrostatic interaction. The core material is first dispersed into a cationic polymer aqueous solution. Then an anionic polymer solution is added. Formation of the shell results when the two polymers form a complex. The complex can be triggered by adding salts, changing pH or diluting the whole system. Gelatin and Gum Arabic are common ingredients used for complex coacervation. They form a complex when a drop in pH is induced. Gelatin needs to be crosslinked with an aldehyde in order to form a rigid shell wall^{20,21}.

Interfacial polymerization creates polymer at the interface of a droplet or particle. Interfacial polymerization allows one to encapsulate hydrophobic or hydrophilic materials. Encapsulation with this method is obtained using a hydrophobic monomer within the dispersed phase and a hydrophilic monomer within the continuous phase, or vice versa. In the microencapsulation process, the dispersed phase and the continuous

phase both supply reactive material at the interface to be created. Interfacial polymerization can encapsulate solid or liquid particles; in the case of liquid particles a core-shell morphology is dominant. Amines can be encapsulated with nylon or polyurethane shells using the interfacial polymerization method. Nylon shells can be made with sebacoyl chloride in an organic solvent and then adding 10% aqueous solution of an amine into the continuous phase. Urethane shells are like the nylon shell but by replacing the sebacoyl chloride with a diisocyanate. The issue here is that the capsules tend to stick together during polymerization and often are made too large to be useful in coatings²¹.

In-situ polymerization, unlike interfacial polymerization, has the reactive ingredients fed from within the dispersed droplet or within the aqueous phase. This technique utilizes the solubility of monomers and insolubility of their polymers in either an aqueous or organic medium. During an encapsulation reaction, the monomer(s) used to encapsulate are polymerized and migrate to the particle interface. At the interface further polymerization occurs and slowly overwhelms the particle and finally encapsulates it^{20,21}.

As described earlier, urea formaldehyde shells are commonly used as an encapsulating material for self-healing systems⁵⁻⁹. Urea formaldehyde (UF) shells are primarily made via in-situ polymerization in an aqueous medium. During aqueous UF polymerization the precipitates of UF are produced and migrate to the surface and slowly engulf the whole droplet to make a capsule. A detailed description of the procedure will be discussed in later sections of this thesis.

Mechanically controlled processes are also widely used in industry to produce microcapsules. Co-extrusion and spray drying are among common procedures used today. Co-extrusion uses a dual fluid stream in which the liquid core and shell materials are pumped through concentric tubes. At the end of the extruder a vibrational force is used to form the droplets. Spray drying is another method and is mainly used for encapsulating fragrances and oils. The core particles are dispersed in a polymer solution and then sprayed into a hot chamber. The hot environment will flash off the solvent leaving a solid shell around the core. Water soluble polymers are typically used as shell material because of potential hazards solvents can be at high temperatures and concentration²¹.

Background on Fracture Toughness

Throughout this thesis the measure of fracture toughness of a brittle material is commonly used to describe healing efficiencies of a system. Fracture toughness, K_c (units of $\text{Pa}\cdot\text{m}^{1/2}$), is a property that is material and geometry dependent. K_c is usually designated as K_{Ic} when the sample size is sufficiently large. With a large sample K_{Ic} becomes the lower limit of the fracture toughness. K_{Ic} is known as the plain strain fracture toughness in Mode I fracture²² (see below).

A specimen can be tested under three different fracture modes. Mode I is known as an opening mode where stresses are applied perpendicular to the crack plane. Mode II is a forward shear or sliding mode, where the stresses are applied parallel to the crack plane, in opposite directions. Mode III is a transverse shearing or tearing mode. Mode I is commonly used for fracture toughness measurements of brittle materials²³.

Beres et al. has designed a tapered double cantilever beam testing sample to keep K_{Ic} constant along the crack plane, as shown in Figure 1-10²⁴.

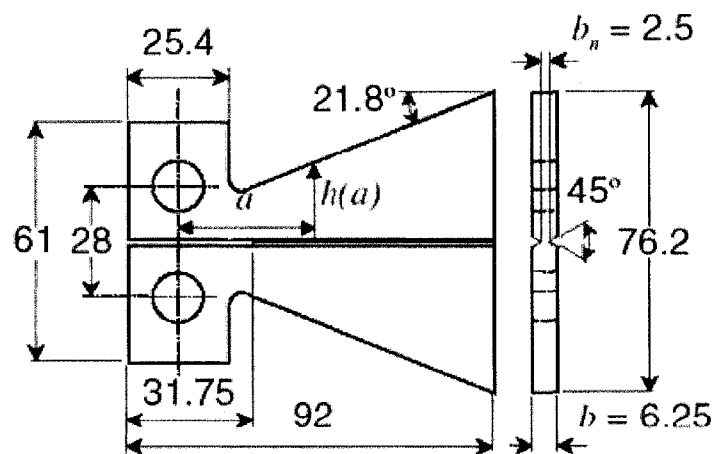


Figure 1-10: TCBD geometry. Dimensions in mm.⁵

With K_{Ic} constant throughout the sample crack plane the fracture toughness is only dependent on the material.

$$K_{Ic} = 2P_c \frac{\sqrt{m}}{\beta} \quad (1.1)$$

The parameter P_c is the critical fracture load which can be measured directly. The parameters m and β are based on geometry of the sample (see Figure 1-10 for a , b , b_n , and h)⁵.

$$\beta = b^{0.61} b_n^{0.39} \quad (1.2)$$

$$m = \frac{3a^2}{h(a)^3} + \frac{1}{h(a)} \quad (1.3)$$

From equation (3), one can see that there is a dependence on crack length, but that has been designed to be constant throughout the crack plane. One can find K_{Ic} by measuring the critical fracture load of a sample. This tapered double Cantilever beam (TDCB) geometry has been utilized to calculate healing efficiencies of this DCPD and Grubbs catalyst system⁵.

$$\eta = \frac{P_{c_{healed}}}{P_{c_{virgin}}} \quad (1.4)$$

Critical fracture loads are measured according to ASTM 638 D for tensile properties of plastics. ASTM 638 D requires use of a tensile testing machine, such as an Instron to measure samples under a constant displacement rate while measuring the load on the sample. The results of such a test are shown in Figure 1-11.

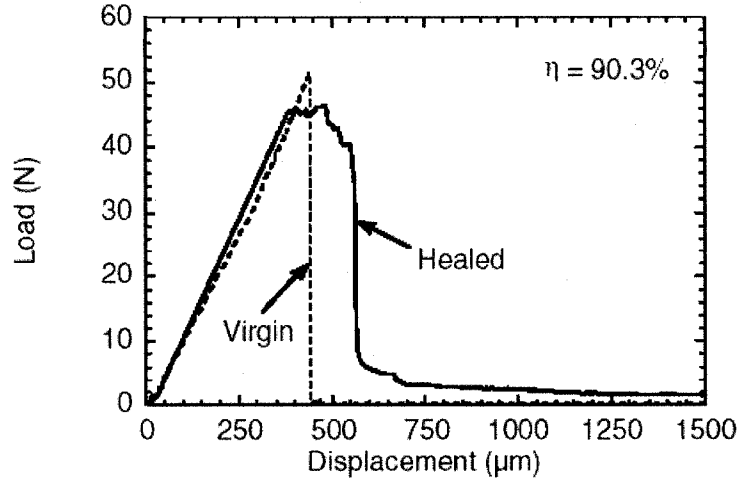


Figure 1-11: Load vs. displacement curve of an in-situ sample⁵.

Virgin samples are broken and are realigned and allowed to heal. It is important to note that the samples often break to failure resulting in two separate pieces. The two pieces are typically realigned by hand and allowed to heal. When placing such pieces together it is difficult to join the two crack surfaces perfectly. Ideally one would like to fracture a specimen a small amount and allow the elastic properties of the sample to realign the crack faces. The healed sample would then be broken again using the same parameters used to break the virgin sample. The ratio of the two fracture loads, equation (1.4), will yield the healing efficiency value η .

CHAPTER TWO

ONE PART AUTONOMOUS SELF HEALING SYSTEM

White et al.⁵ has demonstrated the use of microcapsules and catalyst as an approach to a self-healing system. The system consists of dicyclopentadiene (DCPD) microcapsules and Grubb's catalyst embedded in the epoxy matrix. As a crack propagates through a microcapsule, it releases the DCPD into the crack plane. The DCPD then contacts the embedded Grubb's catalyst, triggering polymerization of DCPD resulting in healing the crack shown in Figure 2-1.

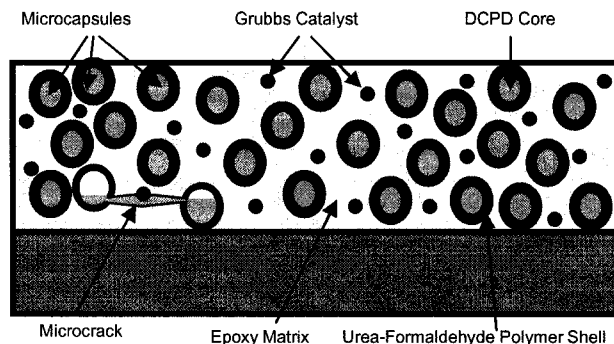


Figure 2-1: Epoxy matrix with DCPD microcapsules and Grubb's catalyst with a crack filled with healing agent.

This system is sufficient to model other systems but there are many potential problems with the high cost of the catalyst including the lifetime of the system, and that the Grubb's catalyst contains a heavy metal that may be harmful to the environment. However, this system will be used as a model in order to develop an understanding of the self healing mechanisms and then applied as a system for anti-corrosion.

Feasibility of Self-Healing System

In order for the self-healing system to work, analysis of the hydrodynamic flow properties of the fluid and kinetics of the polymerization need to be assessed. For the DCPD and Grubb's Catalyst system the DCPD is required to have the ability to fill the crack completely prior to becoming fully polymerized. Intuitively premature curing can lead to inadequate healing of the crack, potentially making the matrix susceptible to further damage.

After microcapsules are broken, the liquid core material fills the crack via capillary action. The filling of the microcrack is modeled by capillary flow in a horizontal tube using the equation below²⁵:

$$v = -\frac{r^2}{(8\mu)} * \left(\frac{\Delta P}{l}\right) \quad (2.1)$$

where r is the radius of the crack, μ is the viscosity of the liquid, ΔP is the pressure drop within the tube, l is the crack length, and v is velocity. Laminar flow is assumed to occur within the crack, making the pressure drop of the crack, ΔP , equal to the pressure in the capillary tube, p_c , by ²⁵:

$$\Delta P = p_c = \frac{2\gamma}{r} * \cos \theta \quad (2.2)$$

where γ is the surface tension of the fluid core material, and θ is the wetting angle of the core material on the matrix polymer surface. Combining equations (1) and (2) becomes:

$$v = \frac{r}{4\mu} * \frac{\gamma}{l} * \cos \theta \quad (2.3)$$

The negative sign (found in equation (2.1)) has been removed because the value of ΔP is negative. One can calculate the time required to fill a crack, t , with the following equation:

$$t = \frac{l}{v} \quad (2.4)$$

Figure 2-2, is a graph of time required to fill a crack with varying crack radii and crack length, while keeping the contact angle, viscosity and surface tension values constant.

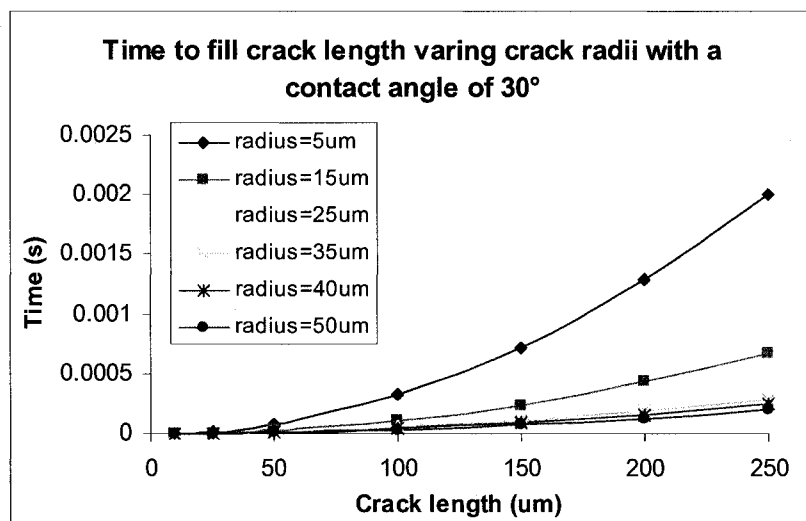


Figure 2-2: Plot of time required to fill various crack lengths and crack radii with a contact angle of 30°

The surface tension and viscosity values are taken as 28.8 dynes/cm (Naphtalene, as a substitute for DCPD as it has a similar structure)²⁶ and 0.01 poise (the viscosity of DCPD is similar to water),²⁷ respectively. The value of 30° for the contact angle has been chosen to produce Figure 2-2. The figure above illustrates the filling of the crack by capillary action occurring in the magnitude of milliseconds. Figure 2-3 (below), shows the sensitivity of the time required to fill a finite crack length of 10µm while varying contact angles. It is difficult to determine the contact angle of the DCPD due to the fact that it solidifies in the pipette used to produce the droplet. This indicates that the surface used to place the DCPD droplet on requires constant temperature control above its

melting point. Therefore a variety of contact angles have been used to calculate various crack fill times. Additional figures regarding crack fill times can be found in Appendix A.

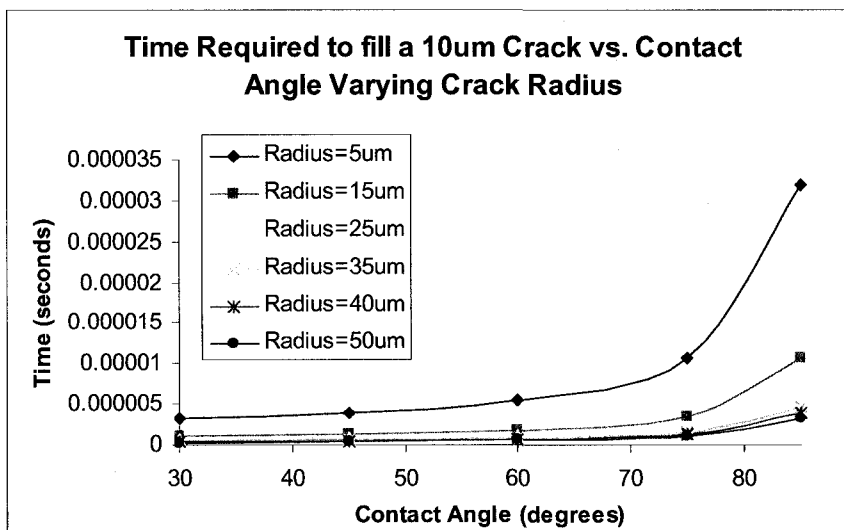


Figure 2-3: Plot of time required to fill a 10um crack varying crack radii and contact angles.

Polydicyclopentadiene (PDCPD) is a highly crosslinked polymer that is produced when DCPD monomer contacts and polymerizes with Grubb's catalyst. The reaction step involves ring opening metathesis polymerization shown in Figure 2-4.

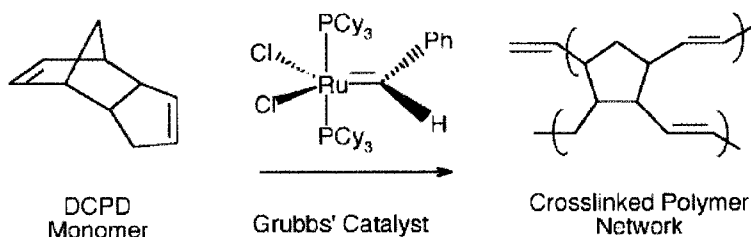


Figure 2-4: ROMP of DCPD and Grubb's catalyst²⁸.

White et al.²⁸ have examined and modeled the kinetics of DCPD with various concentrations of Grubb's catalyst. Results have shown that the rate of curing is dependent on the catalyst concentration, as expected, and as shown in Figure 2-5.

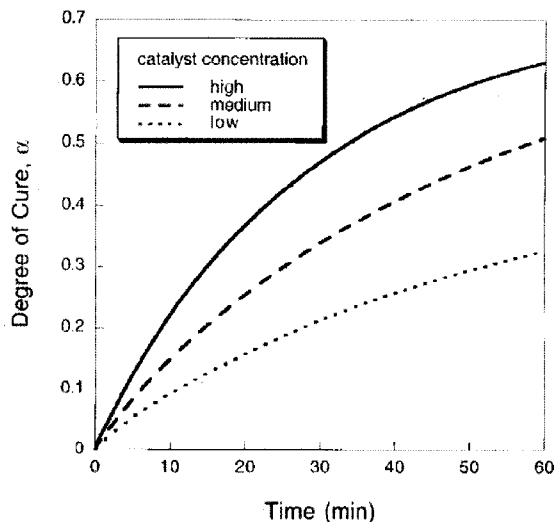


Figure 2-5: Predictions for degree of curing at isothermal conditions (30°C) at low, medium and high catalyst concentrations²⁸.

In Figure 2-5, with 60% curing ($\alpha=0.6$) of the DCPD takes place in a matter of minutes at various catalyst concentrations. Low, medium and high concentrations are designated to be 1.33×10^{-3} g/ml DCPD, 2.00×10^{-3} g/ml DCPD, and 2.67×10^{-3} g/ml DCPD respectively.

One can see that the self-healing system using DCPD and Grubb's catalyst is feasible. The time needed to fill the crack is a small fraction of the time required to polymerize the DCPD to PDCPD. This result makes the system a good model system to gain further understanding of how it works.

Encapsulation of DCPD

Microencapsulation with urea formaldehyde (UF) resins as the shell material has been demonstrated to encapsulate DCPD¹⁹. The UF shell has adequate strength, sufficient adhesion to the host matrix and can be ruptured when a crack propagates through it. This makes it useful in a self healing system. Urea and formaldehyde polymerize under a polycondensation mechanism yielding a highly cross linked polymer²⁵. The overall

reaction sequence for UF polymerization is depicted in Figure 2-6, where the catalytic cross-linking of the resin is performed by the addition of heat and acid. The UF polymerization is performed in water.

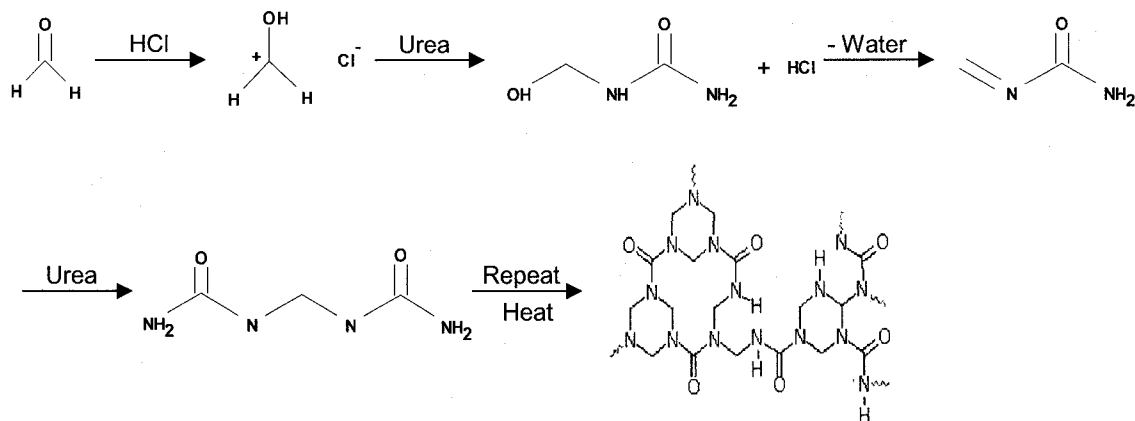


Figure 2-6: Polymerization mechanism for urea-formaldehyde resin

UF polymerization usually takes place in aqueous media where both urea and formaldehyde are soluble. During polymerization the molecular weight (MW) of the polymer increases and becomes insoluble and precipitates out of the aqueous phase.

Figure 2-7 shows potential pathways that precipitated UF polymer can follow. The precipitated polymer can 1) precipitate as a microparticle or 2) migrate onto the oil droplet (DCPD). The precipitated microparticles can either continue to become larger and separate microparticles or coagulate with a droplet producing a rough shelled capsule. The droplets with UF precipitated on them can ideally continue on to produce smooth shelled capsules or coagulate with microparticle producing rough shelled microcapsules.

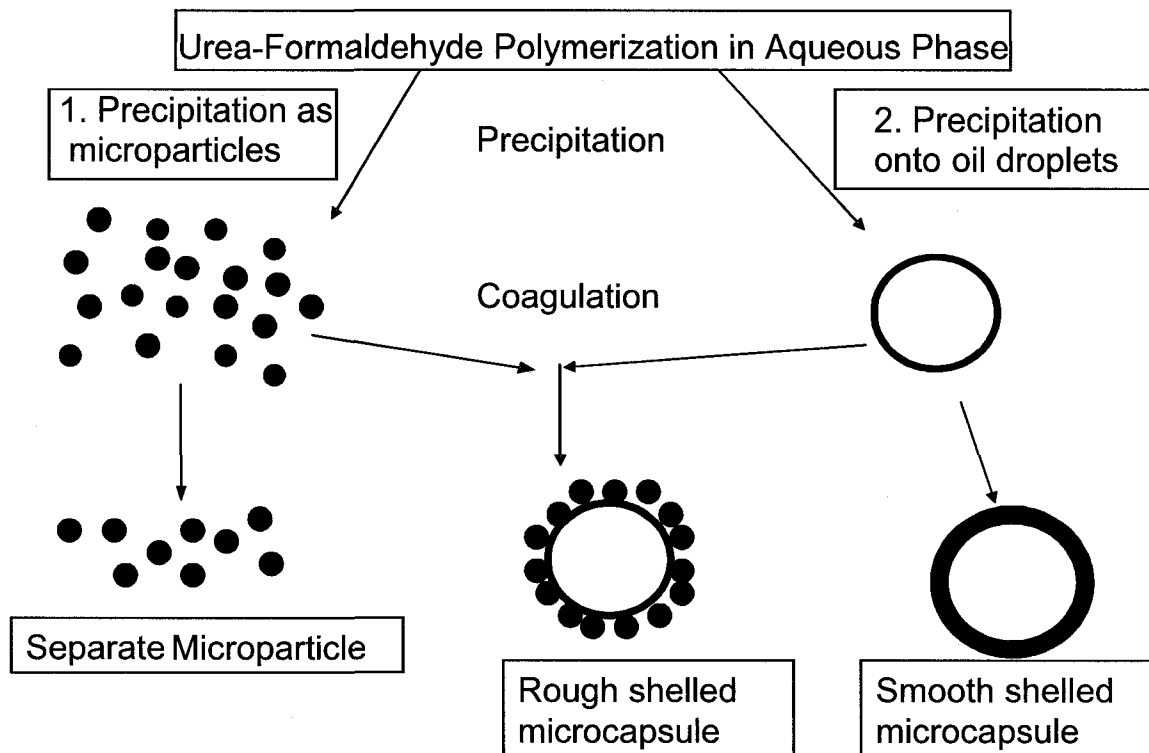


Figure 2-7: Proposed mechanism for UF shell formation²⁹.

The microencapsulation recipe that has been used in the present work follows similarly to what has been presented by White et al¹⁹. In a one liter jacketed reactor, approximately 480 grams of deionized water and 133 grams of 2.5wt% poly(ethylene-maleic anhydride) (PEMA) aqueous solution are mixed, followed by 50g of 2.0wt% polyvinyl alcohol (PVOH) aqueous solution, 13.6 grams of urea, 1.3 grams ammonium chloride, and 1.3grams of resorcinol. To the solution, approximately 160 grams of DCPD is added and dispersed as droplets. The solution is mixed using a Lightnin TS2010 mixer, with a six-blade paddle impeller attachment with a 5 cm diameter, at a rate of 500 rpm.

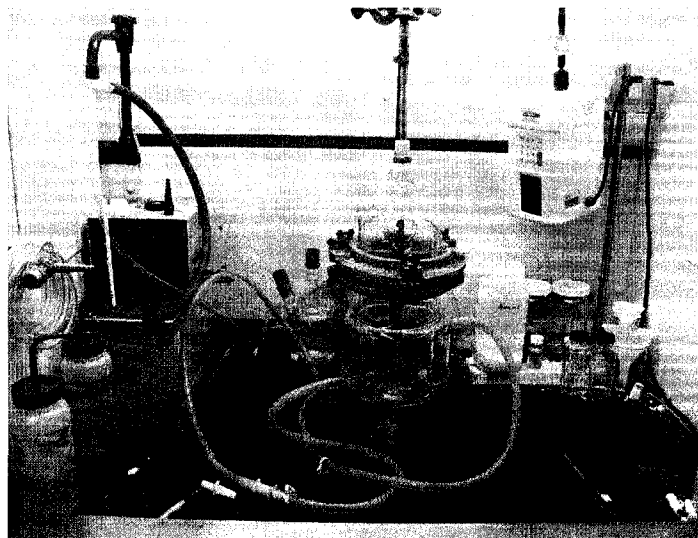


Figure 2-8: Experimental set up for encapsulation of DCPD.

The pH of the dispersion is adjusted to 3.5 using sodium hydroxide and/or hydrochloric acid as required. The reactor content is heated to 55°C, and once the reactor reaches that temperature, 33 grams of 37wt% formaldehyde is added. The dispersion is allowed to react at 55°C for four hours.

PEMA is added to the reactor as a polymeric surfactant to improve the dispersion of the DCPD droplets by reducing the amount of agglomeration^{30,31}. It has been shown by H.Yoshizawa et al³², that PEMA is also essential to the formation of the UF shell around the DCPD droplets. The PEMA adsorbs (like a surfactant) to the DCPD/Water interface and works as a reactive anchor for the UF to adhere to during the condensation reaction³². Polyvinyl alcohol was used as a polymeric stabilizer for the droplets, while the ammonium chloride acts as an acidic-cure catalyst much like HCl for the urea-formaldehyde chemistry. Resorcinol is also a catalyst but aids the UF polymerization differently by providing an already active site for polymerization.

The dispersion is allowed to cool and is placed under vacuum filtration to separate the capsules from the aqueous solution. During the vacuum filtration process the separate microparticles will fall through the filter paper along with the aqueous solution. The capsules are then washed with acetone during filtration process to remove excess surfactant and unencapsulated material. The washed capsules are dried overnight at room temperature, resulting in a free flowing powder. In Figure 2-9, one can see that the particles are approximately 80-120 μm which is confirmed with the use of light scattering measurements (Microtrac S3000 dry mode).

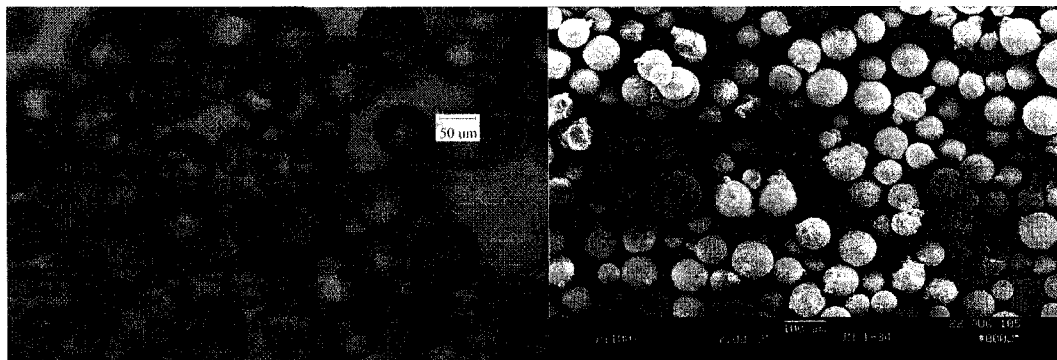


Figure 2-9: Light Microscope (left) and SEM (right) images of DCPD microcapsules²⁵

Differential Scanning Calorimeter (DSC) analysis has determined that there is an 80% payload of DCPD in the microcapsules. DSC data and analysis can be found in Appendix B. Microcapsule payload is defined as the weight ratio of core material to the overall capsule weight. It is important to note that the dried capsules have thin, hard, and brittle shells that can withstand breaking during handling of the material but rupture when needed. Another important characteristic is that the shells have a rough surface which increases the surface area of the capsule, and can lead to better adhesion to the epoxy matrix.

Fracture Testing

In the present work, fracture testing is used to assess self healing of the DCPD and Grubb's catalyst system. The degree of healing can be evaluated by measuring the fracture load of both a virgin and a healed sample. The ratio of those two loads will yield the healing efficiency. Fracture testing similarly follows ASTM 638D which is tensile testing of brittle material. An Instron machine is used to analyze and apply force on the testing specimen at a constant displacement rate and to measure the load over time.

The fracture specimen has a unique design which allows for constant fracture toughness (see chapter one) along the crack plane of the sample (see Figure 1-10). Measuring the crack length of samples optically is a difficult task; therefore the design of the fracture specimen is important. The tapered double cantilever beam (TDCB) specimen allows accurate measurement of fracture toughness without the worry of where the crack ended.

In order to mold samples for testing, a master TDCB template was fabricated out of aluminum. This piece was used to make molds out of silicon rubber. The mold consists of two separated pieces, which are clamped together by two steel plates and four c-clamps. The epoxy mixture was then injected into the mold with a syringe as seen in Figure 2-10. The epoxy mixture was made out of West System Brand Epoxy[®], more specifically the West System 105 resin and 206 slow hardener, with various weight percentages (up to 20wt%) of DCPD microcapsules. The molds were then overfilled into two reservoirs that occupy the holes used for injection, to avoid shrinkage during the curing process.

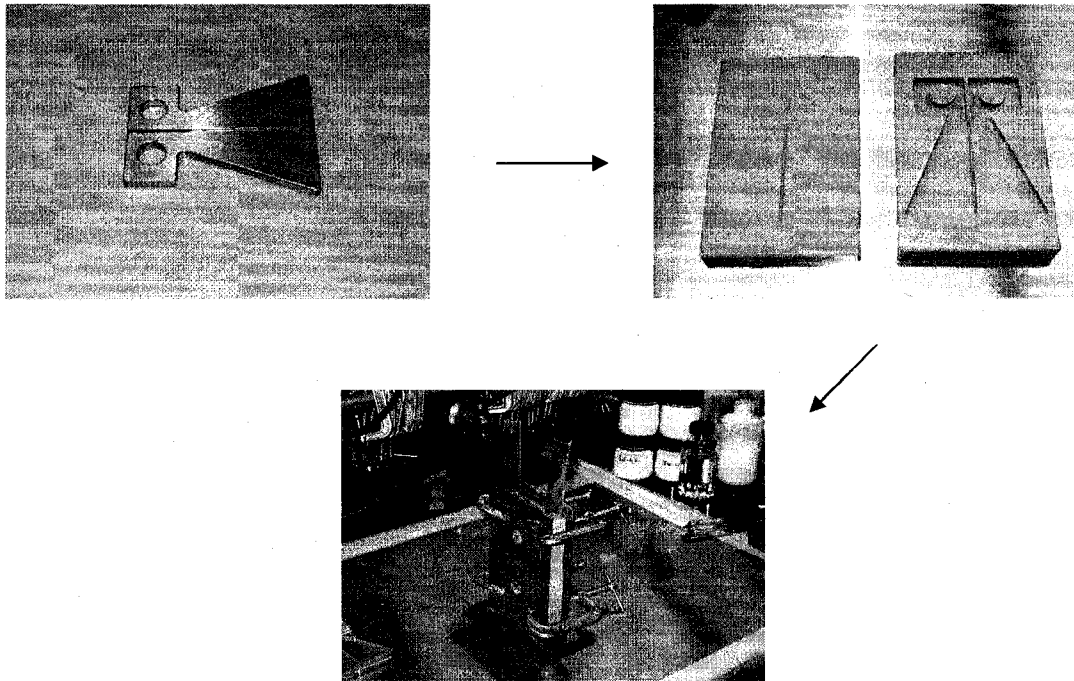


Figure 2-10: Molding process used to make epoxy TDCB specimens.

After twenty-four hours at room temperature, the samples were demolded and allowed to sit at room temperature for additional curing time; approximately six to seven more days. The long cure time allows for complete curing and eliminates any discrepancies in fracture toughness measurements.

The fracture specimens were loaded into an Instron machine and a load applied perpendicular to the crack plane. The displacement was set at a constant rate of crack mouth opening displacement until fracture occurred (e.g. 5.0 $\mu\text{m}/\text{sec}$). Figure 2-11 shows a typical load vs. displacement data for the TDCB epoxy specimen where in this case, the sample exhibited two crack propagations. The crack propagation steps are observed as sudden drops in load. The second drop in load resulted in failure of the specimen (broken into two separate pieces). Typical observed fracture toughness values (K) range from 0.5 to 0.9 $\text{MPa m}^{1/2}$, where handbook values are about 0.6 $\text{MPa m}^{1/2}$ ²².

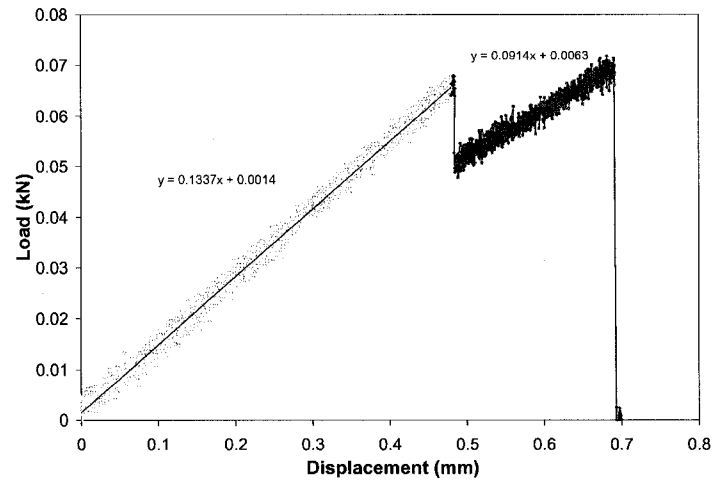


Figure 2-11: Load vs. displacement data for fracture of a microcapsule filled epoxy TDCB specimen²⁵

There are challenges in fracture testing of the TDCB specimens. Prior to sample testing, each specimen needs to be pre-cracked; this leads to the first challenge during testing. Pre-cracking of the samples is performed by tapping a razor blade into a starter notch in the sample, as seen in Figure 2-12.

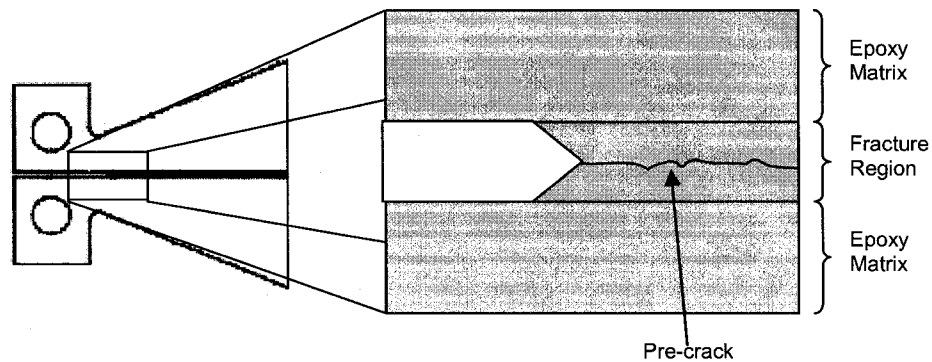


Figure 2-12: Close-up image of pre-cracked region in TDCB specimen.

This pre-crack method most often results in breaking the samples entirely through. A second challenge occurs during testing: samples are often broken to complete failure,

resulting in two halves. In order to evaluate self healing the two halves need to be brought back together and allowed to heal. The physical act of putting them back together by hand does not allow for the crack faces to align perfectly, resulting in inadequate healing. Ideally the sample will only partially crack before the load is released. This allows the sample to naturally come back into perfect contact after removing the load from the sample.

A number of fracture specimens without Grubb's catalyst but with DCPD microcapsules embedded in them have been analyzed. Examination of the fracture surface was made possible by using scanning electron microscopy (SEM). Figure 2-13 shows the fracture surface and numerous cavities are evident. These are from broken capsules which have released their contents. As one can see, there are no protruding microcapsules in the crack plane. Signs of protruding capsules would demonstrate that the cracks propagate around the capsules instead of directly through them. As can be seen in the left hand photo of Figure 2-13, all capsules have been broken completely through. The right hand photo shows the fracture surface for an epoxy matrix without any DCPD microcapsules. The contrast between these photos offers clear evidence for the clean fracture of the DCPD microcapsules.

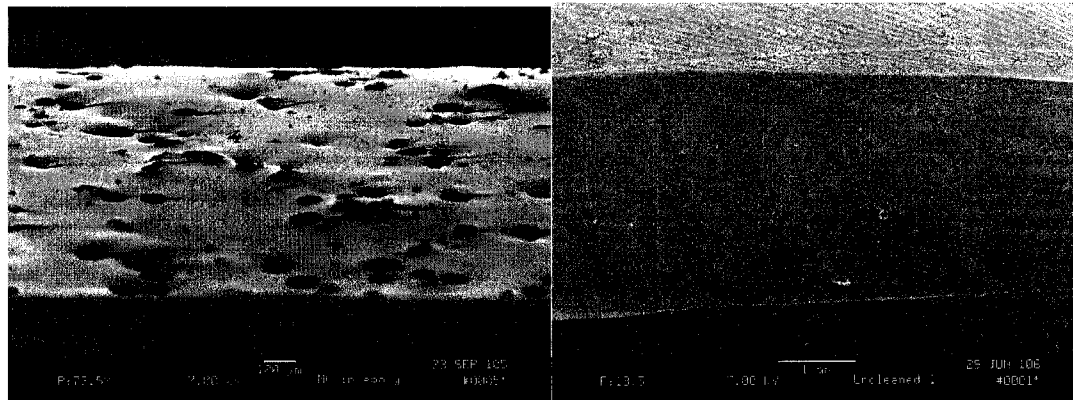


Figure 2-13: SEM picture of a fracture surfaces from an epoxy matrix filled with DCPD microcapsules²⁵ (left) and fracture surface of neat epoxy (right)

Evaluation of self healing was performed with DCPD capsules embedded in epoxy without any Grubb's catalyst. The Grubb's catalyst was omitted from being embedded in the sample due possible deactivation by the amine component. After fracture of an encapsulated DCPD/Epoxy matrix TCBD specimen, a drop of 2wt% solution of Grubbs catalyst in toluene was dispersed along the crack plane and the two specimen halves were put back together and held with c-clamps for a period of 24 hours. Since the specimens typically break into two separate pieces, joining the two crack faces together isn't perfect. In these tests the no additional DCPD was added to the crack plane; the only DCPD present came from broken microcapsules.

As shown in Figure 2-14, the fracture behavior is different from the virgin fracture sample shown in Figure 2-11. The healed sample shows signs of yielding prior to failure. The yielding occurred approximately at a third of the fracture load where the virgin samples break. Using equation (1.4) the healing efficiency, η , is found to be 34.1% for the specific test shown in Figure 2-14.

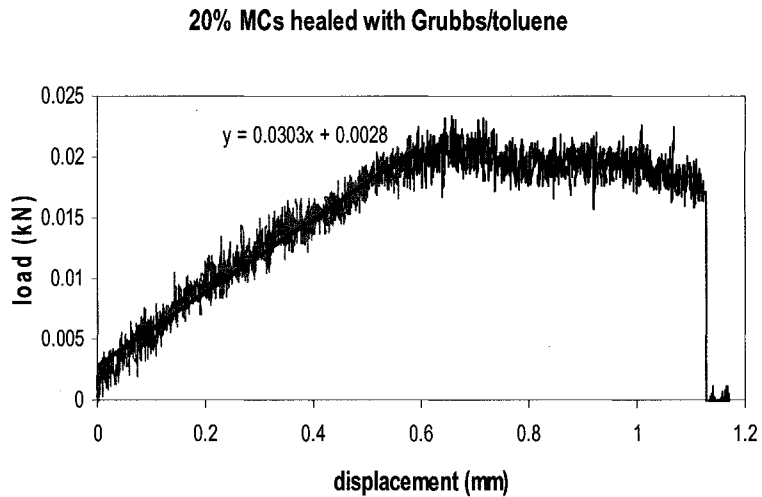


Figure 2-14: Load vs. Displacement curve of a healed sample.

There might be some speculation that the toluene for the Grubb's toluene solution can heal the sample by solvating the epoxy matrix chains, allowing them to inter-diffuse. Various neat epoxy samples have been tested without any DCPD microcapsules embedded within them. A drop of toluene was introduced to the fracture surfaces and the pieces placed together similarly to the DCPD/Grubb's healed samples. Out of ten samples tested, one was able to hold together after removing the clamps. This single sample was unable to hold its own weight and resulted in a break. These results show that the toluene did not heal or contribute to the healing process. Further investigation of this system was halted after reproducing the DCPD/Grubb's catalyst work of Scott White. The understanding of microencapsulation, fracture testing and self-healing was achieved. The optimization of the DCPD/Grubbs process did not become a main focus of the present work because we were much more interested in a two part self healing system that did not contain a catalyst.

CHAPTER III

A TWO MICROCAPSULE AUTONOMOUS SELF-HEALING SYSTEM

A system comprised of two different microcapsules has been devised to be a solution to the problems that exist with the White's DCPD Grubbs catalyst system⁵. This new approach uses components of a two part epoxy to be used as healing agents. The two capsules used in the epoxy system are a resin microcapsule (usually diglycidal ether of bisphenol A (DGEBA)), and a diamine microcapsule as the hardener. Figure 3-1 shows an epoxy matrix filled with microcapsules and a crack filled with the healing agents.

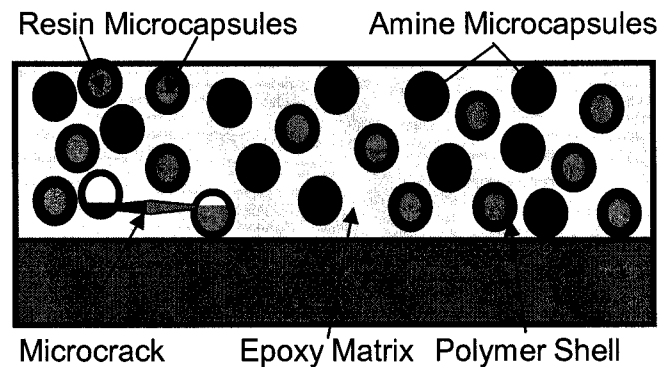


Figure 3-1: Epoxy matrix filled with resin and amine capsules, showing a crack filled with each healing agent.

This system is similar to the DCPD Grubbs' catalyst system, but replaces the Grubb's catalyst and DCPD with epoxy resin and an amine hardener capsules. By replacing the Grubbs catalyst, issues with catalyst shelf life, cost and environmental safety are removed. The new system does require microencapsulation of two different

components in order to preserve them from the outside matrix. The components are ingredients similar to the ones used to make the matrix. Having the healing agents to be the same as the matrix allows for proper adhesion to walls of the crack and similar mechanical strength of the newly formed polymer

Self-healing occurs via a microcrack formed within the matrix that breaks microcapsules as it propagates through the matrix. The crack will break each of the different capsules releasing their contents into the crack plane and filling it by capillary action. This system requires adequate mixing within the crack before it cures. The additional mixing step is performed via molecular diffusion. The filling and mixing steps must be faster than the curing step in order to make a feasible self-healing system.

Feasibility of Self Healing System

For the two capsule epoxy system to become feasible the liquid core materials need to flow into the crack, mix with one another via diffusion and then react and cure after adequate mixing²⁵. Analysis of the hydrodynamic flow properties, diffusion rates and kinetics of the system can determine if the two capsule system is feasible.

Capillary Flow

Within an epoxy matrix the capsules are assumed to be evenly distributed, with equal distances between capsules (shown in Figure 3-2). A calculated distance between microcapsules, h , is approximately $100\mu\text{m}$ (based upon a capsules size of $100\mu\text{m}$ and a capsule loading of 5 wt% in the epoxy matrix).

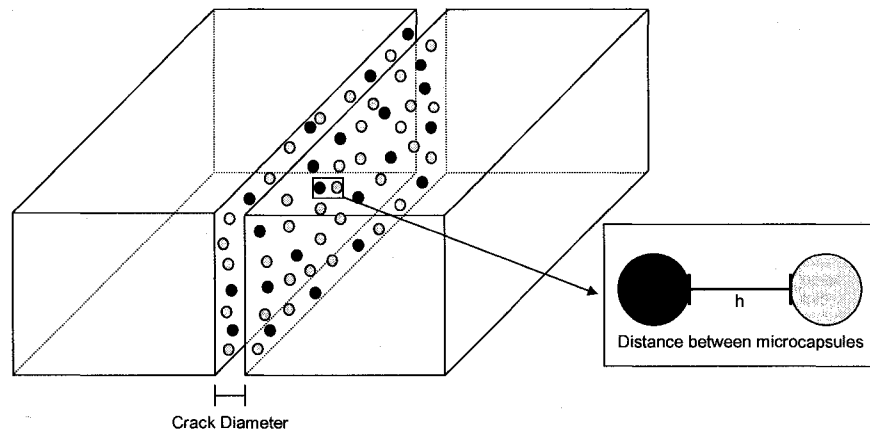


Figure 3-2: Fracture of microcapsules within a matrix.

As a crack propagates through a matrix, capsules within the matrix are ruptured and the contents are released into the crack. Filling of the crack begins when the encapsulated material flows outwards from each capsule occupying all the vacancies within the crack. The filling of the crack can be observed by focusing on a pair of microcapsules and the

distance between them, h . Since the filling process is simultaneously occurring between each pair of capsules one can calculate the time to fill the crack using a distance of h .

The filling of the microcrack can be modeled by capillary flow in a horizontal tube using equation (2.3). The following figures show the time required to fill a crack with resin (Figure 3-3) and amine hardener (Figure 3-5).

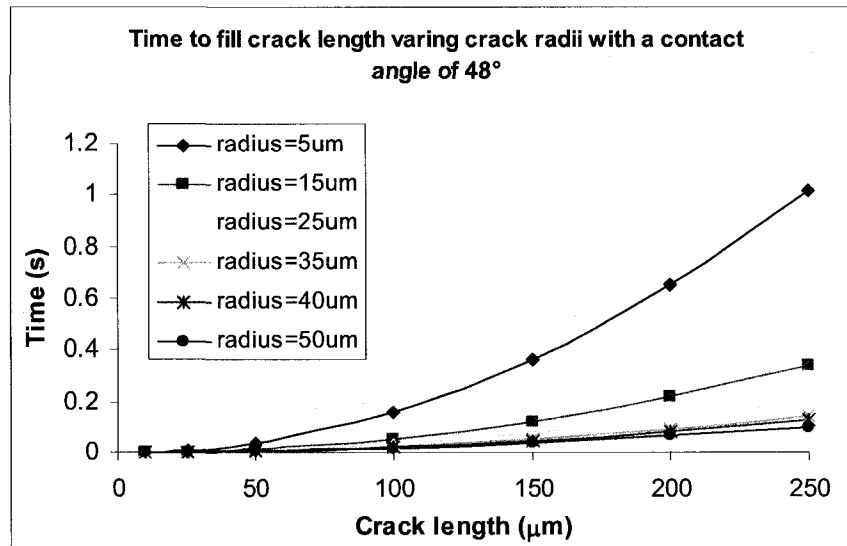


Figure 3-3: Time required to a fill crack with epoxy resin, varying crack lengths and crack radii with a contact angle of 48°

The surface tension and viscosity values in Figure 3-3 are taken as 47 dynes/cm²⁵ and 6.4 poise, respectively (EPON[®]815C, found experimentally using a cone and plate rheometer (model AR 2000) at 25°C). The contact angle for EPON 815C has been found to be approximately 48° on an epoxy surface made from West System Epoxy at room temperature (25°C), shown in Figure 3-4.

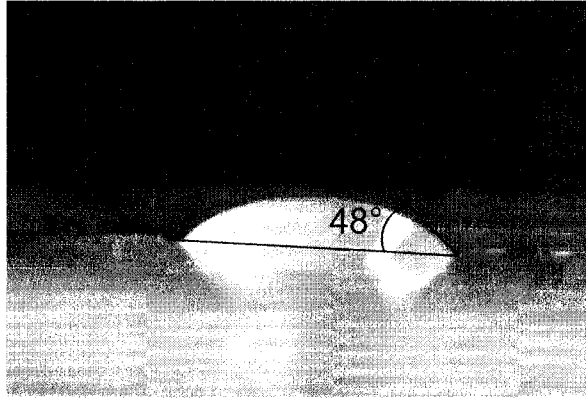


Figure 3-4: Contact angle of EPON 815C on an epoxy surface.

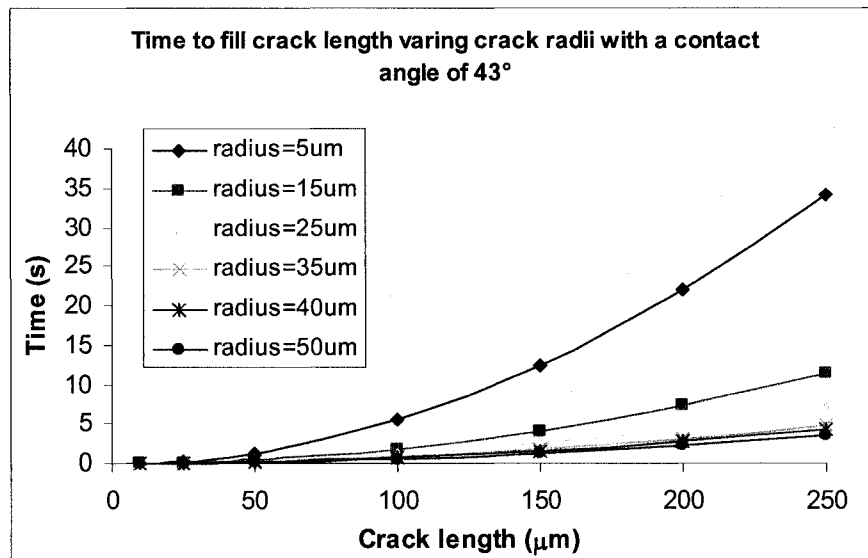


Figure 3-5: Time required to fill a crack with amine hardener, varying crack lengths and crack radii with a contact angle of 43°

In Figure 3-5, the surface tension value for the amine hardener is taken as 44 dynes/cm²⁵ and the viscosity is observed to be approximately 220.4 poise (IDEO adduct found experimentally using a cone and plate rheometer (model advanced Rheometer AR2000) at 25°C). The contact angle for the amine hardener has been found to be approximately 43° on an epoxy surface made from West System Epoxy at room temperature (25°C), shown in Figure 3-6.



Figure 3-6: Contact angle of amine hardener (IDEO adduct) on an epoxy surface

In the above figures (Figure 3-3 and Figure 3-5), one can see that the time required to fill a crack increases as the crack radius increases. The changes in crack radii have no significant impact or magnitude of change to the time required to fill a designated crack volume. The figures above also illustrate that the filling of the crack by capillary action is likely to occur within a matter of seconds. Additional figures regarding crack fill times can be found within Appendix C.

Diffusional Mixing

Once the crack has been filled, shown in Figure 3-7, it is necessary for the epoxy resin and hardener to mix thoroughly before curing can occur. Mixing in the crack can only be achieved by diffusion.

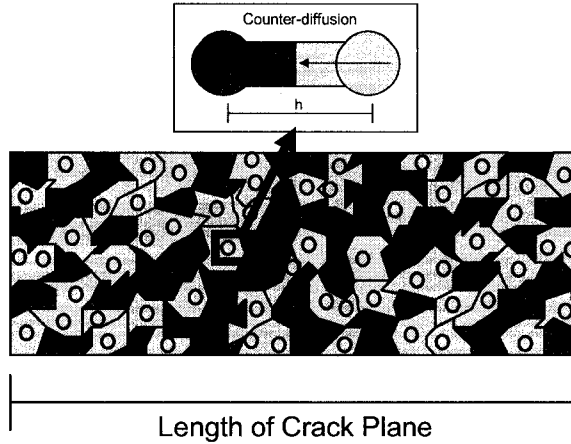


Figure 3-7: Diffusion model of resin and hardener between microcapsules. The colored regions indicate areas that the liquid core materials occupy the crack plane. The circles are the embedded microcapsules.

Diffusion occurs in two directions and this is known as counter-diffusion. This event is occurring throughout the crack plane simultaneously. The diffusion rate can be calculated by observing a set of capsules also shown in Figure 3-7. Although counter diffusion occurs, one can determine the counter-diffusion rate by using the component having the limiting diffusion coefficient.

Diffusional mixing times are approximated using Fick's law of diffusion^{25, 33}:

$$\frac{\partial C}{\partial t} = D \cdot \left(\frac{\partial^2 C}{\partial x^2} \right) \quad (3.1)$$

where t is time, x is distance, C is the concentration and D is the diffusion coefficient. By simply using the inverse relationship between viscosity and diffusion coefficient from the Stokes–Einstein relation, one can estimate the diffusion coefficients for the amine hardener and epoxy resin.

$$D = \frac{k_b \cdot T}{6\pi \cdot \eta \cdot r} \quad (3.2)$$

Assuming that the constants other than diffusion (d) and the viscosity (η) are constant, than one can estimate the diffusion coefficients with the following equation:

$$D_1 \approx \frac{D_2 \eta_2}{\eta_1} \quad (3.3)$$

One can use a simple fluid like water (viscosity of 0.0089 poise and diffusion coefficient of 10^{-4} (simple liquid)) along with the viscosities of the epoxy and amine components to estimate the diffusion coefficients. The viscosities for each of the components, discussed earlier in the chapter are 220.4 poise for the amine hardener (IDEO adduct) and 6.4 poise for the resin. Based on the calculations the diffusion coefficients are likely to be between 10^{-7} and 10^{-9} cm²/sec for the resin and hardener respectively. By applying the following boundary conditions to equation (3.1) calculations of mixing times can be achieved.

$$t = 0 \quad 0 < x < h \quad C = 0 \quad (3.4)$$

$$t > 0 \quad x = 0, x = h \quad C = C_\infty \quad (3.5)$$

The solution to equation (3.1) for finding concentration in a distance between microcapsules h, at time t, and distance x, is calculated below^{25,33}:

$$\frac{C}{C_\infty} = 1 - \frac{4}{\pi} \exp\left(-\frac{D \cdot \pi^2}{h^2} \cdot t\right) \cdot \sin\left(\frac{\pi \cdot x}{h}\right) \quad (3.6)$$

The distance between microcapsules, h, is taken to be 100 μ m. Figure 3-7 shows the concentration profile of a 100 μ m length (distance between capsules) using 10^{-9} cm²/sec for the diffusion coefficient and 0.95 g/cm³ (DETA) for the concentration of the hardener²⁵.

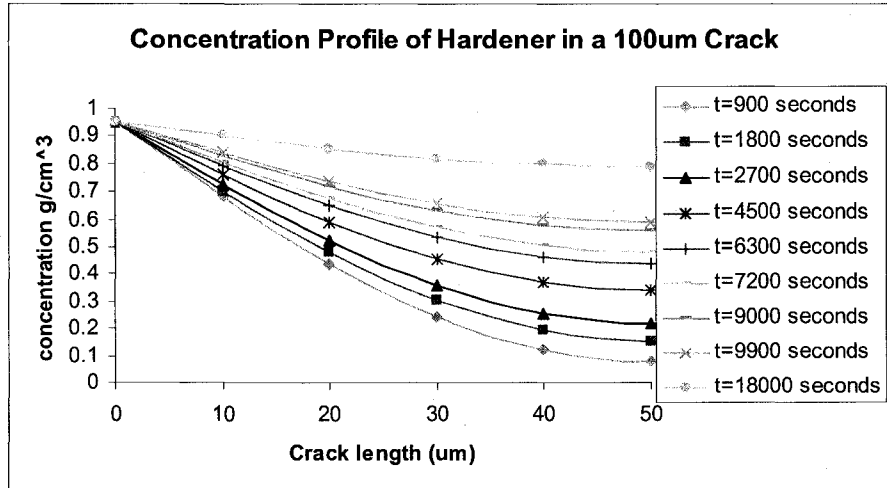


Figure 3-7: Concentration profile of hardener in a 100µm length.

This model is only used to achieve an order of magnitude of time needed to fully mix the self-healing components. The following figure shows the percentage of mixing in the crack defined by comparing the concentration at distance h , to the initial concentration at $h=0$. Assuming equal volume ratios, Figure 3-8 is produced below,

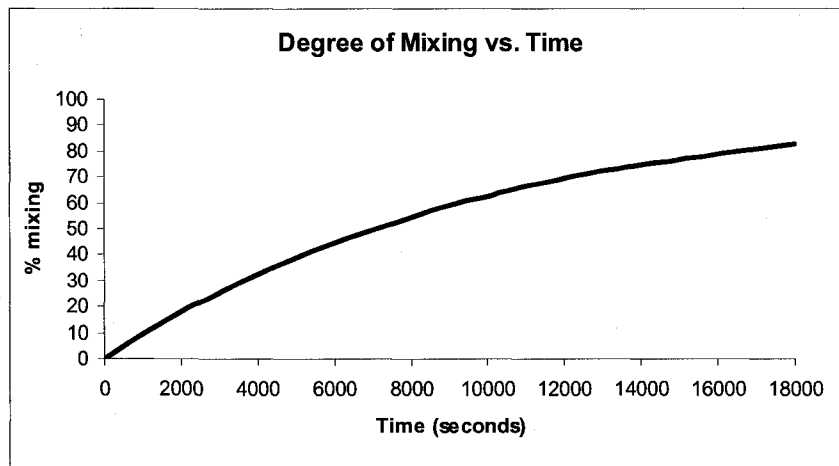


Figure 3-8: Degree of mixing in a crack vs. time.

According to Figure 3-8, the diffusional mixing requires a time of about thirty 5 hours to reach 80% mixing. Now in order to determine if the system is feasible one must estimate the kinetics of the epoxy curing reaction.

Epoxy Curing Kinetics

The epoxy cure reaction typically involves an epoxy resin and a diamine. Both primary and secondary amines can be used where the primary amines are more reactive than the secondary amine. A single nitrogen-hydrogen bond is required to open the epoxide ring and polymerize, thus making primary amine difunctional and secondary amines monofunctional³⁴. The curing reaction leads to a crosslinked three-dimensional network that is shown in Figure 3-9.

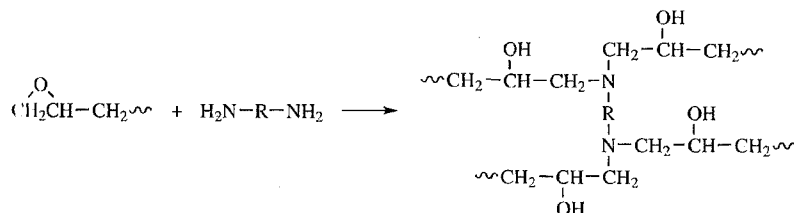


Figure 3-9: Epoxy reaction sequence³⁴.

Epoxy curing times, at room temperature (25°C), are usually of the magnitude of days to fully cure, but the reacting mixture becomes solid within hours. Typical commercial amine based epoxy gel times are within 40-50 minutes (at 25°C)²⁵. Gel times are windows of time required for the reacting material to become a solid or semisolid³². Before the gel time, the viscosity of the epoxy mixture increases indicating that the diffusion rates will decrease as time passes. It is important to mix the components thoroughly before the gel time is reached in order to have a feasible self healing system.

The time needed to fill the crack is of the order of seconds and the time for adequate mixing and in the order of hours. The gel time is in the order of minutes. Though the gel time and diffusion times are far from one another, there is concern that the diffusion of material within the crack will not reach 80% mixing within 40-50 minutes of the curing time of typical epoxies. However, the amine reaction time for the amine adduct, used in this work with EPON 815C has proven to be significantly slower, this will be discussed later in the thesis with a 70% extent of reaction after 12 hours. Therefore this result makes the system a feasible alternative to White's DCPD⁵ and Grubb's catalyst system.

Encapsulation of Resin Capsules

Encapsulation of epoxy resin has been demonstrated using two different routes. The first approach models a 3M patent for a water-based mechanical fastener³⁵, where the encapsulate, EPON® 815C (from Miller-Stephenson) resin is mixed with an aqueous solution of amine hardener. The encapsulation process involves making a pre-polymer known as a urea-formaldehyde-melamine concentrate to make the polymer shell. The second approach uses the same urea-formaldehyde encapsulation process demonstrated in previous work in the encapsulation of DCPD (from Alfa Aesar), which was described in chapter two of this thesis³⁰.

Encapsulation of Epoxy Resin Using the Concentrate Route

The concentrate route reported in the June 30th 2005 ONR Annual Report³⁰ provides the procedure and recipe used to encapsulate the epoxy resin. The shell material that results from using the concentrate route consists of urea, formaldehyde (both from Alfa Aesar), and melamine (UFM) (obtained from Alfa Aesar). The melamine supposedly helps with branching of the polymer therefore increasing crosslinking density within the polymer shell, resulting in a hard and brittle shell material. Prior to encapsulation a pre-polymer concentrate needs to be made.

The concentrate is made as follows: In a 250ml reactor, add 90g of formaldehyde (37% aqueous solution), followed by 23.6g urea, 10.37g melamine and 0.8g triethanolamine (obtained from Alfa Aesar). Triethanolamine is added because it acts as a buffer or control the pH of the solution used to form the UF shell. The solution is heated to 70°C for two hours and then allowed to cool to room temperature and then is diluted

by adding 200ml of de-ionized water. It is important to note that this procedure can be easily scaled up to produce the desired amount of concentrate for encapsulation.

For the encapsulation process, the set up starts with the same apparatus as with the DCPD encapsulation shown in Figure 2-8. Addition of 615g of pre-polymer concentrate into a one liter jacketed reactor is followed by 6.15 grams of sodium sulfate (used as a catalyst for the formation of the UF polymer), and 141.3 g of a 2.5wt% poly(ethylene-maleic-anhydride) (PEMA)(from Polysciences Inc.) solution. The pH of the system is adjusted to 7 with use of hydrochloric acid and/or sodium hydroxide. 200g of EPON[®] 815C is added to the reactor and is emulsified for 30 minutes at 500rpm using a Lightnin TS2010 mixer with a six-blade (5cm diameter) paddle impeller attachment. The pH is then adjusted again to 2.5 by slowly adding hydrochloric acid to the reactor. Emulsify the contents for an additional hour and then begin heating the reactor contents to 60°C. After 30 minutes, adjust the pH to 1.9 and continue heating for an additional 3.5 hours.

The dispersion is allowed to cool to room temperature and is placed under vacuum filtration to separate the capsules from the aqueous solution. During the vacuum filtration process the encapsulated material is separated from the microparticles (shown in Figure 2.7). The microparticles pass through the filter paper with the aqueous solution while the larger microcapsules remain on the filter paper. The capsules are then washed with acetone during the filtration process to remove excess surfactant and unencapsulated material. The washed capsules are air dried overnight (ca. 16 hours) in a fume hood at room temperature.

A number of experiments have been performed using the concentrate route but sizes measured by light microscopy and light scattering yield capsules as large as 300 μ m. Various efforts in changing the surfactant and/or agitation did not yield any decrease in capsule size. The microcapsules have a tendency to agglomerate and adhere to the reactor wall, reducing the overall yield. Another route that can be used is the recipe and procedure used for encapsulating DCPD. This procedure has proven to be very successful, and will be used as another means to encapsulate the EPON[®] 815C.

Encapsulation of Epoxy Resin Using the Urea Formaldehyde

Encapsulation of the epoxy resin without the use of the concentrate has been performed in parallel with the UFM concentrate route. The procedure and recipe that has been used in the present work follows that of the DCPD encapsulation process. In a one liter jacketed reactor, approximately 384 grams of deionized water and 133 grams of 2.5wt% poly(ethylene-maleic anhydride) (EMA) aqueous solution are mixed, followed by 149g of 2.0wt% polyvinyl alcohol (PVOH)(from Sigma-Aldrich) aqueous solution, 13.6 grams of urea, 1.3 grams ammonium chloride, and 1.3grams of resorcinol. To the solution, approximately 160 grams of EPON[®] 815C resin is added and dispersed as droplets. The solution is emulsified using a Lightnin TS2010 mixer, with a 5cm diameter, six-blade paddle impeller attachment at a rate of 500 rpm for one hour. The pH of the dispersion is adjusted to 3.5 using sodium hydroxide and/or hydrochloric acid as required. The reactor contents are heated to 55°C; once the reactor reaches temperature, 33 grams of 37wt% solution formaldehyde is added. The dispersion is allowed to react at 55°C for four hours.

The dispersion is allowed to cool to room temperature before it is placed under vacuum filtration to separate the capsules from the aqueous solution. The capsules are washed and dried in the same fashion as the microcapsules produced by the concentrate route. The dried capsules can be seen in Figure 3-10.

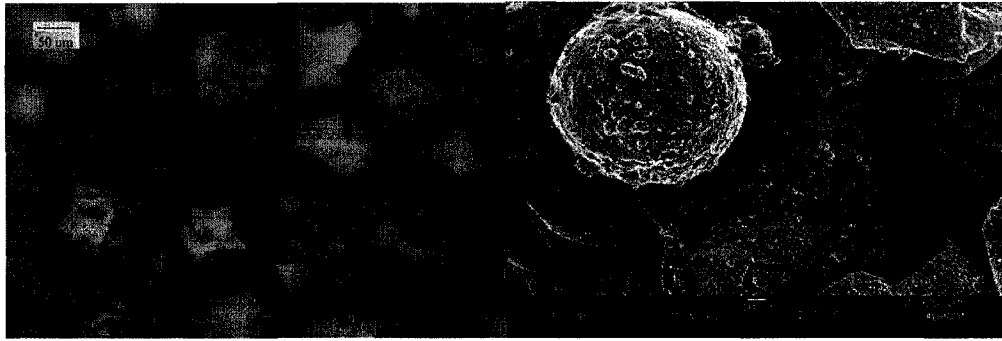


Figure 3-10: Light microscope (left) and SEM (right) photos of Epon[®] 815C Resin capsules using UF process (YD3-56).

The capsules in Figure 3-10 have very thin shell walls that are hard enough to withstand forces required to mix the capsules into epoxy but are brittle enough to rupture by a propagating microcrack. Sizes for the microcapsules are within the 100-150 μ m range. The resin capsules have a high payload up to 83% determined by extraction of the core material. The process starts by weighing the capsule, extracting the core material with a solvent and allowing the shell material to dry. By comparing the starting and end material, one can determine the payload. The microcapsules are recovered to a free-flowing powder that can be easily dispersed into an epoxy coating.

Amine Adduct

Diamines such as diethylenetriamine (DETA), are commonly used as hardening agents for epoxy systems. Other compounds can be used to cure epoxy resins such as polythiols and phenolic prepolymers, but are not as efficient, requiring accelerants in order to cure³⁴. Other compounds such as anhydrides can be used to cure epoxies with low epoxide group concentrations³⁴. Due to the great reactivity and crosslinking, amines are generally used as the curing agent for self-healing.

Encapsulation of amines is a much more difficult task than encapsulating the epoxy resin. Unlike the epoxy resins, amines tend to be soluble in water, but they are also soluble in organic solvents. The amine being soluble in both aqueous and organic phases limits the number of possible processes that can be used to encapsulate it. A majority of encapsulation processes require the core material to be either completely hydrophobic or completely hydrophilic, in order to make droplets in aqueous or organic media respectively. In the current work, modifications of simple amines to amine adducts have been made to produce hydrophobic amines that allow the production of droplets during aqueous based emulsification.

Desired Properties of the Amine Adduct

There are numerous desired properties for the amine adduct in addition to hydrophobicity. The viscosities of the resin and amine adduct need to reasonably match one another in order to allow for the similar hydrodynamic flow and diffusion rates to allow for adequate mixing within the crack plane. The reactivity of the amine adduct needs to be slow enough to allow for flow and adequate mixing, otherwise a barrier has

the potential to form at the resin and amine adduct interface. The ability to sufficiently heal a crack by using a 1:1 (resin capsule: amine adduct capsule) ratio is ideal due to the probability of cracking an off ratio number of capsules being unfavorable. When off ratio amounts are introduced into the crack plane the resultant polymer may not be properly cured, but it will be favorable for the capsule contents to have some degree of curing at off ratio amounts. Crystallization of the adduct would be deleterious and prevent capillary flow out of a fractured microcapsule. Producing an adduct that doesn't crystallize has been a priority and a challenge in this research project

Amine Adduct Synthesis

Adducts can be made by adding linear epoxides to various diamines resulting in more hydrophobic amines. The alkyl group of the epoxide makes the amine substantially more hydrophobic than the starting amines. The epoxide will react with the primary amines making them secondary amines, while leaving adequate amounts N-H bonds for use in self-healing. There is a possibility that the secondary amine can react with the epoxide turning it into a tertiary amine. With primary amines being more reactive than secondary amines, a small percentage of tertiary amines would be only present if such a reaction occurs.

The process used to make these adducts required the use of a 250ml jacketed reactor, water bath, and a stir plate. One mole of a diamine such as DETA (from Sigma Aldrich) and two moles of a mono-functionalized epoxide, such as 1,2-epoxyhexane (from Alfa Aesar), were mixed in a reactor, heated to 65°C and allowed to react over night (ca. 18 hours) resulting in the structure seen in Figure 3-11. This method produces a

much more viscous material compared to the viscosity of each component prior to reaction.

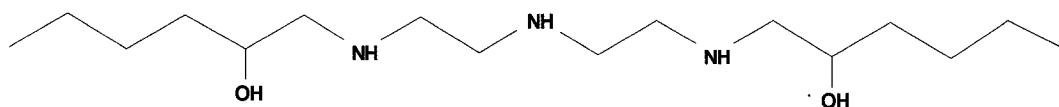


Figure 3-11: one mole DETA plus two moles of 1, 2-epoxyhexane

Numerous types of epoxides for adduct synthesis were used, varying the alkyl chain length from six carbons (1,2-epoxyhexane) to twelve carbons (1,2-epoxydodecane)(all obtained from Alfa Aesar). The resulting compounds are indeed more hydrophobic than the starting amines. The extent of the adducts' hydrophobic nature increases as the length of the alkyl chain on the epoxide increases. Unfortunately, it has been found by experimentation that anything beyond eight carbons (1,2-epoxyoctane) typically results in solidification of the adduct in the reactor or after the adduct has cooled down outside of the reactor. For the adduct shown in Figure 3-11, the adduct will slowly crystallize at room temperature; this is a major problem for use in self-healing. However by, changing the diamine into a more bulky structure (i.e phenol groups or cyclic groups), one has a chance of removing the crystallinity. Figure 3-12, shows 4, 4'-diaminodicyclohexylmethane plus two moles of 1,2-epoxyhexane as the components for the adduct.

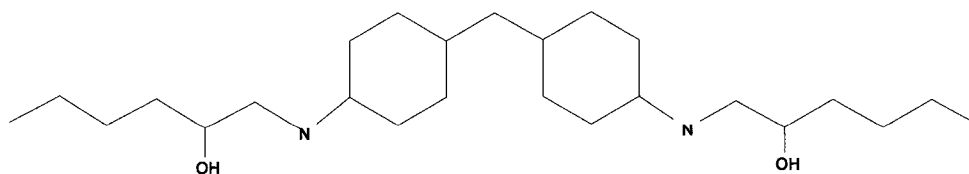


Figure 3-12: One mole 4, 4'-diaminodicyclohexylmethane plus two moles of 1,2-epoxyhexane

Unfortunately this adduct also crystallized at room temperature. A series of other adducts have been produced and are described in Appendix D.

Addition of Inert Component

With various adducts found in Appendix D having issues with crystallinity, one must find a means to avoid this phenomena. One way to remove the crystallinity might be to introduce an inert or essentially un-reactive component into the system. The inert component concept theoretically shows a lot of potential for solving the problems of crystallization. The inert component can act as a plasticizer and reduce the melting point suitable for application. Mineral Oil (obtained from Brooks Pharmacy) was used initially due to its solubility in the components, its insolubility in water, and it is easy to obtain. Various compositions of mineral oil and amine adduct have been made to observe its effects on crystallization. Unfortunately it was found that the mineral oil only hinders the crystallization for a couple of days. When resin, adduct, and mineral oil are mixed together and allowed to cure, results show that the mineral oil phase separated from the epoxy matrix.

The idea of using dibutylphthalate (from Alfa Aesar), a common industrial plasticizer, was considered as another option. Crystallization tests were performed with various compositions of DETA/1,2-Epoxyoctane adduct and dibutylphthalate and were observed over time. The crystallization was retarded up to six days before significant signs of crystallization occurred. Dibutylphthalate and the amine adduct undergo phase separation upon reaction, and did not completely stop crystallization. Though unsuccessful in removing the crystallinity there are some characteristics that inert component can improve. An advantage was to use the dibutylphthalate or mineral oil to

dilute and change the viscosity of the adduct to closely match that of the resin to acquire adequate mixing. Another advantage was that the inert component can also be used as a filler to closely match the required ratios of capsules (i.e 1:1) in an epoxy matrix for use in self-healing.

Addition of a Reactive Component

Due to the phase separation phenomenon that occurred between the inert component and the DETA/Epoxyoctane adduct, one can use a reactive component similar to the amine adduct to stop or hinder the crystallization process. Two types of adducts designed to break the crystallinity seen in the figures below, (Figure 3-13 and Figure 3-14) are to be mixed with the DETA/Epoxyoctane adduct.

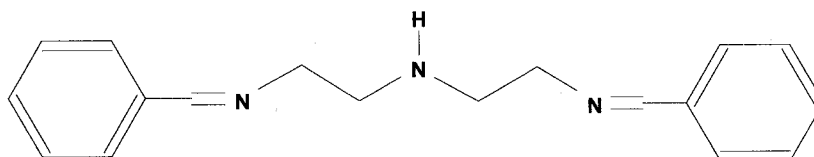


Figure 3-13: one mole DETA plus two moles Benzaldehyde

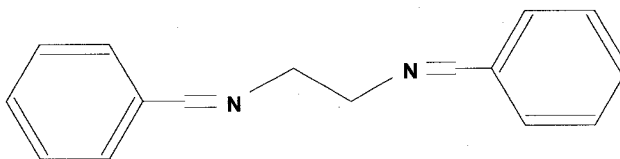


Figure 3-14: one mole Ethylene Diamine plus two moles of Benzaldehyde

The adduct in Figure 3-13, when compared to the one in Figure 3-14, has a better chance of success because the adducts have a similar backbone molecule (DETA). Another reason is that there is a single reactive group (N-H bond) left on the backbone, having the single reactive group might allow reaction with the resin and prevent phase

separation from the epoxy matrix during curing. An adduct blend of DETA/Epoxyoctane (Figure 3-11) adduct and DETA/Benzaldehyde (Figure 3-13) adduct did not crystallize for weeks on its own but addition of a crystalline seed allowed it to crystallize. These findings did not yield great results, but the finding of a new amine, Isophorone diamine has the potential to stop crystallinity. Isophorone diamine and its adduct has become a large focus in the research project.

Analysis of Various Adducts

A characteristic that has been heavily viewed is the octanol-water partition coefficient. The partition coefficient (P) is a measure of the differential solubility of a particular compound in two immiscible solvents, such as octanol and water. This can be defined by the following equation:

$$\frac{[C]_{Octanol}}{[C]_{Water}} = P \quad (3.1)$$

where [C], is the concentration of the soluble material in octanol or in water. The partition coefficient is typically expressed in log form (i.e. log P). Partition coefficients were used to determine how water soluble or oil soluble a specific material (i.e amine adduct) is compared to other materials. In order to obtain partition coefficient, values were either found in the Polymer Handbook³⁶ or using prediction software³⁷. Various adducts have been characterized by their respective log P's to determine which adduct is best to use for microencapsulating. Appendix D has all the adducts listed with their respective log P values. Useful values of log P are 2.0 or higher.

As noted above, crystallization has been a major issue when producing various amine adducts. Many solidify or crystallize during synthesis while others crystallize

slowly at room temperature. Crystallization begins by having various nucleation sites of small crystalline domains, formed thermodynamically or kinetically. Nuclei become sites for crystal growth leading to a fully crystalline material. The adducts that crystallize do so because of the linear molecular structure. The degree of crystallization is dependent on how favorable packing is for a particular structure. Linear molecules are best at crystallization due to having no restrictions to where each segment of a molecule needs to line up to have close packing. When adding long alkyl chains to a diamine, it often tends to allow for the non-crystalline diamine to form a crystalline adduct over time. Addition of large rigid constituents such as phenyl groups and cyclic groups make it difficult to crystallize. One can stop crystallinity by having a mixture of different isomers of the adduct, interrupting the packing of the molecules in an orderly fashion. The crystallization times do vary and are often long, therefore a small sample of already crystalline adduct can be added to the non-crystalline sample to act as a seed to accelerate the crystallization process. The seed is an already thermodynamically stable nucleus to which crystal growth can occur³⁴.

Reactivity of the adducts also measured to see if on and off ratio mixtures allow for adequate curing to be used in self-healing. Various molar ratios of the adduct have been mixed with DGEBA and allowed to cure in an oven at 60°C. The cured samples were observed to see if they were highly crosslinked (hard/glassy), crosslinked (soft/elastic) or non-crosslinked(soft/flowing) material.

Reaction kinetics of the amine adduct and resin are observed to determine if the curing rate can interfere with the time required to diffuse and mix properly. The time required for adequate mixing in the crack plane for self-healing is on the order of minutes

(ca. ten minutes), therefore the gel time between the amine adduct and resin must be much longer than the diffusion time. During observations of the curing of these adducts it was noted that the actual gel times of the adducts were longer than that of the starting amine with the same resin.

Isophorone Diamine Adduct

The isophorone diamine (from Sigma Aldrich) was found to have potential for producing a hydrophobic adduct. Isophorone diamine, as shown below Figure 3-15 has a bulkier structure when compared to DETA and thus was hypothesized to have less tendency to crystallize when formed into an adduct. The amine itself has a log P value of 0.96 and one less amine functional group, when compared to DETA³⁸.

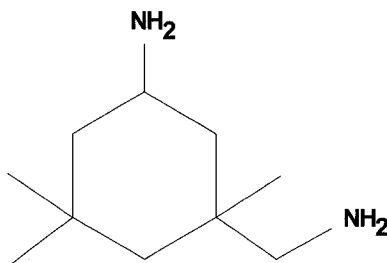


Figure 3-15: Structure of Isophorone Diamine

With further investigation, the isophorone diamine was able to crosslink well with epoxy resin (DGEBA) at closer weight ratios. Weight ratios of 2:1 through 6:1 were found to produce a glassy and hard mixture upon curing. Sufficient curing can take place over a wide range of ratios and can potentially satisfy the objective of employing equal number of epoxy capsules as hardener capsules in the epoxy matrix³⁸. This makes isophorone diamine a good candidate to produce an adduct from.

Isophorone Diamine/ Epoxyoctane (IDEO) Adduct Synthesis

As with most adducts, synthesis is performed simply as a batch reaction with the amine and epoxides. Particularly interesting in this study were, 1,2-epoxyhexane or 1,2-epoxyoctane. When mixing the Isophorone diamine and 1,2-epoxyhexane together, it was discovered that they were not miscible. Therefore a common solvent was used to synthesize the adduct. Initially acetone was used, but attempts to remove the acetone via rotary evaporator have proved unsuccessful. Performing a simple mass balance shows a large amount of acetone was still present in the mixture. FTIR has also shown in Figure 3-16 that the acetone has reacted with the components making a different substance we have hoped to have.

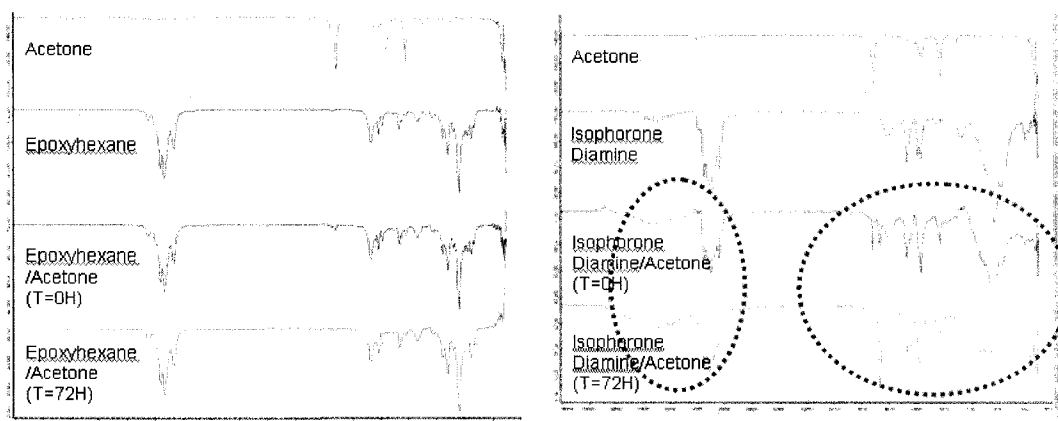


Figure 3-16: FTIR Spectra of Acetone Mixed with 1,2-Epoxyhexane (left) and Isophorone Diamine (right)³⁸.

In Figure 3-16, the spectra on the left do not show any interaction of the acetone with 1,2-Epoxyhexane, however the spectra on the right clearly shows interaction between the acetone and Isophorone diamine thus explaining the difficulty of removing the acetone by rotary evaporation. A suggestion by naval research personnel Dr. Arthur Webb, stated that acetone and isophorone diamine can produce a ketamine. Primary

amines and secondary amines can be used in a reductive amination reaction yielding secondary and tertiary amines respectively³⁹. Tetrahydrofuran (THF) and toluene were also tested as potential solvents, both of which were also found not to be suitable. Based on FTIR results we had some concerns about possible reaction between the THF and the amine therefore abandoned the use of the solvent. Toluene has not shown any signs of chemical interaction but was found not be able to solvate both components. Ethanol however was found to be a suitable solvent as shown in Figure 3-17, as there were no reactive interactions between the components observed by FTIR. Ethanol is easily removed by using a rotary evaporator at full vacuum (ca. 5 torr).

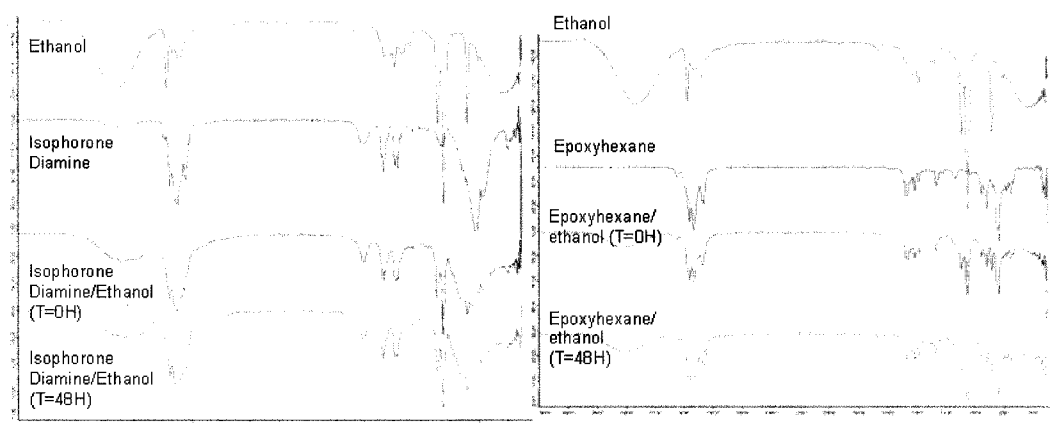


Figure 3-17: FTIR Spectra of Ethanol Mixed with Isophorone Diamine (left) and 1,2-Epoxyhexane (right)³⁸.

After finding a suitable solvent, adduct synthesis was performed in the following fashion: Adduct synthesis was carried out in a 250ml jacketed reactor fitted with a condenser and stir plate. First 30.06g of isophorone diamine (obtained from Sigma Aldrich) was mixed with 9.20 g of ethanol in a beaker. In a second beaker 45.05 g of 1,2-epoxyoctane (obtained from Alfa Aesar) along with 9.20g of ethanol were also mixed. The contents of both beakers were slowly placed into the reactor and are allowed to mix and react at 65°C overnight (ca. 18 hours). The contents were then cooled and removed

from the reactor. The chemical steps to produce the amine adduct can be seen in Figure 3-18 below.

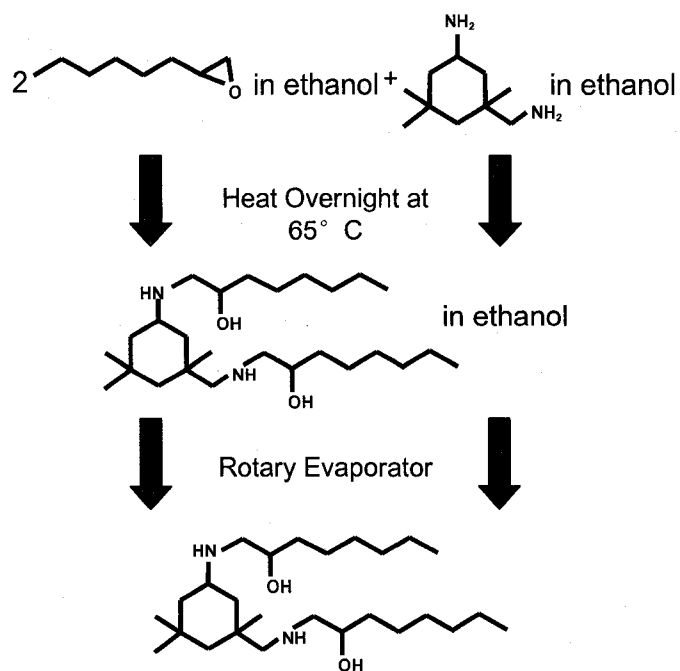


Figure 3-18: Diagram of Isophoronediamine and 1,2-epoxyoctane.

Approximately half of the reactor contents (ca.46.7g) were added to a 250ml round bottom flask and placed into a rotary evaporator (Model Yamato RE 400, and Yamato BM200 Water bath) under full vacuum (ca. 5 torr) at 70°C to remove the ethanol present and unreacted epoxides. The solvent evaporation process leaves a transparent viscous liquid which can be used for encapsulation.

IDEO Adduct Characterization

A series of different characterizations for the IDEO adduct was performed in order to understand the properties and formulate encapsulation experiments accordingly. The resulting adduct had an increased viscosity relative to isophorone diamine and 1, 2-epoxyoctane alone. The viscosity of the adduct surpasses that of common epoxy resins. The experimental viscosity, measured using cone and plate rheometer at 25°C (model Advanced Rheometer AR2000), of the adduct was 220.4 poise compared to that of DGEBA (DER332) at 42.7 poise and EPON[®] 815C at 6.4 poise. The viscosity differences between the IDEO adduct and the EPON[®] 815C resin is very significant.

The solubility of IDEO adduct in water was low enough to allow droplet formation in aqueous media. Using prediction software³⁷, the log P of a di-substituted IDEO adduct is 3.11 which predicted that the amine adduct is approximately 1,200 times more likely to be in an organic solvent than a water phase. The log P of a mono-substituted IDEO adducts ranges from 2.4-2.62, depending on which primary amine the epoxide reacted to. The software also predicted the amine adduct water solubility to be approximately 0.6 grams per liter and the pKa values to be around 8.72 and 10.75.

When various ratios of adduct and DGEBA were mixed and allowed to cure at 60°C for 24 hours, a 1:1 mole ratio (resin: adduct) was found to produce a highly crosslinked sample that fractured upon cooling. The 2:1 ratio produced a pliable but crosslinked sample. The 3:1 ratio material become viscous, but was not crosslinked. There is some concern that these samples were cured at elevated temperatures (60°C), the self healing system will most likely only be in room temperature conditions, therefore determining the appropriate kinetic rates and actual hardness of the material at room

temperature (25°C) is important. A series of room temperature studies were performed using 3:1, 2:1, 1:1, 1:2, 1:3 molar ratios of DGEBA resin and amine adduct. The samples were made and then left over the weekend to cure (ca. 65 hours). The results showed that the optimum reactivity is achieved at 1:1 ratio, while still able to react at slightly off ratio as far as 2:1 and 1:2 molar ratios. By observation, all of them reacted, but only a few (2:1, 1:1, and 1:2 ratio) have seemed to have crosslinked due to their tough and glassy properties. The amine adduct/DGEBA curing reaction is much slower than that of commercial resins with gel times in the matter of hours. With the slower gel times, the time required to fill and diffuse the two self-healing components is very fast by comparison.

Crystallinity of the adduct was a major concern considering the tendency of the prior prepared adducts described earlier in the thesis. In order to probe this new adduct for its propensity to crystallize, several tests were performed. A small sample was stored at room temperature (25°C), a sample was placed into a freezer (0°F), a third was mixed with a seed crystal from a different crystallization prone adduct and left at room temperature (25°C), and a similar sample with a crystal seed was put in the freezer (0°F). From the first preparation of this adduct to the ones presently made, none of the samples showed any signs of crystallization. With the success of producing an adduct that met the desired adduct properties described earlier, and that is not prone to crystallization, the project moved again toward testing encapsulation of the new adduct.

Proton and carbon NMR analyses was chosen to determine the chemical structure of the adduct after synthesis. The starting material used to produce the adduct is a mixture of two moles of the epoxyoctane to one mole of isophorone diamine, therefore one would

expect the amine adduct to be mono substituted or di-substituted or a mixture of the two.

Figure 3-20 shows the possible configurations of the IDEO adduct.

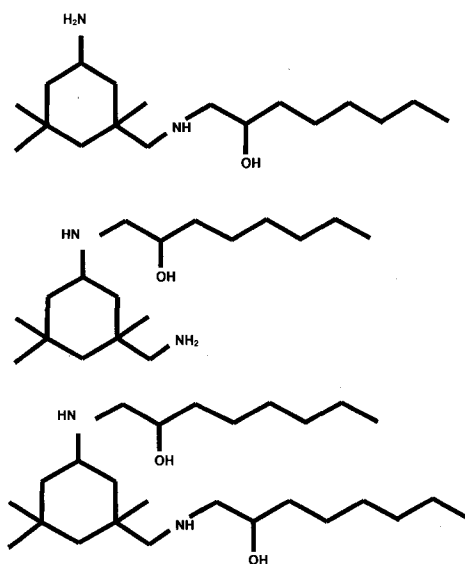


Figure 3-20: Various Configurations of the IDEO Adduct

NMR analysis was performed on the starting material and the final amine adduct.

Proton and Carbon NMR of 1,2-epoxyoctane is shown in Figure 3-21 and Figure 3-22 respectively.

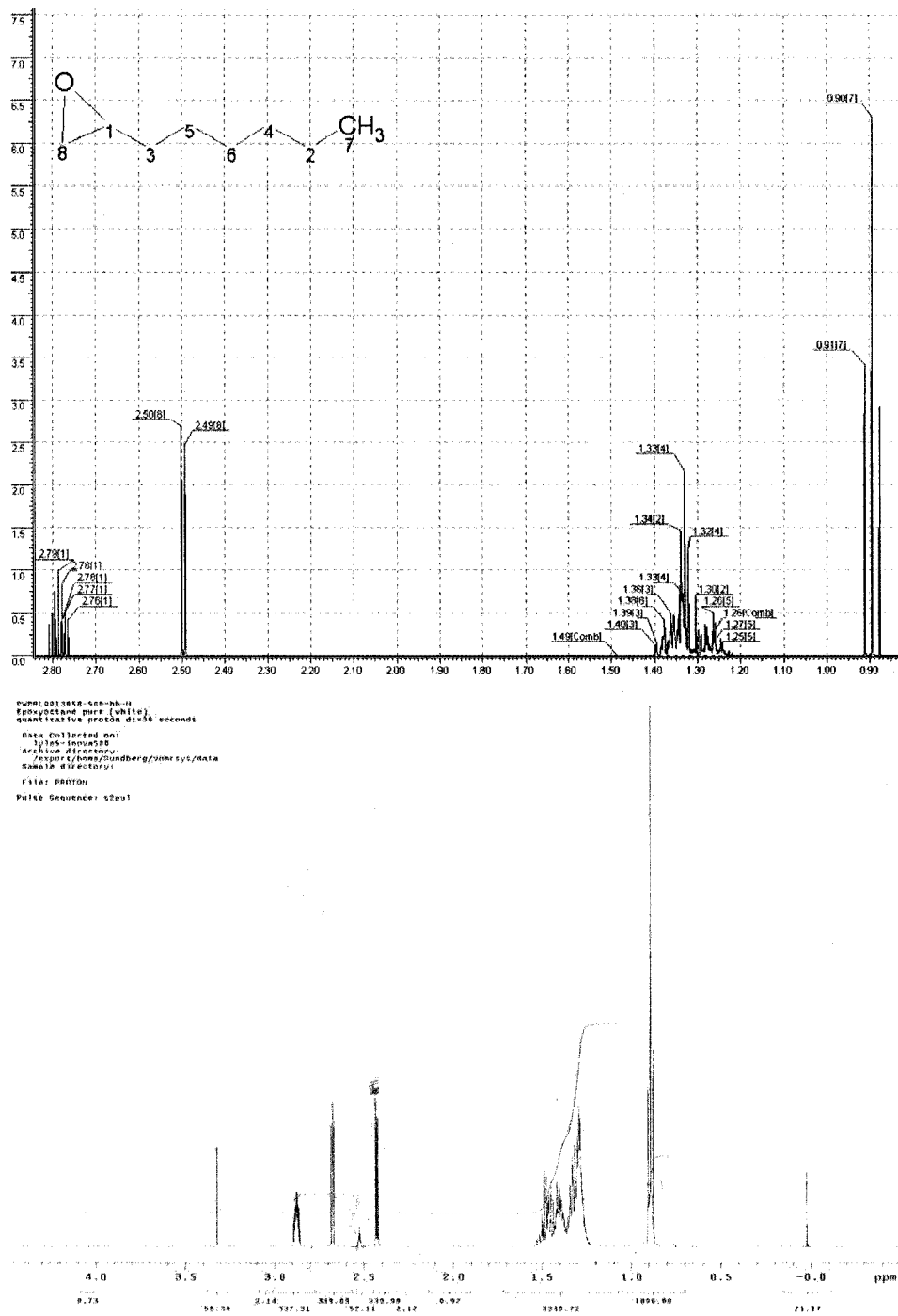


Figure 3-21: Proton NMR of 1,2-epoxyoctane. Prediction (Top), actual spectra (Bottom)

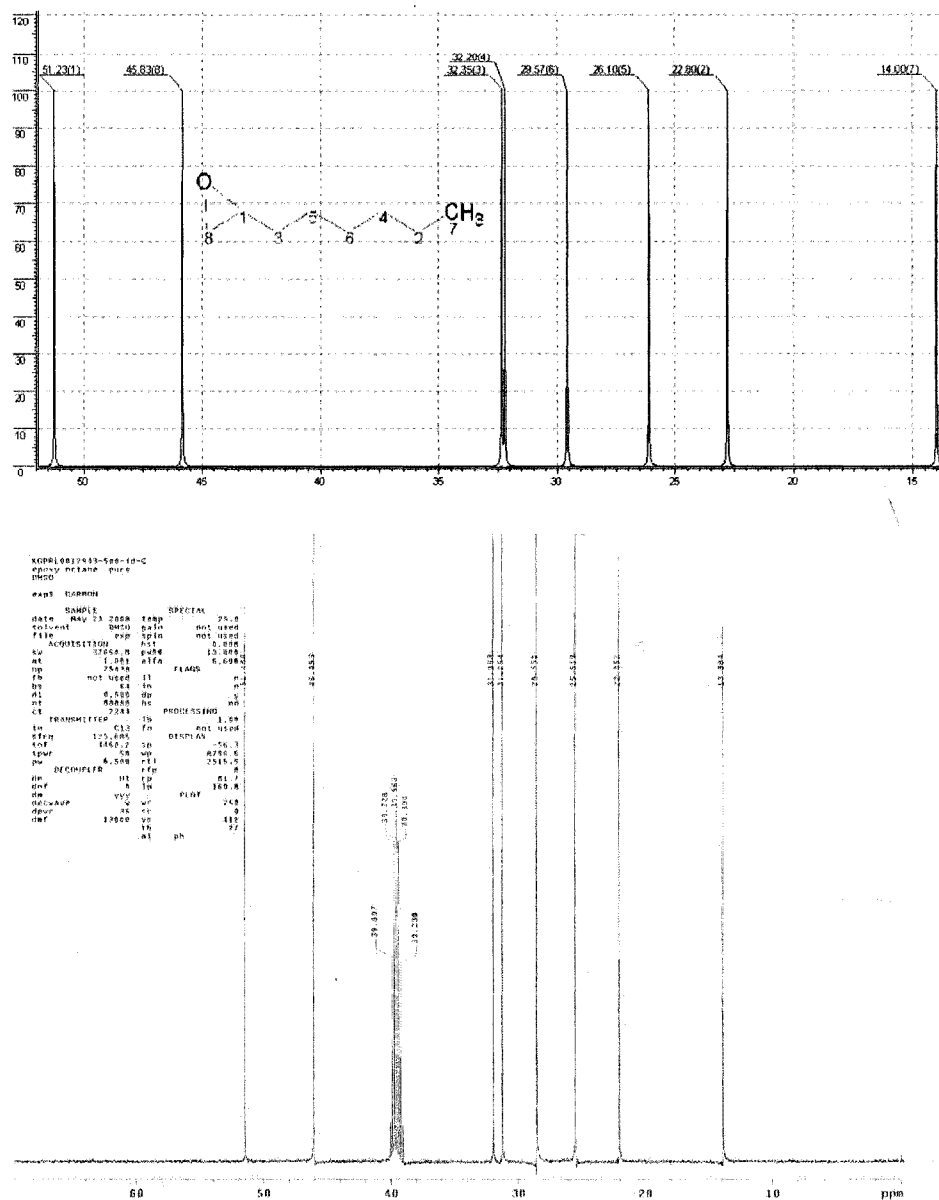
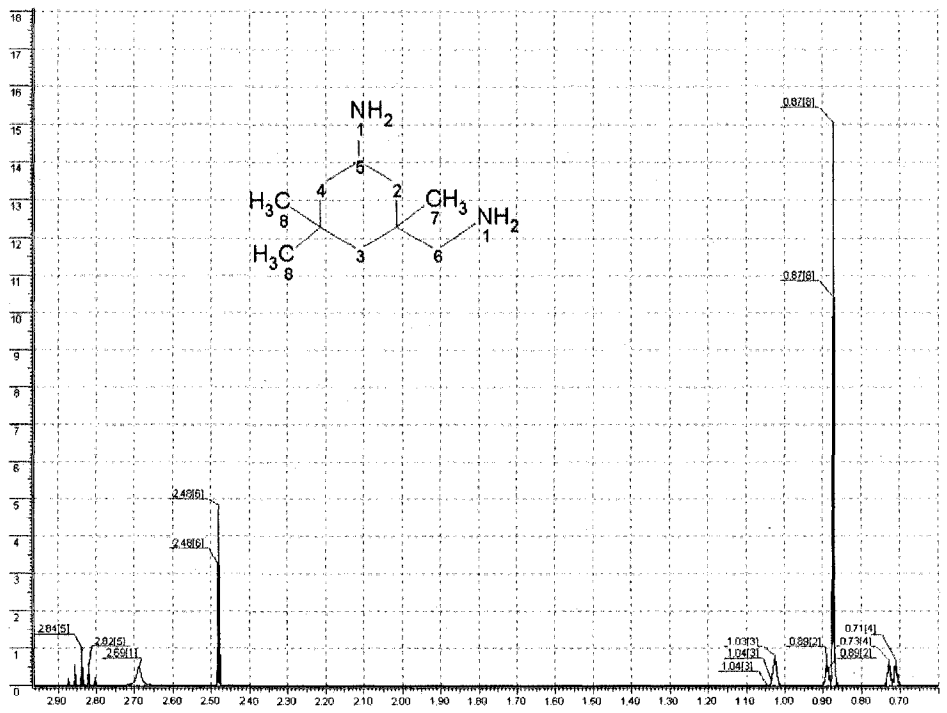


Figure 3-22: Carbon NMR of 1,2-epoxyoctane. Prediction (Top), actual spectra (Bottom)

As one can see in the above two figures, the prediction match the actual spectrum making it possible to identify the 1,2-epoxyoctane peaks in the amine adduct spectra. On the other hand, the spectra for the isophorone diamine are difficult to interpret. Proton and carbon NMR of isophorone diamine are shown in Figure 3-23 and Figure 3-24 respectively.



PUPR19813969-100-bb-H
 isophorone diamine adduct, new
 quantitative proton 43.10 seconds
 Data Collected on:
 spect-impva500
 Archive directory:
 /export/home/olunberg/ommsys/data
 Sample directory:
 file: p00109
 Pulse Sequence: szput

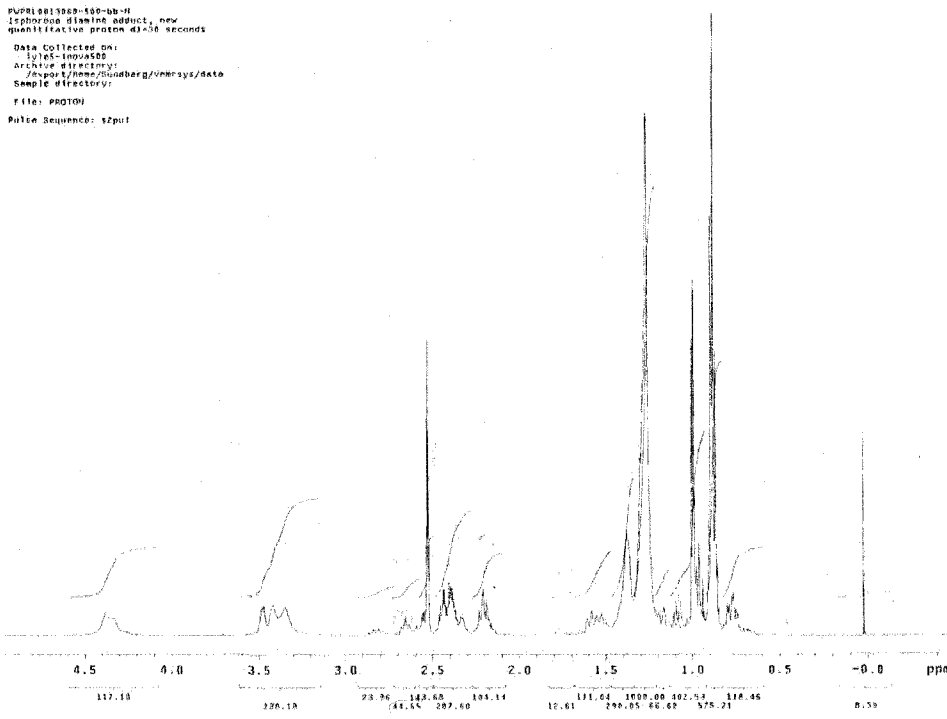


Figure 3-23: Proton NMR of Isophorone Diamine. Prediction (Top), actual spectra (Bottom)

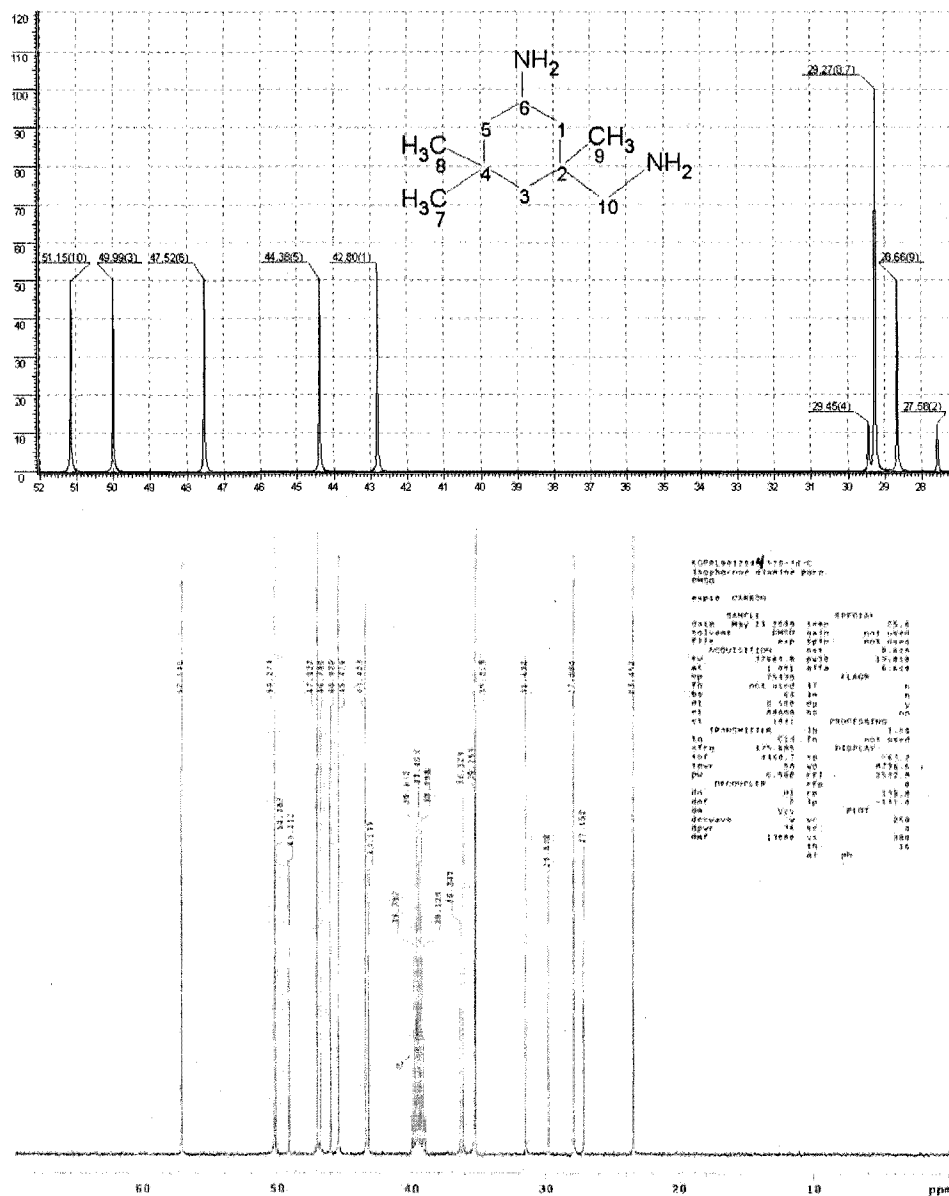


Figure 3-24: Carbon NMR of Isophorone Diamine. Prediction (Top), Actual Spectra (Bottom)

The spectra in Figure 3-23 and Figure 3-24 are more difficult to interpret compared to the 1,2-epoxyoctane spectra. The isophorone diamine was purchased as a mixture of cis and trans isomers, which results in a doubling of proton and carbon peaks in the NMR spectra. Unfortunately, the NMR prediction software^{46,47} does not recognize the difference between cis and trans, therefore making it difficult to interpret the peaks. This in itself is

a major problem in using this technique. Thus the amine adduct is likely produced in various configurations which would make the interpretation for the amine adduct much more difficult to do. NMR results have been inconclusive in determining the mole fraction of 1,2-epoxyoctane that have attached to the isophorone diamine. NMR spectra for the each component and IDEO amine adduct can be found in Appendix E.

The reaction kinetics between the IDEO adduct EPON 815C have been observed through DSC analysis. Equal weight ratios of the resin and adduct have been mixed together and placed into the DSC. The structure(s) of the amine adduct are still inconclusive but molecular weight was estimated to be 382g/mole based on an average of 1.5 moles of 1,2-epoxyoctane reacting with isophorone diamine. EPON 815C is a mixture of various resins and solvent(s) whose molecular weight is stated to be less than or equal to 700g/mole. Diglycidyl Ether of Bisphenol A (DGEBA) is a main component of the EPON which has a molecular weight of 340g/mole. Therefore it is safe to assume that a one to one weight ratio is sufficient.

DSC analysis was performed isothermally monitoring heat flow over time. Experiments monitoring kinetics were performed at 25°C (Figure 3-25) to obtain a conversion vs. time plot for this experiment. See Appendix F for the calculation and production of the conversion vs. time plot in Figure 3-25.

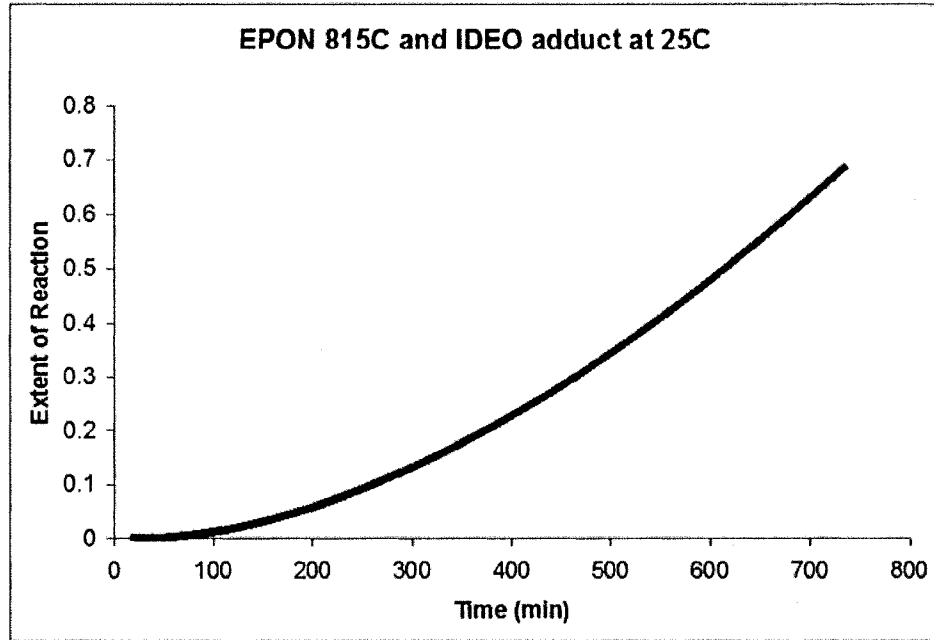


Figure 3-25: Extent of reaction vs. Time for EPON 815C/IDEO adduct curing at 25°C

It is evident from the two figures above that the EPON 815C/IDEO adduct epoxy curing time is substantially longer than the time required to for adequate diffusional mixing to occur (80% mixing after 5 hours as shown in Figure 3-8). At 5 hours the curing of the EPON 815C/IDEO adduct is approximately 15% (at 25°C) This slow curing time would allow sufficient time for the IDEO adduct and EPON resin to fill a microcrack crack and fully mix.

Encapsulation of Amines

After overcoming the challenge of being able to disperse the amine adduct in aqueous media, there has been a concern about the encapsulation process. Amines typically have pKa's between 8 and 10. Many aqueous encapsulation routes require lowering the pH such as for the urea-formaldehyde (UF) process used for DCPD and epoxy resin. With the pKa being so high there is a concern about water solubility when the pH of the system is brought below the pKa's. When the pH drops below the pKa the amine becomes ionized and more hydrophilic. Various encapsulation attempts have been performed using various techniques that do not require a drop in pH.

Interfacial Polymerization

Prior to the discovery of the isophorone diamine/epoxyoctane (IDEO) adduct, interfacial polymerization was a route used to produce amine capsules. Interfacial polymerization is known to work and it allows the use of pure amines²¹ (i.e. DETA). This technique requires a substance in the dispersion to partially react with the core material at the interface to form the polymer shell. The shell thickness is determined by the diffusive properties of the reactive components through the forming polymer shell, providing a constant shell thickness regardless of droplet size. Kondo's²¹ book shows that an aqueous solution of an amine can be encapsulated by introducing an amine (drop-wise) into a sebacoyl chloride (from Sigma Aldrich) and xylene solution. The reaction between sebacoyl chloride and a diamine amine makes a nylon shell. This particular method requires a small percentage of water to be mixed with the amine in order to make spherical capsules. The same idea can be applied to the use of amines and toluene

diisocyanate (TDI). Experiments were performed using 5% toluenediisocyanate (TDI)(from Sigma Aldrich) in a toluene solution with SPAN 83[®] as the surfactant. Droplets of amine are introduced to the solution and instantaneously encapsulated amines are made but often agglomerate and are fairly large in the millimeter size range.

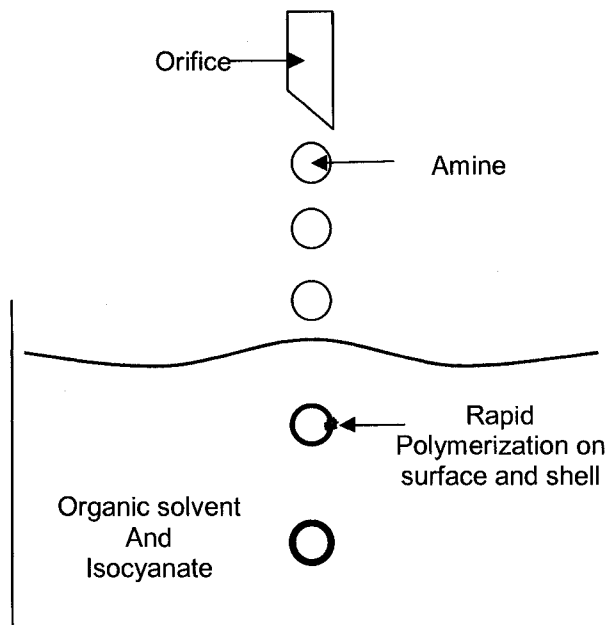


Figure 3-26: Drop-wise interfacial polymerization process.

Using the TDI and DETA chemistry, a new approach has been used to achieve smaller microcapsule size. Different sized orifices were used to achieve smaller droplet sizes. Homogenization was used to achieve a small and uniform size distribution of capsules. A homogenizer (IKE[®] ultra-turrax T-25) was used to homogenize the amine and 5%TDI solution before it reacts. Figure 3-27 is a diagram of the apparatus. The apparatus has an attachment consisting of a cell, where the high shear field is located, and ports to continuously flow of material across the shear field. The TDI and toluene

solutions are fed in one inlet and the diamine (DETA) was feed in another inlet. The two feed streams meet at the high shear field and react upon contact within the chamber.

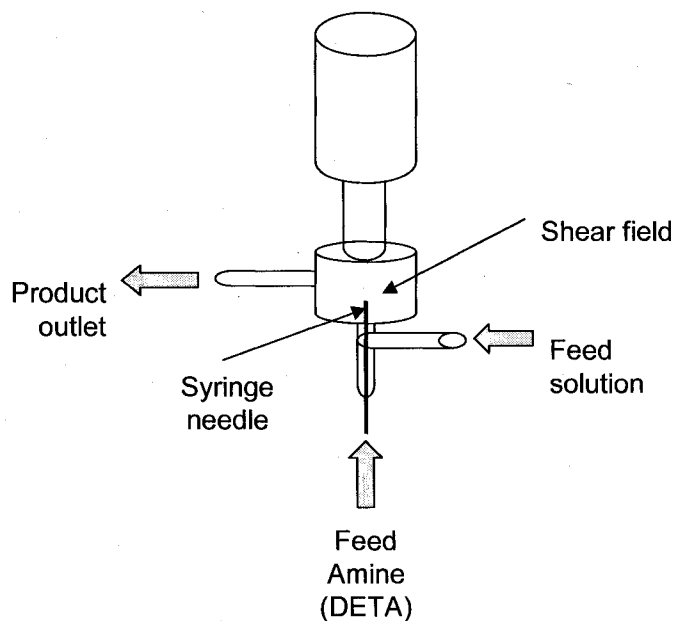


Figure 3-27: Experimental set-up of the ultra-turrax homogenizer

There was a problem with clogging of the chamber where the shear field is located. Another problem was that it is possible that the microcapsules were passed through the shear field multiple times before exiting the chamber. The capsules would break and a majority of the core material would react with the TDI, if passed through the shear field again.

Various attempts of interfacial polymerization have proven unsuccessful. Thus a lot of emphasis was placed on the newly discovered isophorone diamine adduct. The isophorone diamine adduct shows a lot of promise due to its reactivity and resistance to crystallinity. Encapsulating the amine adduct using a variety of different methods seemed to be the only option available.

Complex Coacervation

A proposed approach was to produce a polymer layer around the amine, regardless of its mechanical properties, in order to protect it from ionizing in the acidic environment of the UF process. A UF shell could then be applied as a second step atop the protective layer. Many different types of encapsulation processes have been explored in order to achieve this task.

Complex coacervation uses an aqueous solution of a positively charged colloid and negatively charged colloid. When these two are mixed, a phase separation results due to electrostatic interactions. Typically gelatin is used along with gum arabic or a polyphosphate as the components for coacervation. This process has been successfully performed by a previous student, Charles Beck. The recipe was based on his work⁴⁰ using a type A gelatin (obtained from Sigma Aldrich) and a CALGON[®] (polyphosphate) solution. The polyphosphate has a net negative charge while the gelatin has a net positive charge at low pH and negative charge at high pH. Type A gelatin is widely used for complex coacervation due to its isoelectric point which ranges from 7-9 depending on its preparation. Complex coacervation does require lowering the pH below the pKa's of the amine adduct, however it has been considered that the formation of the initial shell could form before a significant amount of the amine becomes ionized.

Complex Coacervation process is performed as followed. In a 250ml jacketed reactor, 5 grams of gelatin (type A) is mixed with 60ml of deionized water. The dispersion of gelatin is held at 50°C, which is above the gel point of gelatin. 20ml of the core material to be encapsulated is introduced to the dispersion. Soon thereafter 10ml of a polyphosphate solution, (made from mixing 5 g of CALGON[®] Conditioner (a

polyphosphate) in 100ml of water) is added to the system. An additional 60ml of water is charged to the system after the polyphosphate solution is allowed to mix. While maintaining the temperature at 50°C the pH is dropped slowly to a pH of 5 by drop-wise addition of acetic acid. Once at a pH of 5, the pH is reduced at a slower rate until the gelatin phase separates onto the droplets of the core material. Encapsulation occurs around a pH range of 4.2-4.6. The temperature is then dropped to 10°C to harden the gelatin and allow the capsules to either settle or float. Removal of the remaining continuous phase is required and is then replaced with chilled deionized water. 40ml of 37wt% formaldehyde is added soon after to crosslink the capsule walls. Crosslinking is needed due to the fact that the encapsulation process is completely reversible if the pH is ever brought back up, the gelatin will go right back into the continuous phase making it unstable without crosslinking. Crosslinking with formaldehyde takes 12 hours.

To prove capability with the process, a control experiment was performed by encapsulating toluene. The encapsulation of toluene was successful and found to be easy to reproduce. The resultant capsules were quite large, as seen in the figure below, but this was inconsequential as the adduct encapsulation would certainly have a different droplet size.

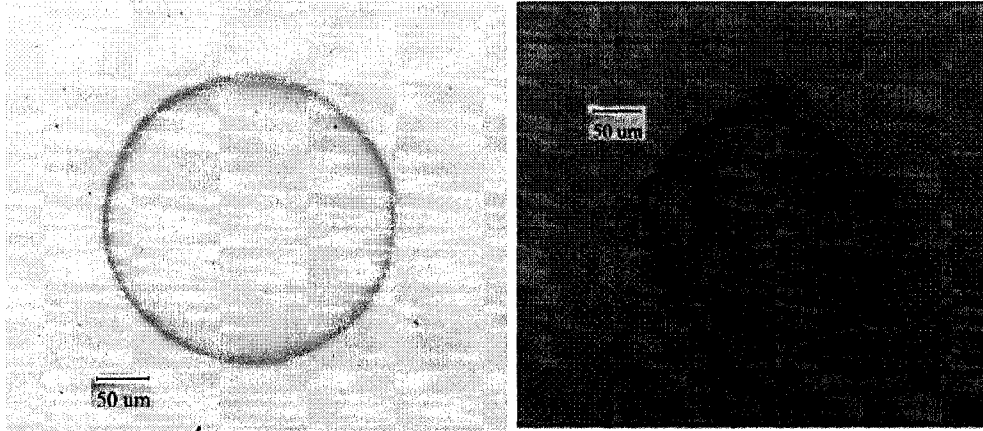


Figure 3-28: Complex Coacervation of Toluene as a Model System (JN3-59)³⁸

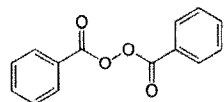
Once substituting the toluene core material in the process to the amine adduct, the encapsulation experiments encountered difficulties. When attempting to lower the pH to 4.2, a considerable amount of acid was required. This quickly suggests there is competition between titration of the amine and the precipitation of the gelatinous shell. For this reason, complex coacervation was abandoned and a different method of encapsulating the amine was sought.

In-situ Polymerization

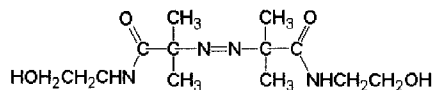
The focus towards encapsulating the isophorone diamine adduct has changed from using complex coacervation to using an in-situ polymerization process. Previous encapsulation techniques clearly indicated that the amine adduct is sensitive to aqueous based encapsulations that involve the reduction of pH. The main focus is protection of the adduct droplet from the acidic environments by placing a polymer shell around the droplet.

An in-situ polymerization process used to protect the amine droplets can be described as a free radical solution like polymerization, where droplets are dispersed in

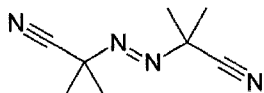
aqueous media containing the amine adduct (IDEH or IDEO), monomer(s), initiator and co-stabilizer. Due to the hydrophobicity of the amine adduct, a co-monomer mixture of methyl methacrylate (MMA) and methyl acrylate (MA) was proposed, where the resulting polymer is more hydrophilic than the adduct and has a tendency to phase separate during formation and move towards the outer surface of the water/droplet interface. PMMA has a high glass transition temperature (119°C) and PMA has a low glass transition temperature (9°C), the co-monomer mixture was used to produce a copolymer of a T_g relative to the reaction temperature. Since the reaction temperature was chosen to be 70°C, the ratio of MMA to MA was chosen to be 70:30 (by weight) such that the copolymer T_g would also be close to 70°C (P(MMA-MA) shell with a dry T_g of 78°C and a wet T_g of 65°C). With the reaction temperature lying between the wet and dry T_g , the polymer formed would phase separate to the outer surface of the adduct droplet and should have enough mobility at the reaction temperature to coalesce with neighboring polymer domains and form a continuous shell. Numerous experiments have been performed using a variety of initiators (shown in Figure 3-29) to determine which one best encapsulates the amine adduct.



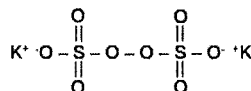
Benzoylperoxide (BPO)



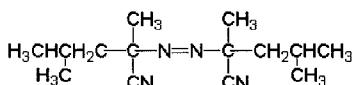
2,2'-Azobis[2-methyl-N-(2-hydroxyethyl)propionamide] , VA-086



2, 2'-Azobis 2-methylpropionitrile (AIBN)



Potassium persulfate (KPS)



2,2'-Azobis(2,4-dimethyl valeronitrile) , V-65

Figure 3-29: Initiators used for in-sit polymerization encapsulation process^{41,42}

First attempts to encapsulate the amine used BPO (obtained from Sigma Aldrich) as the initiator. A mass ratio of the polymer to the adduct was first chosen to be 2:1 in order to produce a sufficiently thick shell to be observed in the optical microscope. At this stage ratio, the payload would be quite low (around 33%), but the point was to test the efficacy of this technique in encapsulating the amine adduct. As seen in Figure 3-23, a successful encapsulation was observed, however the shell thickness was considerably thinner than predicted, although the success of forming a shell around the amine adduct was promising.

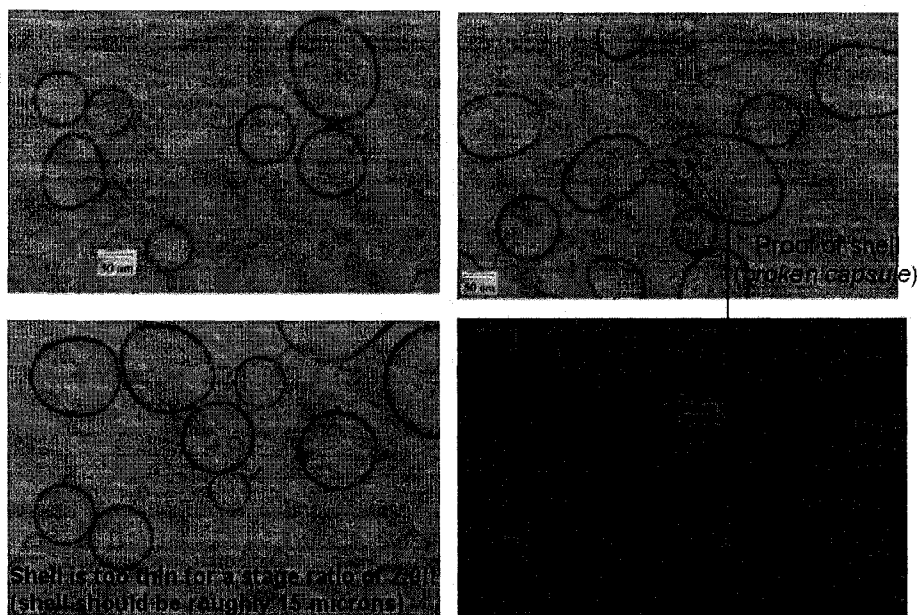


Figure 3-30 First Attempt at Free-Radical Polymerization Based Encapsulation of the IDEH adduct by a p(MMA-MA) Shell (JN3-80)³⁸.

Although the shell was thinner than expected, the photos at the right side of Figure 3-30 clearly shows a broken capsule retaining its shape under the microscope. The capsule was broken by placing a glass cover slip over the material. Clearly a droplet would not retain its shape, so this was a simple proof that a shell has formed. However, the monomer conversion of this polymerization was found to be low, which helps to explain the thinner polymer shell. A second attempt (JN3-81) of encapsulation at a higher stage ratio (5:1) also showed a significantly thinner than expected shell and a noticeably low monomer conversion.

In the portion of the procedure where the droplet size is established, the amine adduct (mixed with the monomers and the benzoyl peroxide initiator, BPO) is agitated in the reactor at room temperature for over one hour. It turned out that the benzoyl peroxide initiator actually forms a redox couple with the amine adduct⁴³ and was decomposing during this pre-mixing period at room temperature. The high radical decomposition rate

of the redox system may produce a high radical flux initially and polymerization quickly consumed the initiator, resulting in forming only a thin shell. This explains why later, as the reactor was brought to temperature no further polymerization occurred.

To salvage the low conversion of a particular run (JN3-82), azobizbutyronitrile (AIBN), (obtained from Alfa Aesar) was fed to the reactor in an aqueous solution with a small fraction of acetone to aid its solubility and dispersibility. AIBN was chosen as a potentially more appropriate initiator. The monomer conversion was found to easily increase and form a much more pronounced shell on the capsules. Although the resulting capsules were much too large (1-2 millimeters), Figure 3-31 and Figure 3-32 shows the promise and success of this system.

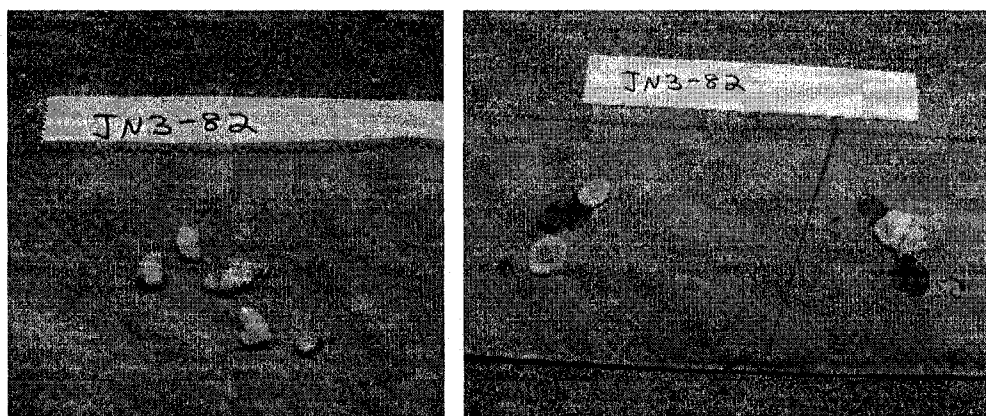


Figure 3-31: Clusters of JN3-82 Amine Adduct Capsules Encapsulated by P(MMA/MA) (left), Capsules after Being Crushed and Amine Adduct Liquid Content Released (right)



Figure 3-32: Close-up optical microscope image of broken JN3-82 capsule releasing IDEH amine adduct liquid

Figure 3-31 uses a paper wetting test to determine the amount of encapsulated material present after being crushed between a folded paper towels. One can see that there is some indication of liquid core material inside the capsules, though the capsules were large and agglomerated. Figure 3-30 shows a single microcapsule releasing a large amount of IDEH liquid, indicating that encapsulation was successful.

In order not to consume any of the amine adduct which was observed with the BPO and amine redox coupling, the same recipe was reattempted (JN3- 84) utilizing only the AIBN initiator feed. The experiment consisted of a stage ratio of 2 using a 70:30 MMA:MA monomer composition. 2 wt% of AIBN (compared to monomer) was mixed with a 50:50 water and acetone solution (20ml) and for two hours. Optical microscopy images of those capsules are shown in Figure 3-33.

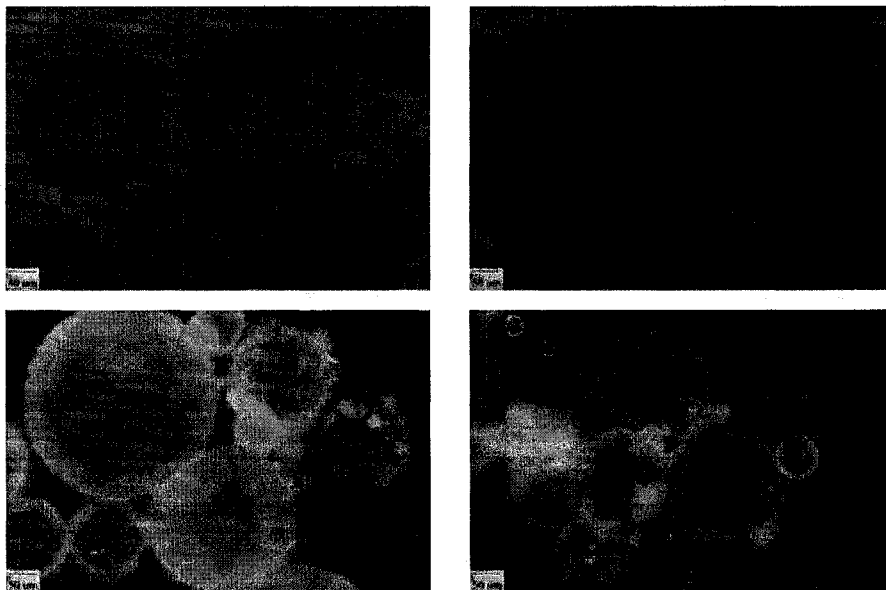


Figure 3-33 Optical microscopy of JN3-84 capsules from free-radical polymerization based encapsulation of the IDEH adduct by a P(MMA-MA) shell with AIBN initiator

However, when those capsules were subjected to the isolation and crushing test to prove release of the amine adduct hardener, only a small payload of amine was released as shown in Figure 3-34 below.

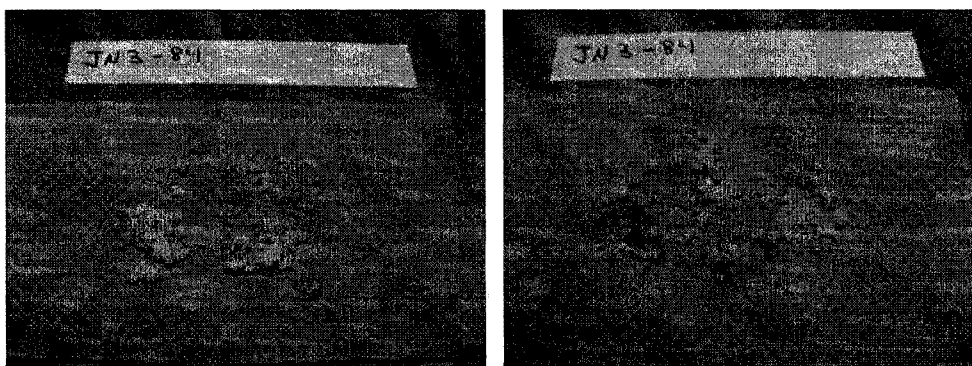


Figure 3-34: Clusters of JN3-84 IDEH amine adduct capsules encapsulated by P(MMA-MA) (left), capsules after being crushed and amine adduct liquid content released (right)

The low yield in the release of these capsules could potentially be due to a variety of issues. It was suspected that there was a poor degree of phase separation between the adduct core and the polymer resulting in a highly occluded morphology which might be

more difficult to crush. When compared to previous runs (JN4-80, JN4-81), the difference is found to be the very fast polymerization of an initial shell when the BPO/amine redox was occurring. To test this concept, a different amine adduct was made which would be slightly more hydrophobic than the IDEH adduct, the only difference being the addition of four more carbon units via two epoxyoctane units versus epoxyhexane units³⁸, as shown in Figure 3-35.

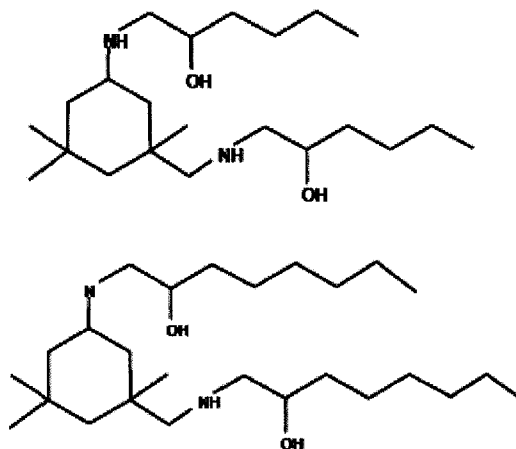


Figure 3-35: Adduct of Isophorone Diamine and 1,2 Epoxyhexane (top), Adduct of Isophorone Diamine and 1,2 Epoxyoctane (bottom)

Now with a more hydrophobic core (IDEO adduct) the phase separation of the p(MMA/MA) polymer to the outer surface of the droplets should occur more easily. The resulting optical microscopy images and crush test of those capsules are shown in Figure 3-36 and Figure 3-37 respectively.

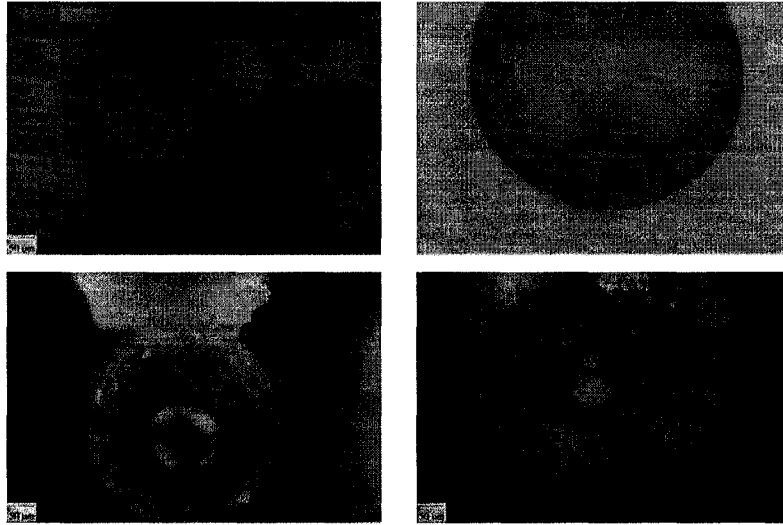


Figure 3-36: Optical microscopy of JN3-85 capsules from free-radical polymerization based encapsulation of the IDEO Adduct by a p(MMA-MA) shell with AIBN initiator

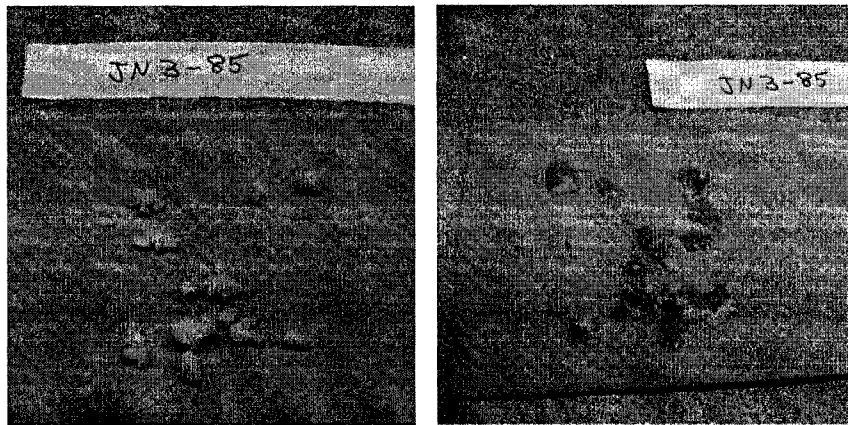


Figure 3-37: Clusters of JN3-85 amine adduct capsules encapsulated by pMMA/MA (left), capsules after being crushed and IDEO amine adduct liquid content released (right)

Clearly from the two figures above, this encapsulation technique shows significant promise as spherical capsules were obtained which on crushing released a considerable amount of amine hardener liquid. This result was a significant achievement for this project. The capsules were far from optimized for application with the resin capsules, but the amine component has some promise for encapsulation.

Many attempts to lower the stage ratio of the encapsulation process below 1.5 have been unsuccessful and focus changed towards water-soluble initiators. Such initiators experimented with were potassium persulfate (KPS) (obtained from Alfa Aesar) and VA-086 (obtained From WAKO Chemicals) an azo-initiator. The water soluble initiators were fed into a reactor containing dispersed monomer and adduct droplets. KPS was used to test if feeding water-soluble initiators could improve the capsule properties. The results of the KPS run were not successful due to a large amount of unencapsulated adduct floating on top.

VA-086 is a water soluble azo-initiator which produces carbon centered radicals compared to KPS that produces oxygen centered radicals. Feeding of VA-086 compared to feeding AIBN resulted in smaller sized capsules and produced a larger yield of microcapsules compared to BPO. The stability was much better than any other encapsulation attempted on the IDEO adduct so far. The capsules can be seen in the light microscope shown in Figure 3-38.

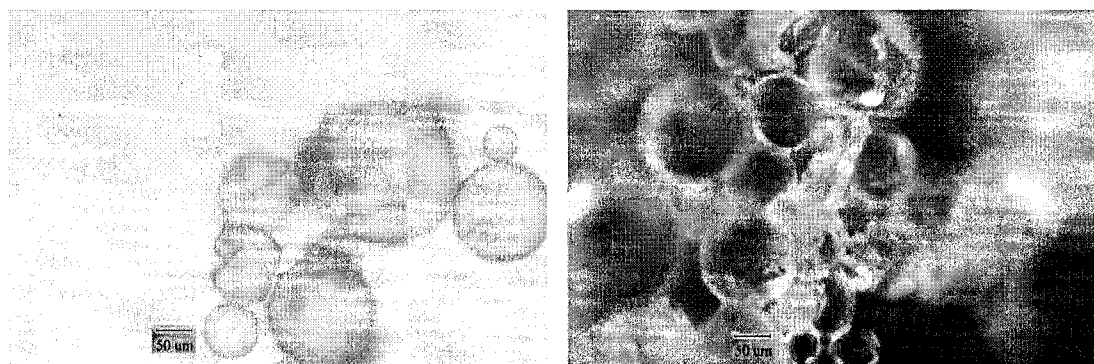


Figure 3-38: Light microscope images of JN4-11 wet (left) and dried (right, polarized lens)

As one can see from Figure 3-38, the polymer shell seems thinner than calculated; but there are signs that a definite shell is formed around the droplets. Attempts to lower the stage ratio below 1.5 have been unsuccessful due to large amounts of unencapsulated adduct that floats.

It is important to note that there is formation of a second crop of polymer particulates in the aqueous dispersion. It was suspected that the second crop is made up of smaller sized polymer particles (nanoparticles) due to the dispersion having limited stability. It was also noted that the second crop would affect the actual stage ratio of the encapsulation due to the loss of polymer from adduct droplets to the dispersion. This might explain why the shells were significantly thin in the majority of experiments and why one cannot further decrease the effective stage ratio. Before moving on, a step towards determining the effects of a second crop to the encapsulation process was assessed.

Second cropping

With many encapsulation attempts so far, a second crop of polymer has formed in the aqueous phase. This is possibly due to nucleation of polymer particles in the aqueous phase. Nucleation of polymer particles can be caused by the partial solubility of the monomers in water and the partial or complete solubility of the initiators. MMA monomer has a 1.5% solubility (25°C)³⁶ in water and MA has a 5% solubility (25°C)³⁷ in water which is very high compared to many vinyl monomers. With much of the monomer residing in the aqueous phase, one would believe the effective amount of monomer used for encapsulation is less than what was put in the reactor initially. As an example, a stage ratio of 1.5 used in most experiments could actually be a stage ratio lower than 1.5 due to loss of polymer used to form the shell material, therefore reducing the stage ratio that was put in the reactor at the start of polymerization. Therefore the amine adduct and monomer droplets experience a different stage ratio or “effective” stage ratio. One must either

determine what the new “effective” stage ratio is to compare to theoretical values or introduce the use of an aqueous free radical scavenger such as Fremy’s salt (potassium nitrosodisulfonate) or sodium nitrite⁴⁴, to reduce or eliminate the second cropping of polymer formation in the aqueous phase.

Aqueous Radical Scavenger

Aqueous radical scavengers such as Fremy’s salt and Sodium Nitrite (NaNO_2) are used to deactivate free radicals in the aqueous phase and therefore potentially stop a second crop of polymer from forming. The aqueous radical scavenger primarily attacks carbon based radicals found in the aqueous phase⁴⁴. Before attempting the addition of the radical scavengers, a few experiments were performed in order to obtain a better understanding of how the polymerization behaves with radical scavengers present. Separate batch emulsion polymerizations of MMA(JN4-26) (Figure 3-39) and Styrene(JN4-27) (Figure 3-40) have shown decrease in conversion after charging an equal molar amount (compared to the KPS initiator used) of the radical scavenger, Sodium Nitrite (from Sigma Aldrich), after 30 minutes of reacting.

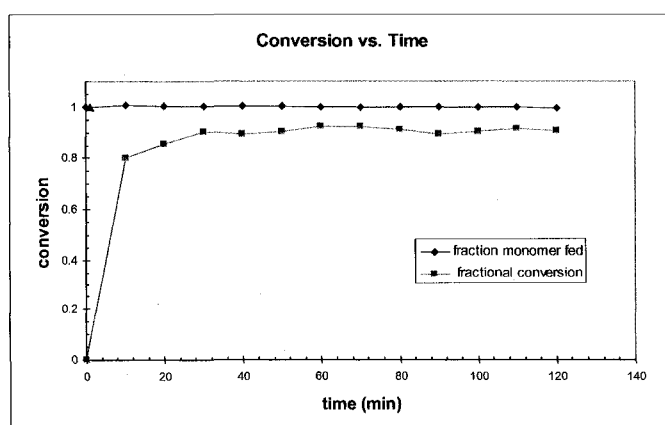


Figure 3-39: Conversion curve of MMA batch emulsion polymerization with AIBN. A charge of radical scavenger was placed at t=30Min

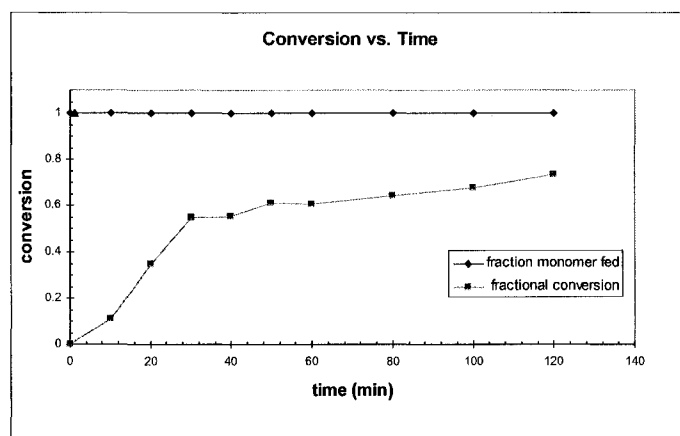


Figure 3-40: Conversion curve of Styrene batch polymerization with AIBN. A charge of radical scavenger was placed at $t=30\text{Min}$

As one can see in the above figures the decrease in polymerization rate is more obvious in the styrene batch reaction rather than the methyl methacrylate batch reaction. The reason that the scavenger did not perform well with the MMA batch reaction is that the polymerization was effectively complete before the addition of the radical scavenger. For the styrene reaction (Figure 3-40) the addition of the radical scavenger caused the monomers to polymerize slowly as the scavenger becomes consumed.

When using the radical scavenger, one can no longer use water soluble initiators or feed initiators into the system. Feeding of the initiator across the aqueous phase will cause deactivation of free radicals with sodium nitrite present. Experiments involving radical scavengers have been performed as batch reactions using azo-initiators. Azo-initiators such as AIBN have been performed with the radical scavenger but have resulted in producing a second crop. A new type of azo-initiator, 2,2'-Azobis(2,4-dimethyl valeronitrile) known as V-65 from Wako Chemicals, is similar to AIBN but is predominantly oil soluble. The transition to V-65 was justified by reducing the amount of

second cropping from forming. The combination of the radical scavenger and V-65 has shown significant reduction or elimination of second cropping.

Amine Capsule Properties

With the numerous experiments performed thus far, various characterizations of the encapsulated amines were performed to determine properties and information which can be used in preparation for the next experiment to further optimize the encapsulation process. Properties such as amine capsule payload, capsule size, stability, and the ability to protect itself from ionization, have been used as guides on how to carry on a new set of experiments.

Microcapsule Payload

The microcapsule payload is important data to determine how well the encapsulation process was performed. Many encapsulation attempts have shown various shell thickness and payloads by observation. To differentiate which of the attempts are better, one must be able to analyze microcapsule payloads in a quantitative manner.

Typically, payload data can be achieved by using a Differential Scanning Calorimeter (DSC), measuring heat flow vs. temperature. A first order transition was observed and integration of the peak will result the heat required to soften the material in the units of J/g. The results for pure core material and the microcapsules are compared to determine the capsule payload by simply dividing the value received for the capsules divided by the value of the pure core material. (eg. 5.766 J/g for pure DCPD and 4.615

J/g (JN1-27 DCPD microcapsules) divide values to get payload. $(4.615/5.766)*100 = 80\%$ payload by weight)

For the case of the IDEO amine adduct, a first order transition was not present but a second order transition was. A second order transition is characteristic of a T_g rather than the melting point, therefore determining the payload is difficult to achieve but can be calculated using the heat capacities of the resulting capsules and the heat capacities of the IDEO adduct and polymer shell. There is a possibility that the amine adduct can still leave residue on the outside of the capsules, which would make the DSC analysis to be invalid. Another method to determine payload requires adequate washing of the capsule without rupturing and removing the core material. Once cleaned, capsules were weighed then crushed. The crushed capsules were washed again to remove the core material as much as possible and then allowed to dry. The dried sample was weighed again and then compared to its initial weight. The ratio determines the payload of the capsules. This process has a lot of potential in producing a large error. The process requires no loss of material between steps which is difficult to achieve when working with a small amount of material.

Since the first set of experiments, reduction of the stage ratio (grams of polymer: grams of amine adduct) was important to achieve a practical system. Below is a graph (Figure 3-41) of theoretical payload and shell thickness of a $100\mu\text{m}$ particle with various stage ratios.

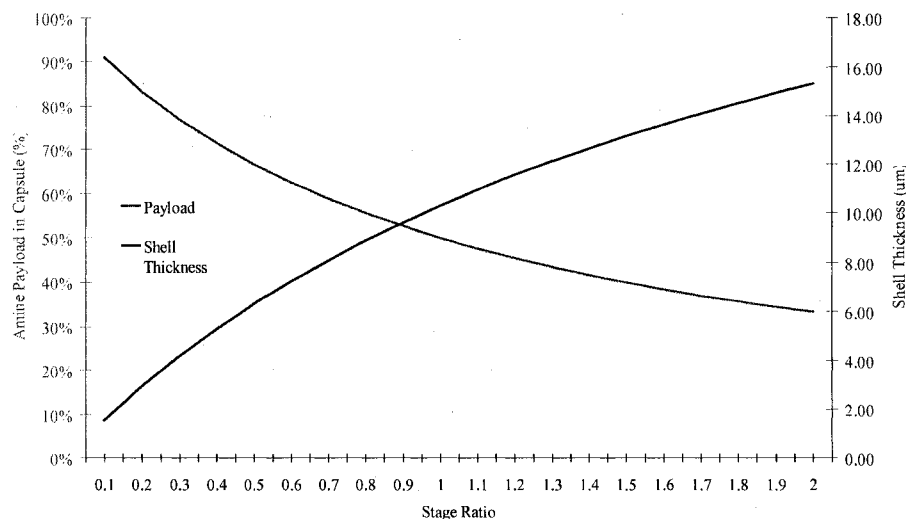


Figure 3-41: Graph of theoretical payload and shell thickness of a 100µm diameter microcapsule.

A payload of approximately 80% (by weight) is desired to match that of the resin microcapsules, which would mean a stage ratio of 0.2 is required. The most successful encapsulation attempts had a stage ratio of 1.5, which would theoretically give a payload of 40% and a shell thickness of 13µm. After observing the capsules from the numerous experiments using light microscopy techniques, we have seen that the capsules actually have a larger payload than 40% and the actual shell thickness is thinner than the theoretical 13µm shell thickness. With this knowledge one can suspect that second cropping can be the cause of this phenomenon.

IDEO amine adduct density

With many successful encapsulations, the typical result was capsules that tend to float on top of the liquid dispersion while the second crop polymer particles sank to the bottom. Since the capsules float, one would suspect that the density of the amine adduct was less than that of water and polymer. Assuming the density of the P(MMA/MA) polymer to be 1.147g/ml⁴⁵ and the density of IDEO adduct is 0.74g/ml (JN4-19, found

experimentally at 25°C), it has been calculated that a stage ratio of 2:1 is required to have the capsules sink in the dispersion. The recipes thus far have only successfully encapsulated with a stage ratio of 1.5, therefore the microcapsules produced will always float to the top. With the density being less than that of water, separation of the capsules from the dispersion becomes an easier process by simply removing the top layer of capsules and placing them in a container of water and allowing that to separate again. But the floating of microcapsules proves to be an issue later when adding these capsules to an epoxy matrix. Upon curing of the epoxy matrix the capsules have a tendency to float and congregate at the top. This phenomenon can cause problems with preparing samples to test self-healing and in end-use applications.

Sonication and Homogenization

Initially magnetic stirrers were used to make and maintain droplet sizes in the reactor, but resulted in large microcapsule sizes in the range of 500 μ m to 1500 μ m. The use of a magnetic stirrer was not sufficient to make small droplet sizes. Investigations for obtaining smaller droplet sizes and stable particles have been performed using a homogenizer and sonicator. The use of the sonicator or homogenizer could produce smaller droplet sizes in the desired range of 50-80 μ m. Producing smaller droplets can improve the stability of the monomer/adduct droplets from coalescing therefore improve droplet stability.

Investigation of sonication and homogenization methods have been applied to a beaker of water, polyvinylpyrrolidone (PVP), hexadecane and mineral oil to observe if each of the processes can produce droplets that are in the 50-80 μ m range. Mineral oil was

used as a substitute for the amine adduct since it has a similar viscosity to the amine adduct/monomer droplets, and to explore how the equipment worked and how to optimize settings for the appropriate droplet sizes.

Droplet sizes with both the sonicator and homogenizer ranged from 10-80 μm . The droplets were shown to be stable for at least 90 min after introduced to sonication/homogenization without the use of a co-stabilizer. The homogenizer was chosen over the sonicator due to having the ability to produce a narrower size distribution of mineral oil, in the range of 20-100 μm with the majority of the droplets being 50 μm (JN4-46) determined by light microscopy. Experiments then led to the use of the adduct instead of mineral oil. Using the same setting on the homogenizer and same reactor set up, smaller droplet sizes were achieved and the dispersion turned white very quickly. After 5-10 minutes of homogenization the dispersion was very white in color with sizes around 10-20 μm . Clearly one obtains much smaller droplet sizes with the use of the adduct than with mineral oil likely due to the more polar nature of the adduct and the reduction of the interfacial tension.

Polymer Shell Properties

Microcapsules obtained during and after polymerization often have a tendency to agglomerate to one another. This phenomenon is also observed after having the capsules vacuum filtered washed, and dried. The agglomeration can be caused by numerous things such as a low T_g polymer (polymer drift during polymerization), plasticized shell, or that the washing method was not adequate therefore there is residue that remains on the capsule walls. During the polymerization reaction agglomeration between droplets can

occur especially in a “sticky” period around 50-70% conversion. In the 50%-70% conversion range polymer is produced while having the unreacted monomers reside within the polymer, plasticizing the polymer and make them sticky. The sticky droplets can collide with one another and end up agglomerated together.

A simple experiment (JN3-87) was performed to determine if the IDEO adduct could plasticize the p(MMA-MA) copolymer. A solution polymerization containing MMA, MA, IDEO adduct (1.5 stage ratio), and AIBN was performed. The polymerization yielded an opaque solid with large occlusions contained inside. The occlusions were found to be filled with a viscous liquid of IDEO amine adduct. Along with the opaqueness of composite this proves that the P(MMA/MA)/adduct system sufficiently phase separates. The polymer chunk is solid and glassy at room temperature which would indicate that the copolymer is not significantly plasticized by the amine adduct.

One might think that the agglomeration is a result of adduct being on the outside of the capsules and making them stick together. Attempts to wash them have been performed but capsules still have a tendency to stick to one another. It is important to use a washing solvent that doesn't plasticize or swell the shell material and potentially affect the core material. Current washing methods use a mixture of 50% methanol in water to wash the capsules. During the vacuum filtration process, the methanol mixture is poured over the capsules. This procedure is done two to three times to ensure proper cleaning. After performing this procedure many capsules still continue to stick to one another. With this information one must suspect the stability of the droplets during polymerization is insufficient.

Amine Capsule Titration

The reason that the in situ-polymerization process was used was to have a protective layer that encapsulates the amine, while ignoring other desired properties of the shell. The reason for the protective layer was to prevent ionization of the amine which is a concern when using many other types of encapsulation techniques. If the amine adduct was successfully protected, then one can try to place a urea-formaldehyde shell around it, to match the mechanical properties of the resin microcapsules. To determine if protective polymer shells are adequate, titration experiments were performed to determine how the adduct capsules behave, during the titration of the amine adduct with acid in the aqueous dispersion. Using a pH probe and pH meter (Venier Lab Pro System), the pH was monitored and plotted over time. Figure 3-42 (below) contains separate titration curves for 2wt% JN4-11 capsules (VA-086 capsules) in water, DI Water alone, and 2wt% IDEO adduct dispersed directly in water.

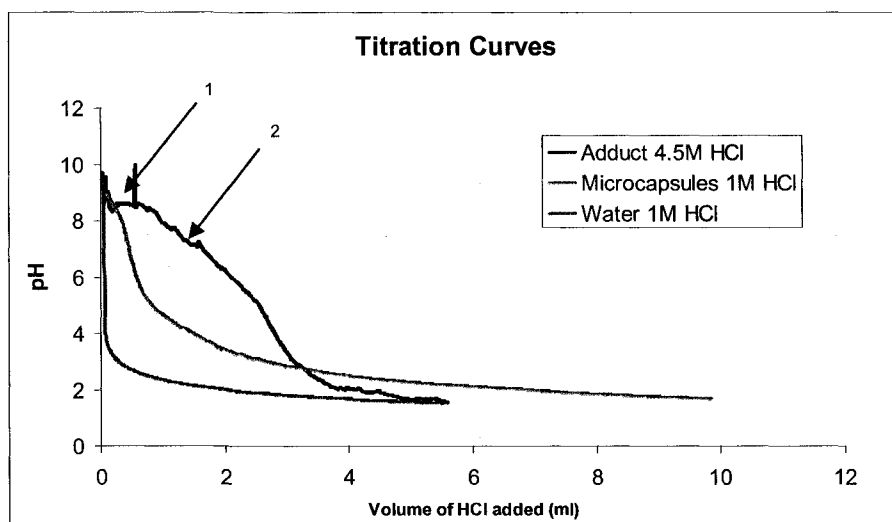


Figure 3-42: Titration curves of adduct, water, and JN4-11 microcapsules with the specified acid fed at a rate of 5ml per hour

One can see in Figure 3-42, that the IDEO adduct (dark blue curve) has two pKa's approximately around nine and seven (designated by arrow 1 and 2 respectively), while the pure water and the microcapsule curves have no signs of a pKa. The microcapsule titration curve (green curve) lies in between the adduct curve and water curve. The fact that the microcapsule curve lies in between the pure water curve and the adduct in water curve (red curve), makes one suspect that there is some trace of amine adduct on outside of the capsule walls or that the adduct could be slowly leaching through the shell wall.

With the JN4-11 capsules (polymerized with VA-086), attempts to optimize the washing was performed with no further improvement. In addition, the capsules that have been titrated were saved and were exposed to acidic conditions (pH=2) over a week's time. Unfortunately, the capsules no longer floated, which would make one believe that the capsules have ruptured or leached their contents within that period. Figure 3-41 shows a light microscope image of JN4-11 microcapsules in acidic conditions for one week.



Figure 3-43: Light microscope images of JN4-11 in pH 2 after seven days Light microscope(left), Light microscope with polarized lens (right).

In Figure 3-43, one can clearly see that there are broken capsules present. This information is very discouraging, but encapsulation of the amine adduct has been achieved. Our focus thus shifted to produce a thicker shell around the capsules by means of increasing the stage ratio or eliminating the second crop. The actual payload of the

JN4-11 capsules was unknown due the challenges in determining the actual capsule payload.

Encapsulations Using V-65 Initiator

Although AIBN generated in some successful encapsulations, it unfortunately still partitions into the water phase. Having the free radicals in the aqueous phase often results in the formation of a second crop, therefore a new azo-initiator that is predominantly oil soluble might be suitable. An oil soluble azo-initiator, VA-65 is very similar to AIBN but is predominantly oil soluble. Below in Figure 3-44, one can see that the initiators have similar structures with the double bonded nitrogen groups in the center. Dissociation of the both initiators results in carbon centered radicals that are highly reactive with monomer.

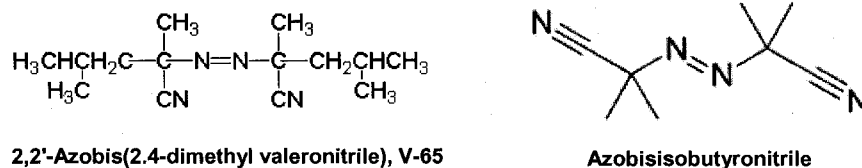


Figure 3-44: Chemical structures of V-65(left) and AIBN (right)^{40,41}

In the figure above, one can see that the V-65 has a longer alkyl chains in the molecule compared to the structure in AIBN, making V-65 a much more hydrophobic initiator.

VA-65 has a 10 hour half life at 51°C⁴⁰. Reduction of the polymerization temperature to 65°C was used to have a reasonable half-life during the polymerization process (1.53 hours). A series of batch reactions were performed with V-65 and radical scavenger. Results were much better than any previous encapsulation attempts with the amine adduct, with higher yield and the amount of polymer formed as a second crop has

decreased significantly. The dispersion was opaque rather than milky white. However the capsules were still large (eg. 300-800 μ m) and most of them still agglomerated to one another.

The issue of second crop formation seems to have been eliminated with the use of an aqueous radical scavenger in conjunction with V-65. Unfortunately, experiments trying to drive the stage ratio lower than 1.0 have been unsuccessful. Stability is still a key issue with encapsulation.

Agglomeration during polymerization has been a common result when trying to encapsulate the IDEO adduct using MMA/MA co-polymer. An experiment has been performed (JN4-50) which has the IDEO adduct omitted from the recipe to see if the adduct has anything to do with the system being sticky and cause the capsules to agglomerate. After running an experiment (JN4-51) without the adduct conversions have been calculated to be approximately 49%. The low conversion of the polymer is a puzzling result. A possible reason for the low conversion is the radical scavenger present during polymerization. Even though the scavenger is dominant in the aqueous phase, it can cause the resulting low conversion. However an experiment (JN4-52) without adduct and without scavenger still resulted in a low conversion, approximately 45%.

In order to determine what is going on with the low conversion a series of small scale experiments (20ml vials) have been performed. A series of bulk polymerizations were performed to answer a few questions about the system that was currently employed. Investigation of temperature, monomers, and initiator concentrations has been a priority. The relationship between conversion and temperature has been observed in the following series of bulk polymerizations found in Table 3-1 below:

Table 3-1: Bulk polymerization experiments JN4-53

Vial#	MMA, g	MA, g	V-65, g	Reaction Temperature, C	Properties
1	4.8	3.2	0.137	65	Polymerized but sticky
2	4.8	3.2	0.137	80	Polymerized but sticky

The polymer T_g 's should be around 80°C(Dry T_g) and 63°C (Wet T_g); it clearly shows that the T_g of the experiments in Table 3-1 is below that. Investigation of the polymerizations of the individual homonomers has been performed using BPO and V-65 as initiators to determine if there are any anomalies that occur during polymerization.

Table 3-2: Bulk polymerization experiments JN4-54

Vial#	MMA, g	MA, g	Initiator, g	Reaction Temperature, C	Properties
1		8	0.137 V-65	65	Polymerized, soft
2		8	0.137 V-65	80	Polymerized, soft
3	8		0.137 V-65	65	Polymerized, hard
4	8		0.137 V-65	80	Polymerized, hard
5	4.8	3.2	0.137 BPO	65	Polymerized, hard
6	4.8	3.2	0.137 BPO	80	Polymerized, hard

With the data from Table 3-1 and Table 3-2, one can see that V-65 used to polymerize a copolymer of MMA and MA was soft and therefore unsuccessful (Table 3-1) but when using BPO, polymerization is easily achieved resulting in a hard material (Table 3-2). This result is very puzzling since MMA and MA should be easily copolymerized.

With this puzzling result, a substitution of MA with BMA has been made. The use of BMA lowers the polarity of the copolymer but still it remains higher than the adduct.

Bulk experiments (JN4-53) with V-65 and MMA/BMA have shown that these monomers polymerize properly. With the success of BMA polymerizing, phase separation and plasticization between the co-polymers and the adduct needed to be investigated. At 1 wt% V-65 initiator based on the monomer, the BMA/MMA co-polymer clearly phase separated from the IDEO adduct yielding a cloudy solid piece of polymer as shown in the Figure 3-43 below.

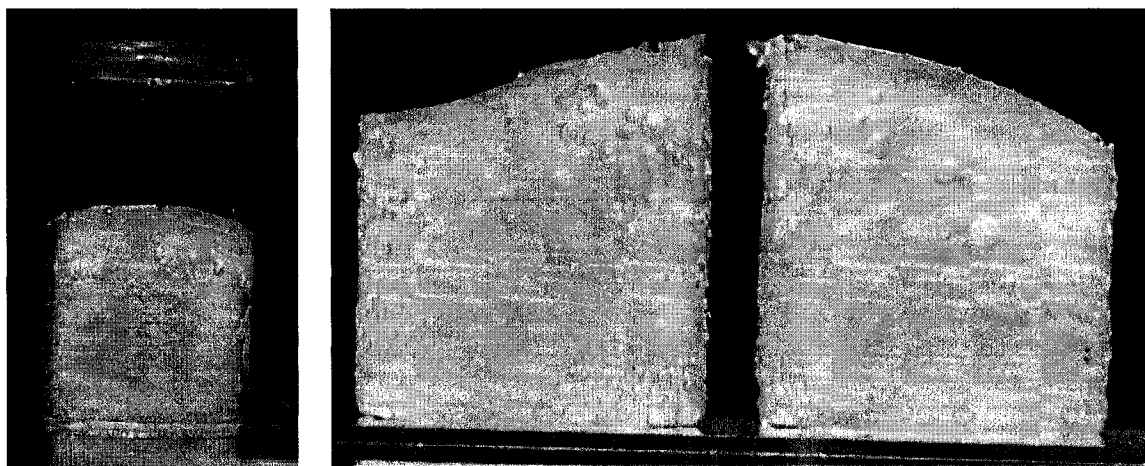


Figure 3-45: Solution polymerization of MMA/BMA/IDEO adduct. 20ml vial (left), broken halves (right)

A sample of the polymer was analyzed in the DSC to achieve a T_g , to determine if the sample is plasticized by the adduct. Prior to placing it into the DSC the sample was crushed into small pieces with a hammer and then placed in the oven to evaporate any residual monomer, while leaving any amine adduct within the copolymer (IDEO adduct does not evaporate at 60°C over a two hour period). The results of the DSC gave a T_g of about 54°C. The MMA/BMA monomer mixture was tailored to have a dry T_g close to 80°C and wet T_g of 63°C. The apparent decrease in T_g indicates that there may be some plasticization of the MMA/BMA copolymer, by the adduct, or that we did not remove all of the residual monomer from the sample. See Appendix G for further details.

An encapsulation attempt was performed using a 1.5 stage ratio with MMA/BMA as the co-monomers. Reaction was subjected to homogenization during the entire polymerization process. The experiment yielded 50-150 μ m microcapsules that float to the top of the dispersion and removed to be dried and washed with a 50% methanol solution. The resulting dried capsules can be seen in Figure 3-46 and Figure 3-47 below.

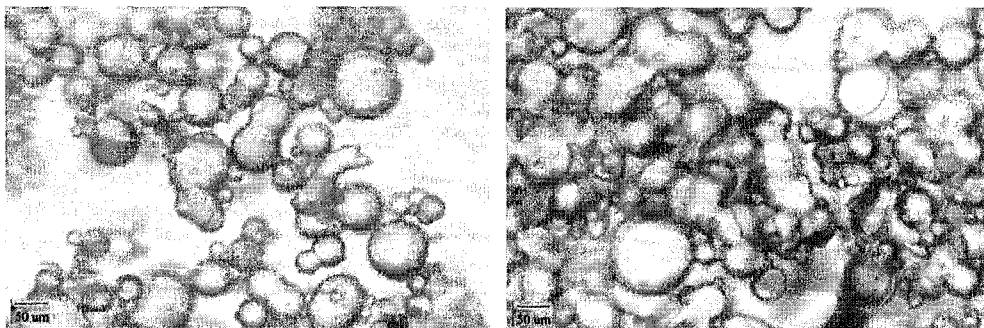


Figure 3-46: Light microscope images of washed and dried JN4-64 microcapsules. Whole capsules (left) and crushed capsules (right)

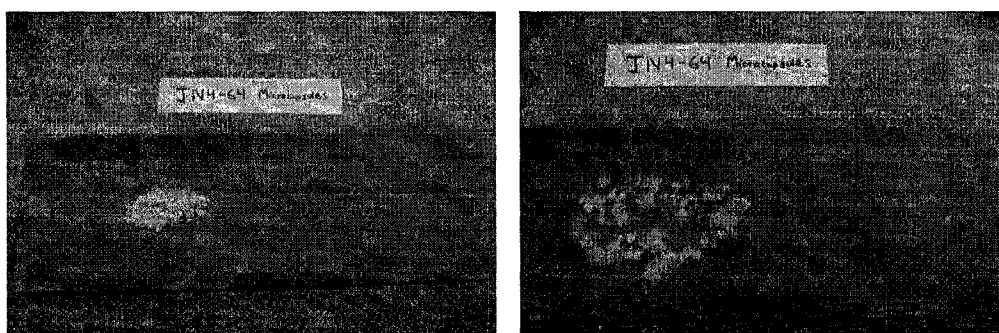


Figure 3-47: Paper test of dried and washed JN4-64 microcapsules. Whole Capsules (left) and crushed capsules (right)

Under the light microscope (Figure 3-46), one can see some liquid on the glass slide after applying pressure onto the capsules. With the paper test (Figure 3-47), one can not see the liquid core material. A titration experiment on the capsules has been performed to see if the shell walls are sufficient in the protection of the core material from ionization. Figure 3-48 shows the data obtained from the titration experiment JN4-65.

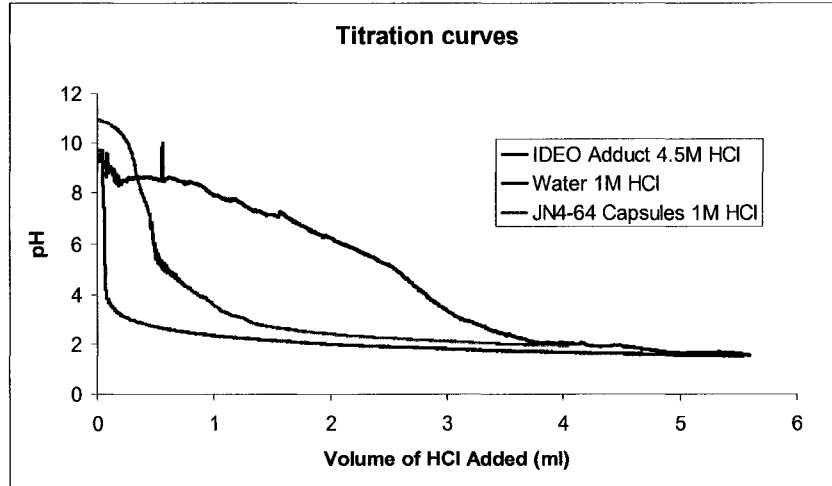


Figure 3-48: Titration curve of JN4-64 capsules, water, and IDEO adduct in water.

The JN4-64 microcapsule curve lies between the water and adduct titration curves, similar to the JN4-11 microcapsules made with VA-086. This can indicate that the washing process was still not sufficient or that the adduct continues to leach out of the shell wall. Interestingly after a day, the JN4-64 capsules sank in an acidic solution with a pH of 2. This is also a characteristic of the JN4-11 microcapsules previously mentioned. Though the protection of the core material from being ionized was not completely successful, the IDEO adduct was indeed encapsulated.

A series of tests have been performed trying to drive down the stage ratio closer to 0.2 to achieve an 80% payload. There was success at a stage ratio of 1:1, but lead to the formation of a “crust” near the homogenizer shaft after an hour of reaction. The capsules tend to be agglomerated into large (ca. 1mm) particles.

Typically the homogenizer has been run for 3-4 hours, during the whole reaction, to maintain the same droplet size throughout the free radical polymerization. But in one specific experiment JN4-72, the homogenizer started to make some odd grinding noises around the motor. Immediately homogenization was halted in the early part of the

reaction. It was approximately 45-50 minutes when homogenization was stopped . The first 15 minutes was used for dispersing the liquid droplets at room temperature and the remaining 30-35 minutes was the time for the water bath to be heated from room temperature to 65°C. With the reactor contents already at temperature, it was best to let the reaction proceed for the rest of its time, without using the homogenizer. This incident yielded capsules that floated in the dispersion and were 70-150um in size according to light microscopy and multi angle light scattering techniques (Microtrac, wet setting). The microcapsules were much more dispersed and a higher yield of capsules was produced but did agglomerate slightly after washing and drying. Light microscope images in Figure 3-49, and paper towel test Figure 3-50 show a lot of promise compared to other previous attempts.

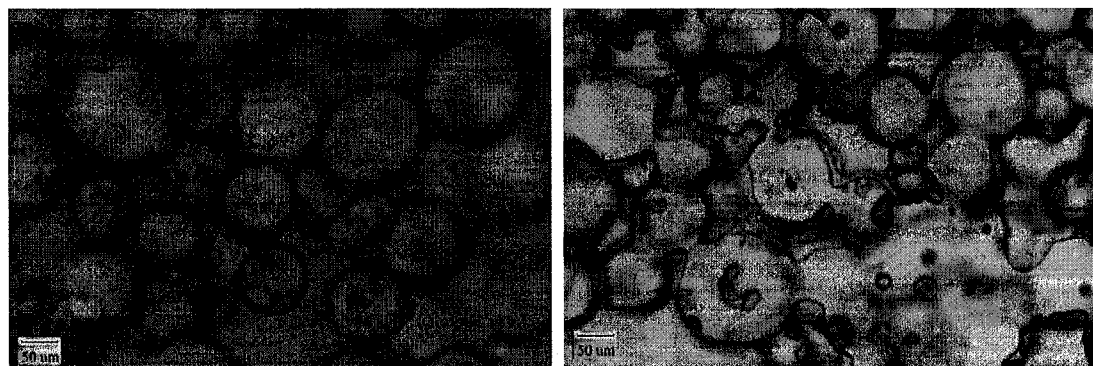


Figure 3-49: JN4-72 capsules in dispersion (left) and dried crushed capsules (right)

As one can see from Figure 3-49, the capsule sizes are smaller than achieved with any other attempt so far. On the right side of Figure 3-49, there is a significant amount of liquid core material released from the ruptured capsules

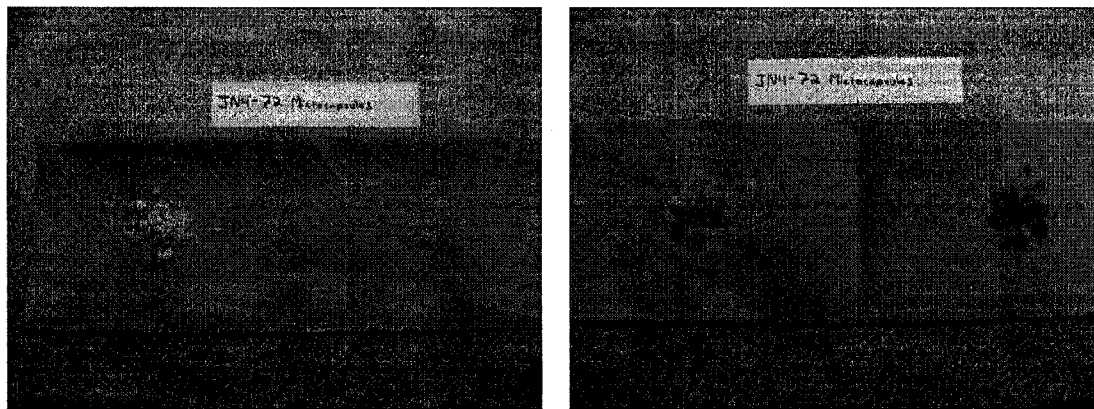


Figure 3-50: Paper test of JN4-72 capsules. Whole capsules (left) and crushed capsules (right)

Figure 3-50 shows that there is a significant amount of liquid amine adduct that was released by wetting the paper towel.

The following is a detailed procedure and recipe used to make the capsules from JN4-72 with a stage ratio of 1 to 1. In a beaker, 128ml of deionized water, 5.12g poly(vinylpyrrolidone) and 0.0892g sodium nitrite are added and well mixed. In a second beaker, 6.4g of MMA, 4.26g BMA, 0.106g hexadecane 0.106g V-65 are well mixed. Once mixed 10.66g of IDEO adduct is added to the monomer mixture until dissolved. The contents are then placed into a 250 ml jacket reactor at room temperature. Attached to the reactor are a condenser, homogenizer, and a nitrogen gas feed line. The homogenizer is not sealed, therefore parafilm[®] is used to produce a gas tight seal. The contents are dispersed using the homogenizer (IKE[®] Ultra-turrax T-25) with a setting of 9500 RPM in conjunction with a magnetic stir plate and oval shaped (30mm in length) stir bar at a setting of 11 (Barnstead/Thermolyne Cimarc) for 15 minutes. In Figure 3-51, the experimental set-up is shown below.

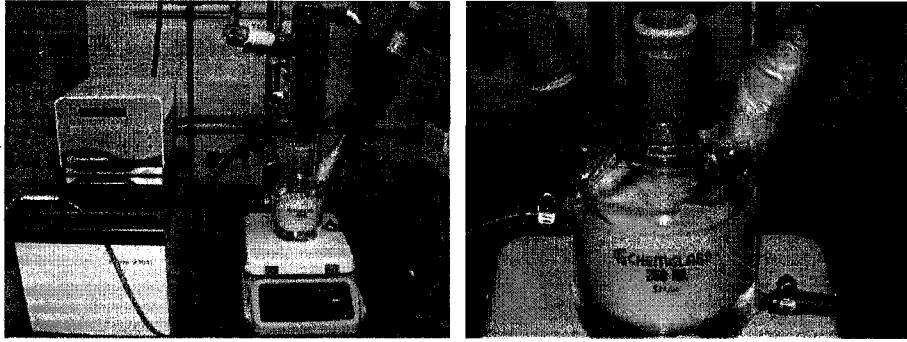


Figure 3-51: Experimental set-up of encapsulation process used in JN4-72.

Once the 15 minutes for homogenization has expired, the water bath (Fisher Scientific Isotemp 3016HD) is turned on to heat up to 65°C while homogenization and magnetic stirring continues. Once the bath reaches 65°C, homogenization is stopped and the homogenizer is removed from the reactor. At this time the stir plate is set at a lower rate, a setting of 7. The contents are allowed to react for an additional four hours.

Characterization of JN4-72 Microcapsules

Characterization and drying of the capsules has now become a priority. Sizes of the microcapsules range from 70-150 μm based on multi-angle light scattering (Microtrac S3500) analysis of the dispersion found in Figure 3-52.

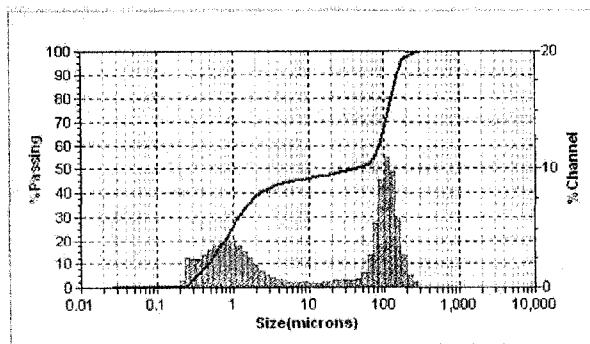


Figure 3-52: Dynamic light scattering data (Microtrac S3500) of JN4-72 dispersion.

By observation one can see that there is a second crop in the dispersion shown as by a bi-modal distribution in sizes. Isolation of the particles is typically done by using vacuum filtration but the second crop (at about $1\mu\text{m}$) would typically clog the filter paper making it difficult to isolate and dry. To get around this, the capsules were allowed to float. The microcapsules were then removed from the top and placed into the vacuum filtration apparatus to be washed with a 50% methanol in water solution two times. Capsules were then placed in the hood to dry overnight (ca. 16 hours) at room temperature.

Scanning Electron Microscopy

The microcapsules were analyzed using Scanning Electron Microscopy (SEM) (AMRAY 3300FE) to determine the characteristics of the shell when intact or crushed. The images shown in Figure 3-53, show a fairly smooth shell material (compared to Urea-formaldehyde), and that the capsules did not break when crushed.

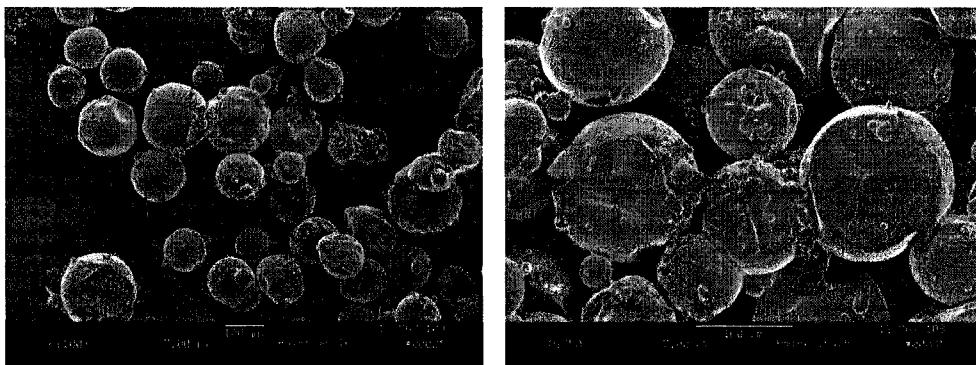


Figure 3-53: SEM Images of JN4-72 capsules. Whole capsules (left). Crushed capsules (right).

The SEM images showed an interesting microcapsule shown on the left of Figure 3-51. This capsule shows some substance pouring out of the capsule while keeping a majority

of the capsule intact. A more interesting piece of information is the thickness of the shell wall, which is shown in the right image of Figure 3-54.

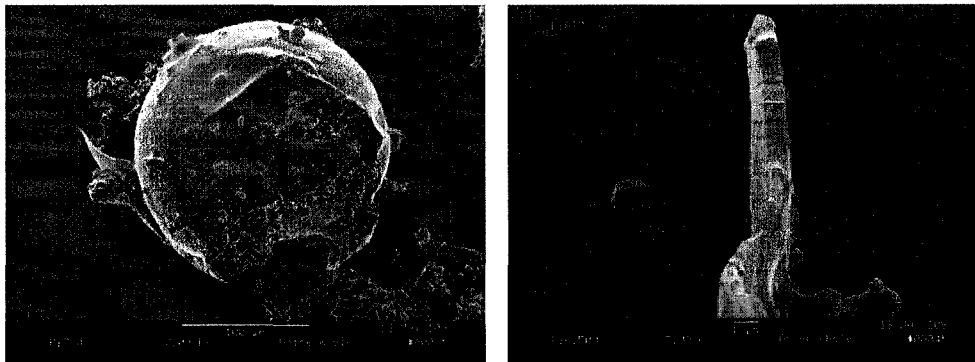


Figure 3-54: SEM Images of JN4-72 capsule (left) and a section of its shell (right).

The shell thickness is predicted to be $10\mu\text{m}$ thick based on a 1.0 stage ratio used to produce the capsules (see Figure 3-41) but images show a $1\mu\text{m}$ thick shell. This discovery would suggest that the second cropping that is present can be the cause of this phenomenon by lowering the effective stage ratio.

Fourier Transform Infrared Spectroscopy (FTIR)

The dried capsules were analyzed by FTIR (with attenuated total reflectance (ATR)), to ensure that core material is indeed IDEO adduct inside of the capsules. By using basic peak comparison of IDEO adduct, MMA/BMA copolymer, and JN4-72 capsules, one can confirm that the adduct was successfully encapsulated with the following FTIR-ATR spectra found in Figure 3-55.

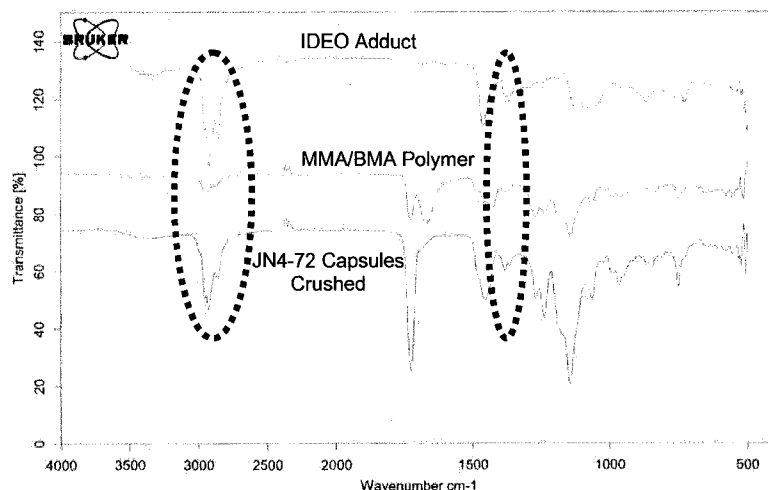


Figure 3-55: FTIR Spectra of IDEO Adduct, MMA/BMA copolymer, and JN4-72 microcapsules.

In the above figure one can do a peak comparison between the IDEO adduct, MMA/BMA copolymer, and JN4-72 capsules. By looking at the regions pointed out in Figure 3-55 one can see that the IDEO adduct is present upon crushing of the JN4-72 amine capsules. One would like to see the difference of an uncrushed and crushed microcapsules but it was difficult to perform FTIR-ATR on the uncrushed microcapsules since it required applying some pressure onto the sample. Applying any pressure on the microcapsules could result in rupturing the microcapsules.

Encapsulated Adduct Reactivity

To crudely test if the capsules have useful adhesive properties, the dried capsules were then mixed (not crushed) with JN2-37 epoxy resin microcapsules at a 1:1 molar (amine to resin) ratio. Based on the approximate payloads, the calculated the ratio is 0.58g resin capsules to 1 gram of adduct capsules. The calculation is shown below:

$$Ratio = \frac{\frac{Mw_1}{Payload_1}}{\frac{Mw_2}{Payload_2}} = 0.58 \quad (3.5)$$

where Mw_1 is the molecular weight of the epoxy resin (340g/mole), Mw_2 is the molecular weight of the adduct (362 g/mole assuming 1.5 moles of epoxide reacted). $Payload_1$ is the payload of the resin capsules JN2-32 (80%) and $Payload_2$ is the payload of the amine adduct capsules JN4-72 (50%). The blend of capsules was placed between two glass slides and then the slides crushed together. After being clamped together over night (ca. 16 hours), the contents were found to strongly bond the two glass slides together as shown in Figure 3-53.

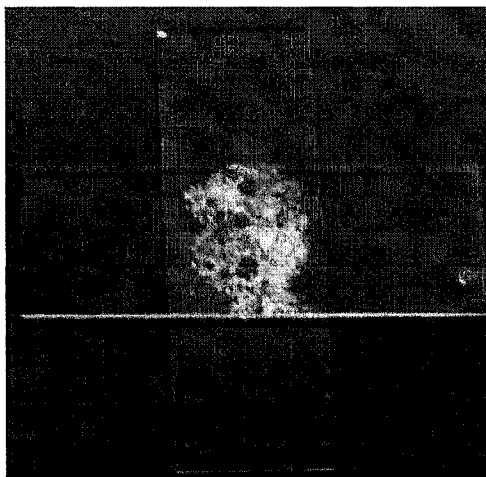


Figure 3-56: Image of crushed JN2-32 Resin Capsules and JN4-72 IDEO adduct capsules between two glass slides.

As a control experiment adduct capsules and resin capsules were placed between glass slides and they revealed no adhesive properties by themselves, as expected. This result is very promising since it confirms that the adduct is encapsulated within the acrylate shell and that a 1:1 molar ratio can adhere the two glass slides together. Another test, similar to the adhesion of the glass slides, was performed trying to adhere to two

sheets of epoxy. The sample was allowed to cure for 24 hours and resulted in successful bonding of the two sheets. It is important to note that the molecular weight of the resin is approximately 340.41 g/mole and the adduct (assuming 1.5 moles of epoxyoctane groups react with the amine) is 362.6 g/mol. If an 80% payload (similar to the resin) can be achieved with the adduct capsules, one can produce a blend that requires 1 resin capsule to 1 adduct capsule in order to cure properly.

Microcapsule Payload

Obtaining payload data through DSC analysis is difficult, since the adduct does not have a melting temperature, unlike DCPD. Without a melting point, obtaining the microcapsule payload of the amine capsules requires data obtained from the DSC in the form of heat capacities. The heat capacities of the adduct (Figure 3-57), shell material (Figure 3-58), and the overall microcapsules (Figure 3-59) are found in the figures below.

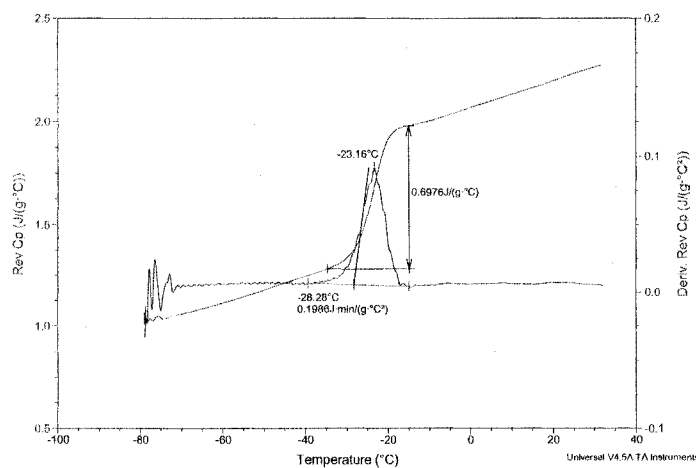


Figure 3-57: DSC trace of JN4-63 IDEO adduct

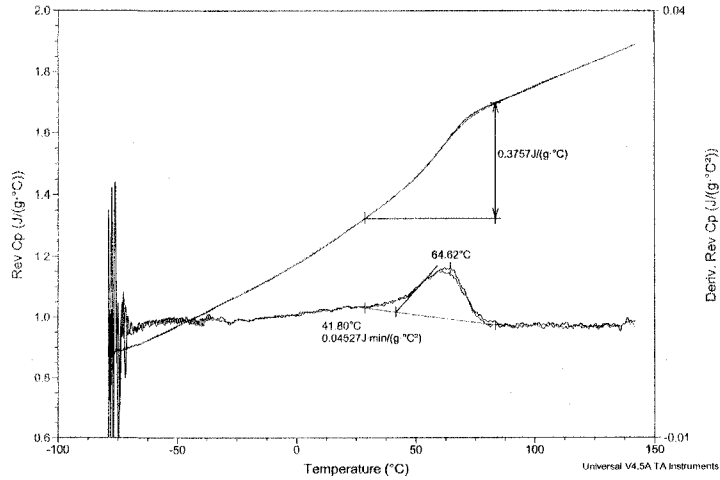


Figure 3-58: DSC trace of JN4-68 MMA/BMA polymer

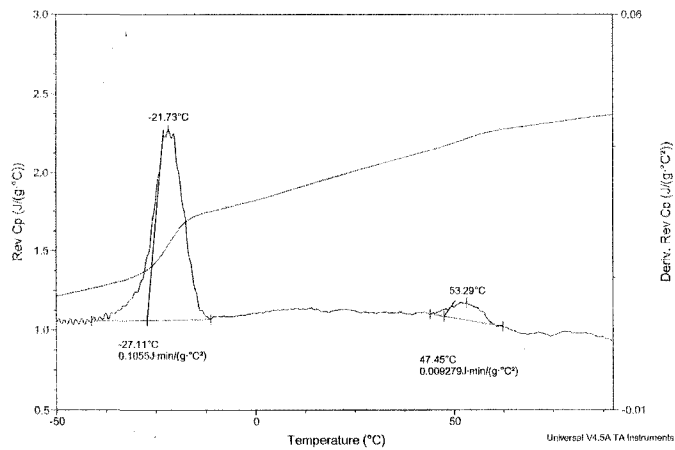


Figure 3-59: DSC trace of JN4-72 IDEO amine adduct capsules.

From the figures above, the ΔC_p values of the amine adduct and the polymer shell along with the integrated peak areas of the amine microcapsules were calculated from the DSC trace observing the reversible heat capacity and derivative of the heat capacity vs. temperature. With the appropriate data, one can now calculate the payload with the following equation:

$$\text{Payload} = \frac{\Delta C_{p_{\text{polymer}}} * A_{\text{adduct}}}{\Delta C_{p_{\text{polymer}}} * A_{\text{adduct}} + \Delta C_{p_{\text{adduct}}} * A_{\text{polymer}}} \quad (3.6)$$

where $\Delta C_{p_{\text{polymer}}}$ is the change in heat capacity for the shell polymer, $\Delta C_{p_{\text{adduct}}}$ is the change in heat capacity for the amine adduct, A_{adduct} is the integrated area of the derivative reversible heat capacity for the amine adduct, and A_{polymer} is the integrated area of the derivative of reversible heat capacity for the polymer shell. The resulting payload is:

$$\text{Payload} = \frac{0.3757 * 0.1055}{0.3757 * 0.1055 + .6976 * 0.009279} * 100 = 85.9\% \quad (3.7)$$

The resulting payload is approximately 86%, which is significantly higher than the predicted 60% payload.

However, a payload can also be calculated based on the amount of polymer in the second crop. With the second crop present, the effective payload is higher (stage ratio is lower) than what was put in the reactor. By this technique (as determined from the measurement of the second crop for experiment JN4-72) the maximum payload that these capsules can achieve is 78%, making the actual payload fall in between the range of 60%-78% for the 1.0 stage ratio experiment. With the SEM images found in Figure 3-52, one can also estimate the payload by back calculating from the size of the capsule and the apparent shell thickness. A shell thickness of 1 μm (from SEM) and a capsule size of 150 μm were used to calculate a payload of 95% or a stage ratio equivalent of 0.075. This result is very surprising, but one can not determine the average payload with this method. This method only utilizes a few microcapsules and the shell would most likely to rupture at the weakest point of the polymeric shell, therefore skewing the data. The three methods used to determine the microcapsule payload resulted in three different answers. It is still uncertain which of the payload values are correct.

Reproduction of JN4-72 Microcapsules

With the limited success of encapsulating the IDEO adduct, one can move on and employ them into an epoxy matrix for self-healing testing. In order to do self-healing tests, producing a large amount of capsules is needed. Attempts to replicate the experiment JN4-72 have been very difficult to achieve. Subsequent attempts have encapsulated the amine adduct but often led to large microcapsules and/or agglomerate during the encapsulation process. A series of experiments has been performed to try to produce more IDEO adduct capsules to be used in self-healing testing.

The first set of tests was attempted to replicate the experiment JN4-72. The recipes to produce the capsules are identical but the magnetic stir rate was adjusted to obtain a similar vortex in the reactor between runs. Results have shown that the capsules float and often agglomerate into large particulates in the millimeter size range. A second crop of polymer particle was present in all of the experiments. A table of experiments for repeating JN4-72 can be found in Appendix H, Table H-1.

A next set of experiments used mechanical stirring (paddle stirrer attached to a mixer) instead of magnetic stirring (magnetic stir plate with 30mm oval stir bar). Magnetic stirring has shown to be unreliable in maintaining the same speed (RPM) throughout and between experiments. Therefore, mechanical stirring might resolve the uncertainty in using magnetic stirring. A list of experiments performed are found in Table F-2 in Appendix F. Numerous variables have been changed, such as surfactant concentration, solid content, stirring speed, and homogenization speed, but always resulted in undesirable results. A majority of the experiments often led to capsules that are very large 300-800um with yields varying from very low to moderate.

With numerous attempts to encapsulate the amine adduct only one experiment, JN4-72, has been successful in producing a high yield of capsules in the correct size range and payload. Based on the information from the experiments trying to reproduce JN4-72, it is clear that the conditions for a successful encapsulation are very sensitive to changes in the reactor conditions and the recipe. To date we have not been able to reproduce the results of JN4-72.

CHAPTER 4

CONCLUSIONS AND RECOMMENDATIONS

Conclusions

The work in this thesis has shown that the concept of self-healing can be achieved. Work with the dicylopentadiene microcapsule and Grubb's catalyst system has furthered our understanding on how to test and produce a previously demonstrated self-healing system. A new system involving a dual microcapsules system became the main focus of the thesis.

Computational results have suggested that the epoxy resin and amine microcapsule system is feasible for self-healing. Modeling results have revealed that a set of microcapsules, once broken, may release their contents, fill a microcrack by capillary flow, and sufficiently mix by diffusion prior to significant reaction of the healing agents. Providing that sufficient adhesion between the new polymer and the walls of the crack is achieved, this appears to lead to successful self-healing.

Encapsulation of the epoxy resin was easily achieved. Encapsulation with urea formaldehyde resulted with capsules in the 80-120 μ m range and has an 80% payload. The capsules can be dried into a free flowing powder and can be easily dispersed in an epoxy coating. Adhesion between epoxy resin capsules and the host epoxy matrix was sufficient to allow a crack to properly cleave the microcapsules.

With amines being soluble in aqueous and organic media, traditional encapsulation methods are difficult to perform. Various amine adducts were produced to be hydrophobic but often crystallized over time. However, an isophorone diamine and 1,2-epoxyoctane (IDEO) adduct was made and has been shown to have a low water solubility, achieve good reactivity with the epoxy resin, and does not crystallize. It has been discovered that the amine adduct does become ionized at lower pH, therefore making the adduct more water soluble. This result limits the number of possible encapsulation techniques that can be used to encapsulate the amine adduct, however free radical in-situ polymerization was successful in encapsulating the amine adduct when using an acrylic polymer as the shell. The microcapsules range in sizes from 70-150 μm and have a reasonable payload. The capsules are able to be dried into a free flowing powder and can be dispersed into an epoxy coating. However, reproducing the encapsulation process has proven to be very difficult.

Though reproducibility is an issue, the adhesive properties with a mixture of amine adduct capsules and epoxy resin capsules have proven to be successful by binding two pieces of epoxy strongly together. This result shows the great potential of the dual microcapsule self-healing system.

Recommendations

There are still multiple issues that must be addressed with the chemical analysis, and encapsulation of the amine hardener. The chemical properties of the IDEO adduct, the reproduction of amine encapsulation, and the self-healing two part microcapsule

system requires further investigation. Analysis of the amine adduct via NMR has proven difficult because the isophorone diamine is obtained as a mixture of cis and trans configurations. The two configurations make it difficult to identify peaks in carbon and proton NMR. The time to identify each peak requires extensive knowledge about NMR analysis of amines. If possible, one can purchase or purify the isophorone diamine to have one specific configuration and then perform NMR studies. Other techniques such as Carbon Hydrogen Nitrogen (CHN) analysis, Gel Permeation Chromatography (GPC), Liquid Chromatography (LC), and Mass Spectrometry (MS) should be performed to determine the number of epoxide groups that have reacted with the isophorone diamine to produce the IDEO amine adduct.

Epoxy resin microcapsules were easily produced but, encapsulation of the adduct has been very difficult. The current investigation has shown that this encapsulation process is very sensitive to the reaction conditions. Though encapsulation of the amine adduct is achieved, the microcapsules tend to be very large and agglomerate together. Further investigation of the free radical in-situ polymerization process is needed. More specifically, studies on how the second crop is formed and what kind of influences the second crop has on the production and properties of the IDEO microcapsules are needed. Other variables such as solid content, surfactant concentration, and mixing should be thoroughly addressed. Production of large quantities of microcapsules is important to have ability to perform tests on self-healing. Encapsulation by other means should be studied in conjunction with in-situ polymerization. Methods such as spray drying and co-extrusion could be used to encapsulate an amine or the amine adduct.

Proving the concept of self-healing with the two-part microcapsules system is important to this project. After producing a significant amount of amine capsules, fracture testing with the tapered double cantilever beam specimens should be performed to compare healing efficiencies with the ones published by Scott White⁵ and the ones achieved with DCPD capsules and Grubb's catalyst system mentioned in this thesis. A second mechanical testing method suggested by Dr. Michal Kaperski to monitor the time evolution of self-healing process with the Dynamic Mechanical Analyzer (DMA) is suggested. In the present literature, there is no test proposed or proven to monitor the dynamics of self-healing, where most methods perform tests before and after healing. This test has the potential to supply unique data, such as the rate of the self-healing system and also to determine if self-healing can be achieved with the continuous variation of stress in the healing sample held in the DMA instrument.

LIST OF REFERENCES

- 1) Dry, C. *Composites Structures*, 1996, 35, 263-269.
- 2) Pang, J.W.C.; Bond, J.P. *Composites: Part A: Applied Science and Manufacturing*, 2005, 36, 183-188.
- 3) Pang, J.W.C.; Bond, J.P. *Composites Science and Technology*, 2005, 65, 1791-1799.
- 4) Bleay, S.M.; Loader, C.B.; Hawyes, V.J.; Humberstone, L.; Curtis, P.T. *Composites: Part A*, 2001, 32, 767 -1776.
- 5) E.N. Brown; N.R Sottos; S.R White. *Experimental Mechanics*, 2002, 42, 372-379.
- 6) A.S. Jones; J.D. Rule; J.S. Moore; N.R Sottos; S.R White. *Journal of the Royal Society Interface*, 2007, 4, 13, 395-403.
- 7) M. R Kessler; S.R White. *Composites Part A: Applied Science and Manufacturing*, 2001, 32, 5, 683-699.
- 8) Brown, E.N.; White, S.R.; Sottos, N.R. *Journal of Materials Science*, 2004, 39, 1703- 1710.
- 9) Brown, E.N.; White, S.R.; Sottos, N.R. *Proceedings of the Materials Research Society*, Fall 2002.
- 10) Wudl, F.; Chen, X.; Nutt, S.R; Shen, H. *Macromolecules*, 2002, 295, 1698-1702.
- 11) Wudl, F. *Thermally re-mendable crosslinked polymers*, United States Patent Application: 20040014933, January 22, 2004
- 12) Toohey, Kathleen S.; Nancy R. Sottos; Jennifer A. Lewis; Jeffrey S. Moore; Scott R. White.. *Letters to Nature*, June 2007.
- 13) Williams G.J.; Trask R.S.; Bond I.P. *A Self-Healing Carbon Fibre Reinforced Polymer for Aerospace Applications*, 12th European Conference on Composite Materials, Biarritz, France, Aug.29-Sept. 1, 2006.
- 14) Trask, R.S.; Bond, J.P. *Smart Materials Structures*, 2006, 15, 704-710.
- 15) www.merriam-webster.com
- 16) Bejan, A.; Lorente, S.; Wang, K.-M. *Journal of Applied Physics*, 2006, 100.

- 17) Therriault D.; Robert F. Shepard; Scott R. White; Jennifer A. Lewis; *Advanced Materials*, 2005, 17, 4.
- 18) Rule J.D.; E.N. Brown; N.R Sottos; S.R White; J.S. Moore; *Advanced Materials*, 2005, 17, 2, 205-208.
- 19) E.N. Brown; M.R Kessler; N.R Sottos; and S.R White; *In Situ poly(urea-formaldehyde) microencapsulation of dicyclopentadiene*, Submitted to Journal of Microencapsulation, 2003.
- 20) Ghosh S.K. *Functional Coatings by Polymer Microencapsulation*, Wiley-VCH Verlag GmbH & Co., 2006.
- 21) Kondo A. *Microcapsule Processing and Technology*, University Microfilms International: Michigan, 1992.
- 22) Courtney T.H. *Mechanical Behavior of Materials second ed.*, McGraw Hill: Boston, 2000.
- 23) <http://www.matter.org.uk/glossary/index.asp?dbid=171>
- 24) Beres, W.; A. K. Koul; R. Thamburaj ; *Journal of Testing and Evaluation*, *JTEVA*, 1997, 25, 536-542.
- 25) Sundberg D.C.; J.P Claverie; Y.G Durant; *Innovative Multifunctional Anti-Corrosion Coatings Semi-Annual Report January 15, 2006*.
- 26) Weast R.C. *Handbook of Chemistry and Physics 50th Edition*, 1969-1970, F-31.
- 27) Gupta, R.K. *Polymer and Composite Rheology Second Edition Revised and Expanded*, Marcel Dekker: New York, 2000.
- 28) Kessler, M.R; White, S.R. *Journal of Polymer Science: Part A: Polymer Chemistry*, 2002, 40, 2373-2383.
- 29) Sundberg D.C., J.P Claverie, Y.G Durant. *Innovative Multifunctional Anti-Corrosion Coatings Semi-Annual Report December 23, 2004*.
- 30) Sundberg D.C., J.P Claverie, Y.G Durant. *Innovative Multifunctional Anti-Corrosion Coatings Semi-Annual Report June 30, 2005*.
- 31) K. Dietrich; H. Herma; R Nastke; E. Bonatz; W. Tiege; *Acta Polymerica*, 1989, 40, 243-251.

- 32) Yoshizawa, H. E.; Kamio Hirabayashi; J. Jacobson; Y. Kitamura; *Journal of Microencapsulation*, 2004, 21, 241-249.
- 33) Vergnaud J.M.; T.M. Aminabhavi; H.T.S. Phayde; J.D. Ortego; *Polymer* 1996, 37, 1677-1684.
- 34) Odian G. *Principles of Polymerization 4th ed.* Wiley Interscience: New York, 2004.
- 35) Willett P.S.; R.D. Wald; R.S. Frank; R. Carrozzella; *Water-based Adhesive Compositions with Polyamine Curative and Binder*; United States Patent Application US2004/0258922 A1, Dec. 23, 2004.
- 36) Howard, P.H.; Meylan, W.M. *Handbook of Physical Properties of Organic Chemicals*. Lewis Publisher: Boca Raton, 1997.
- 37) www.Chemsilico.com
- 38) Sundberg D.C., Y.G Durant. *Innovative Multifunctional Anti-Corrosion Coatings Semi-Annual Report June 13, 2007*.
- 39) McMurray, J. *Organic Chemistry 6th ed.* Thomson:United States 2004.
- 40) Beck, Charles L., *Diffusion Controlled Delivery of Antifouling Agents from marine coatings*; Masters of Science Thesis University of New Hampshire 1997, 150-153.
- 41) <http://www.wako-chem.co.jp/specialty/oilazo/V-65.htm>
- 42) www.Wikipedia.com
- 43) Sarac, A.S. *Progress in Polymer Science* 1999, 24, 149-1204.
- 44) Tsavalas J.G.; F.J Schork; Hans de Brouwer; Michael J. Montiero; *Macromolecules*, 2001, 34, 3938-3945.
- 45) Sundberg, D.C., Stubbs J.; Carrier R. *Kmorph 3 Software*. University of New Hampshire 2005.
- 46) ACD/HNMR ver. 1.0, ACD/Labstm
- 47) ACD/CNMR ver. 1.1, ACD/Labstm

APPENDICES

APPENDIX A

Hydrodynamic Flow Calculations for the One Part Autonomous Self Healing System

The surface tension and viscosity values of Dicyclopentadiene are taken as 28.8 dynes/cm and 0.01 poise respectively.

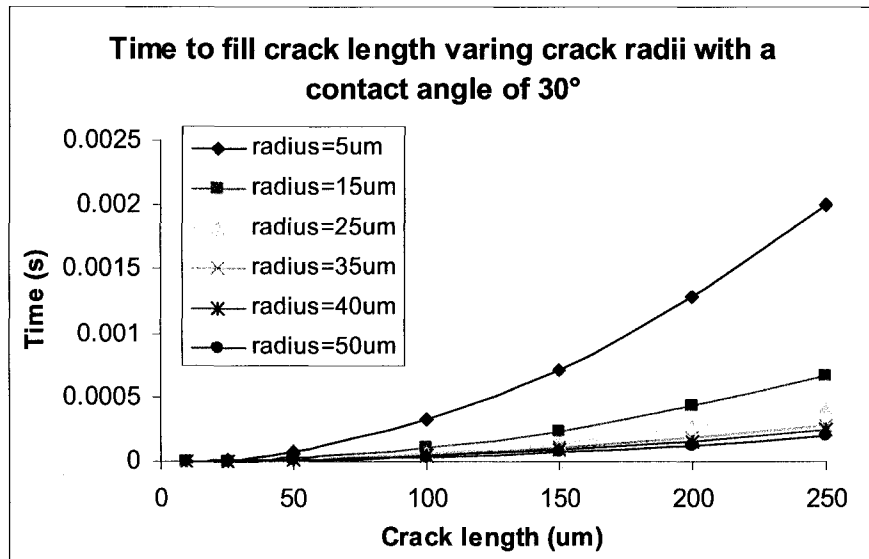


Figure A-1: Plot of time required to fill various crack lengths and crack radii with a contact angle of 30°

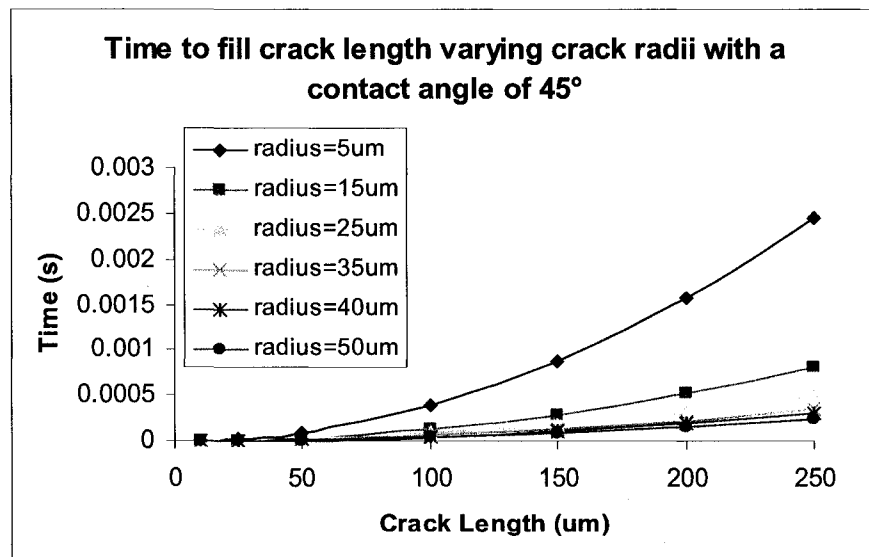


Figure A-2: Plot of time required to fill various crack lengths and crack radii with a contact angle of 45°

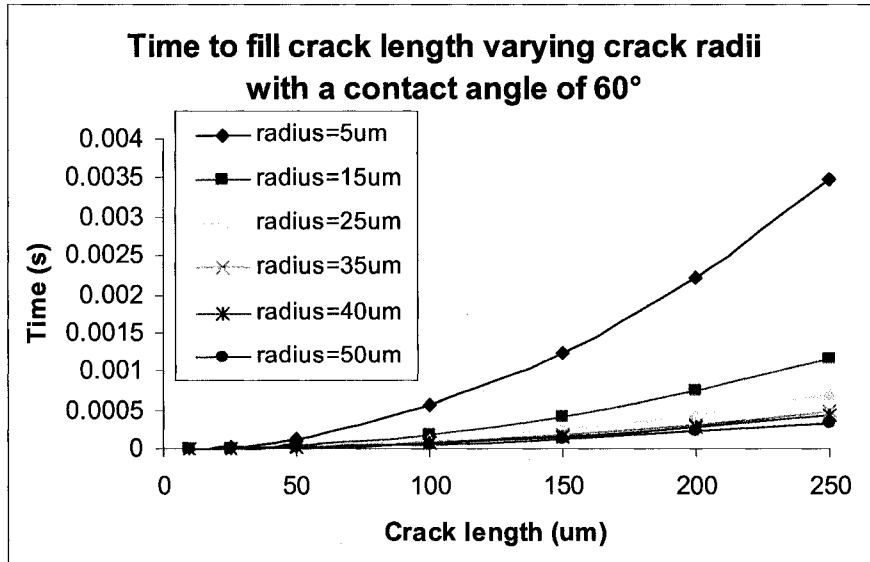


Figure A-3: Plot of time required to fill various crack lengths and crack radii with a contact angle of 60°

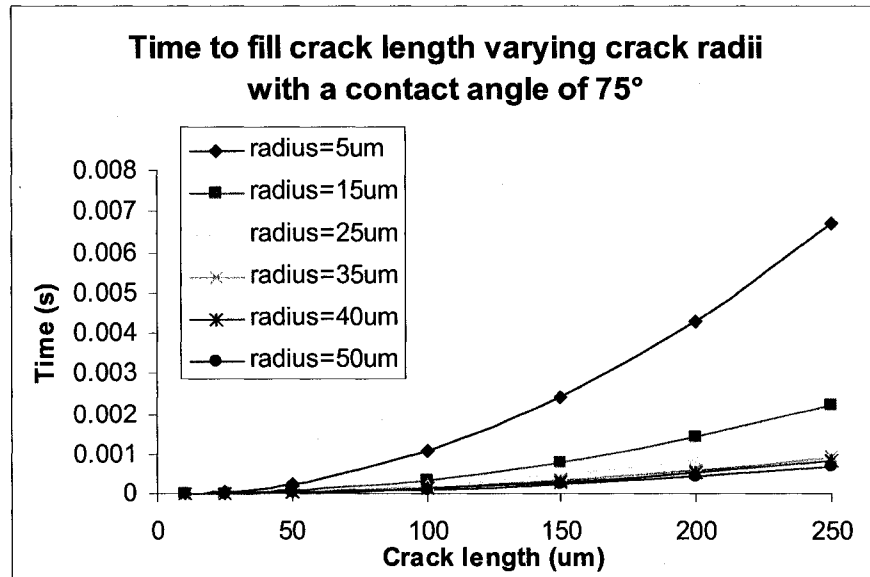


Figure A-4: Plot of time required to fill various crack lengths and crack radii with a contact angle of 75°

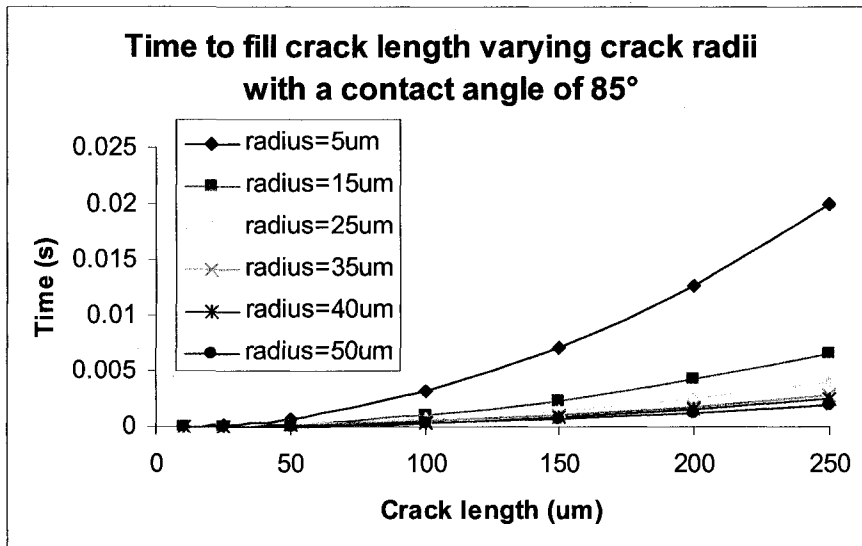


Figure A-5: Plot of time required to fill various crack lengths and crack radii with a contact angle of 85°

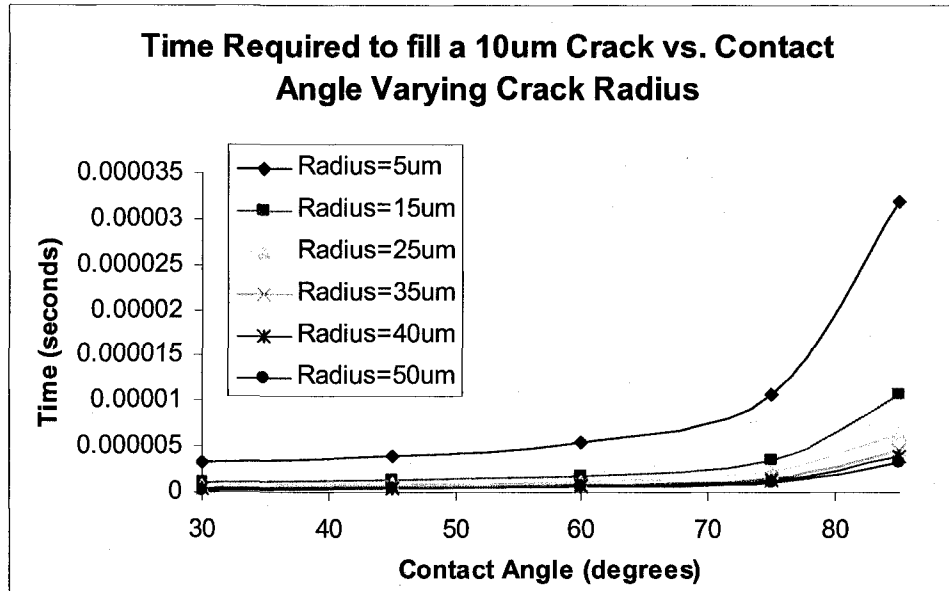


Figure A-6: Plot of time required to fill a 10um crack varying crack radii and contact angles.

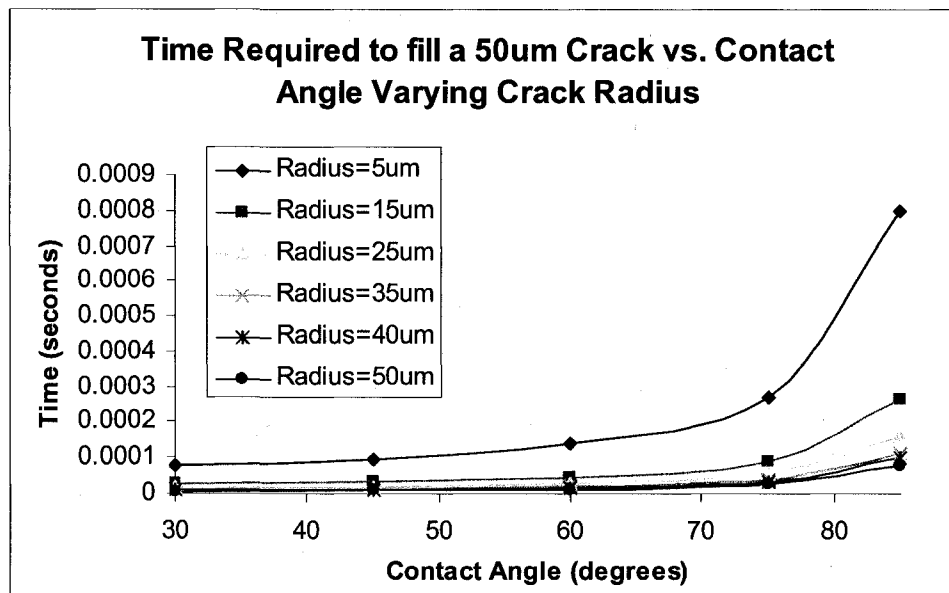


Figure A-7: Plot of time required to fill a 50um crack varying crack radii and contact angles.

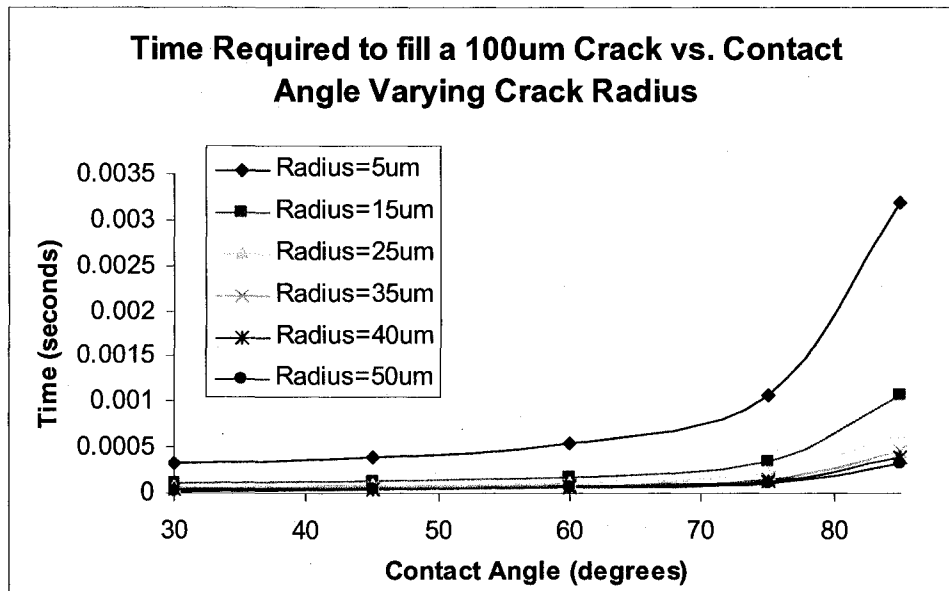


Figure A-8: Plot of time required to fill a 100um crack varying crack radii and contact angles.

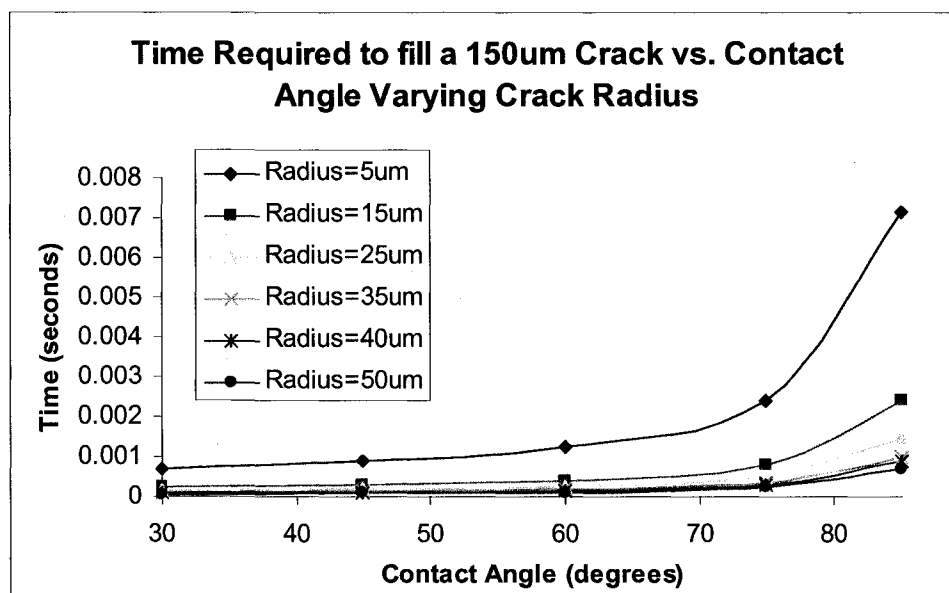


Figure A-9: Plot of time required to fill a 150um crack varying crack radii and contact angles.

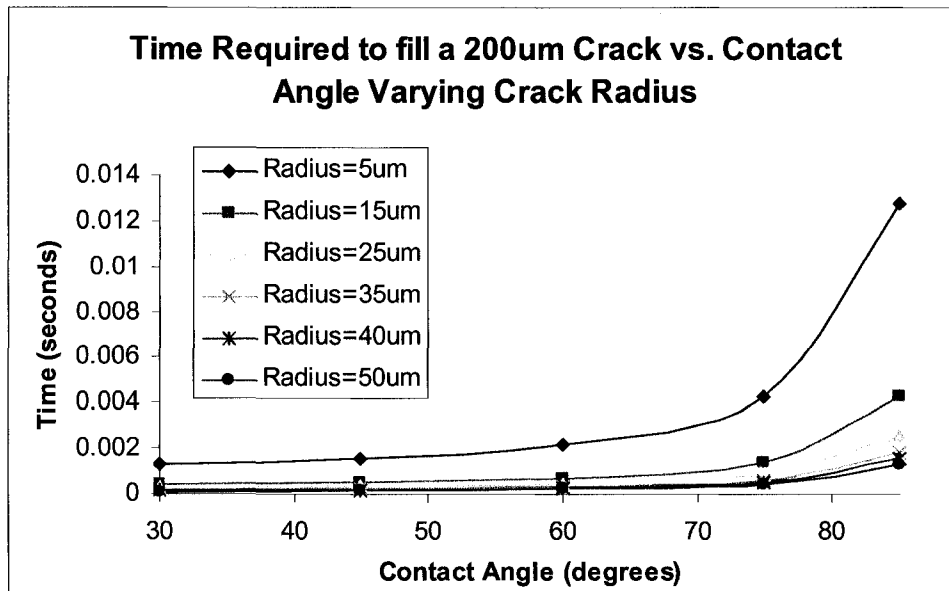


Figure A-10: Plot of time required to fill a 200um crack varying crack radii and contact angles.

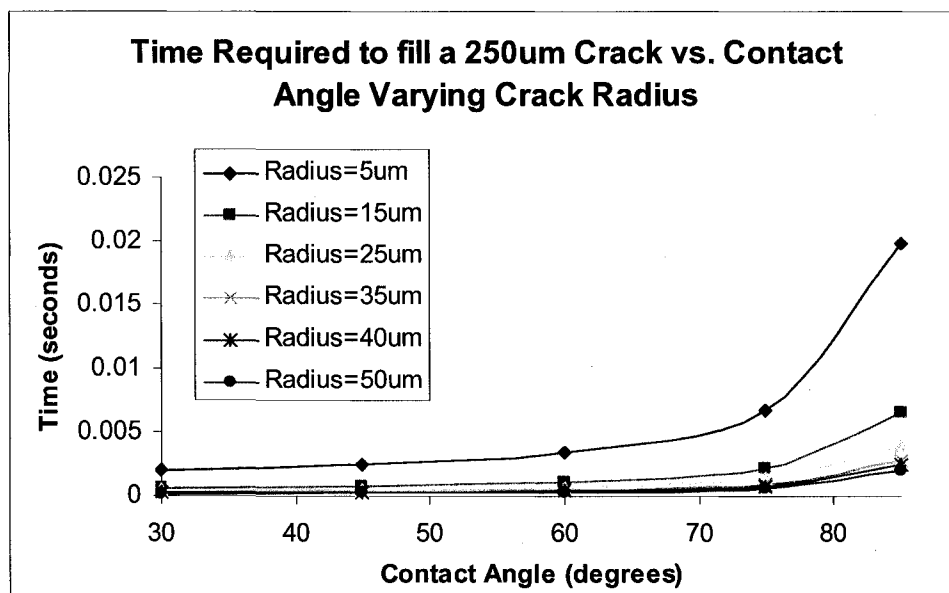


Figure A-11: Plot of time required to fill a 250um crack varying crack radii and contact angles.

APPENDIX B

Dicyclopentadiene Microcapsule DSC and Payload Data

Sample: DCPD across
Size: 15.4000 mg
Method: standard two ramp

DSC

File: C:\DSC\Jon\DCPD standard across.001
Operator: Jon
Run Date: 2005-07-08 11:47
Instrument: DSC Q100 V8.2 Build 268

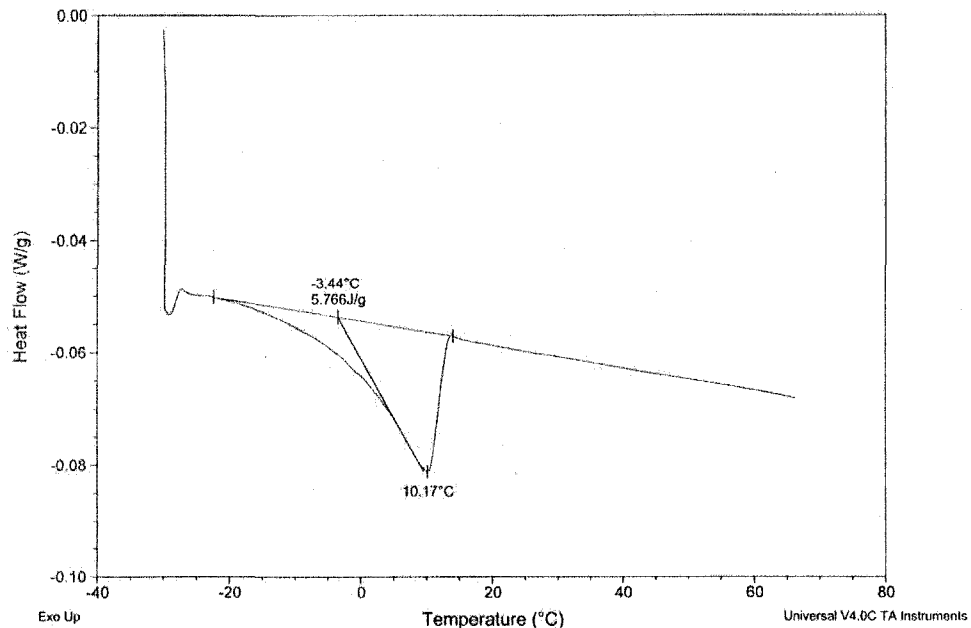


Figure B-1: DSC Trace of pure DCPD

Sample: JN1-27
Size: 13.1000 mg
Method: standard two ramp

DSC

File: C:\TA\Data\DSC\Jon\JN1-27.001
Operator: Jon
Run Date: 2005-07-11 11:28
Instrument: DSC Q100 V8.2 Build 268

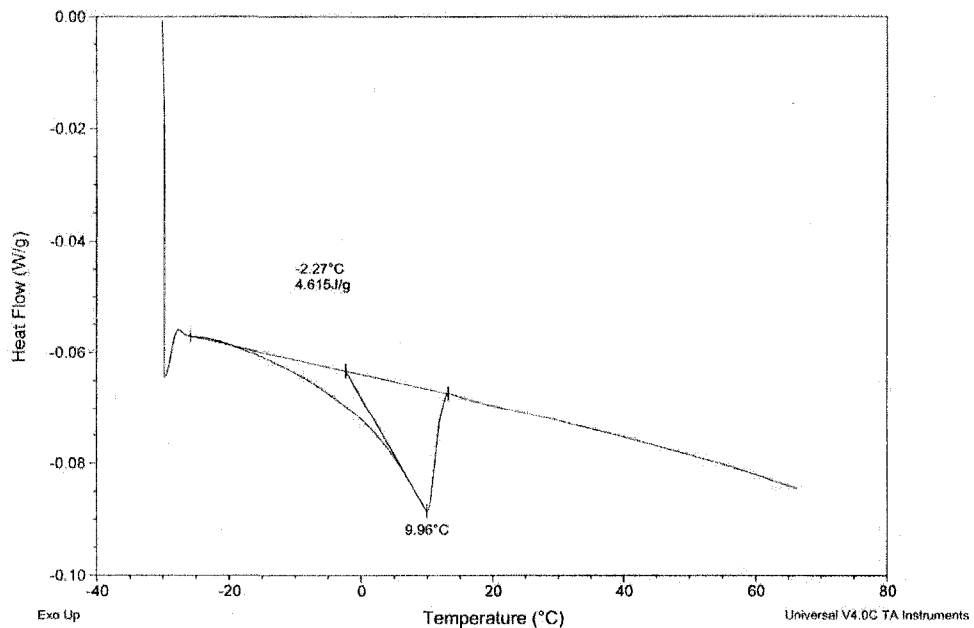


Figure B-2: DSC Trace of JN1-27 Microcapsules. Payload $= (4.615/5.766) \times 100 = 80\%$

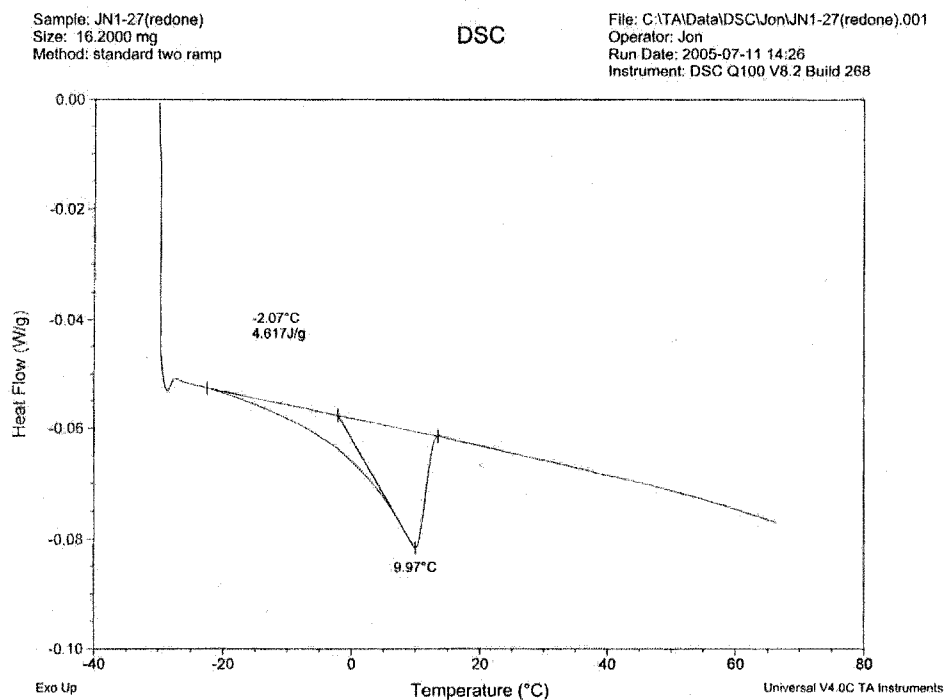


Figure B-3: A second DSC Trace of JN1-27 Microcapsules. Payload $= (4.617/5.766) \times 100 = 80\%$

Sample: JN1-29(2nd)
Size: 17.1000 mg
Method: standard two ramp

DSC

File: C:\TAI\Data\DSC\Jon\JN1-29(2nd).002
Operator:
Run Date: 2005-07-18 10:18
Instrument: DSC Q100 V8.2 Build 268

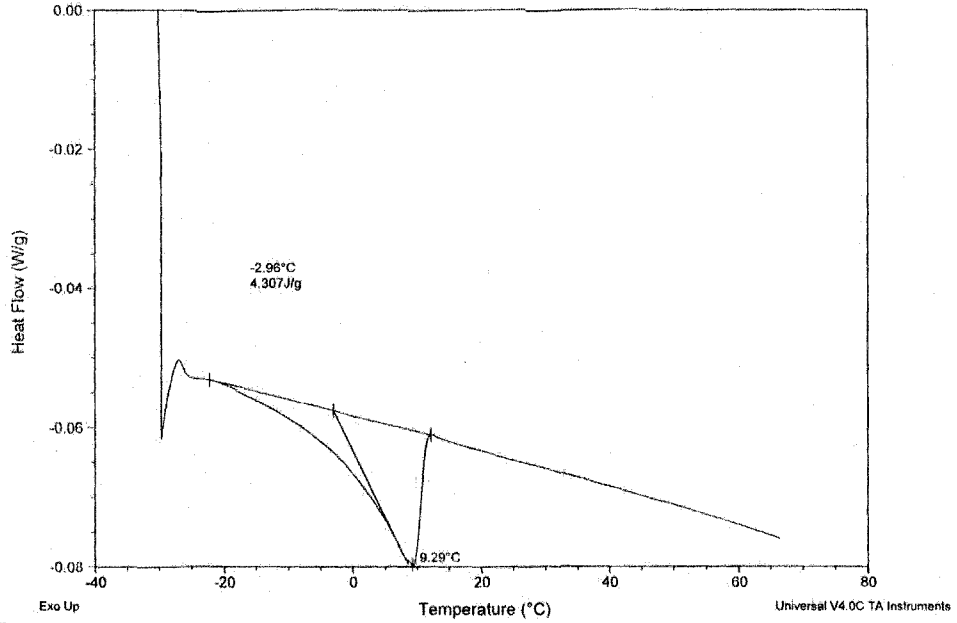


Figure B-4: DSC Trace of JN1-29 Microcapsules. Payload = $(4.307/5.766) \times 100 = 74.6\%$

Appendix C

Hydrodynamic Flow Calculations for the Two Part Autonomous Self Healing System

Epoxy Resin:

The surface tension and viscosity values of epoxy resin are taken as 47 dynes/cm and 6.4 poise respectively.

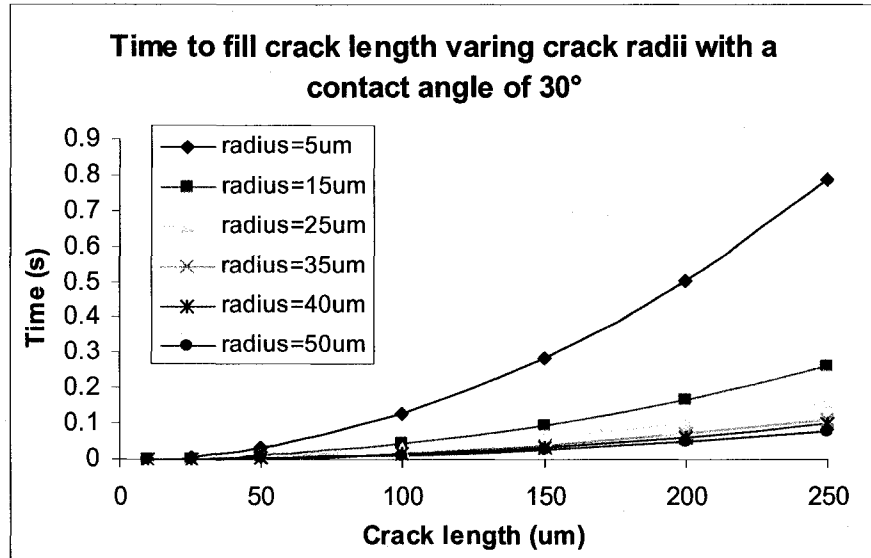


Figure C-1: Plot of time required to fill various crack lengths and crack radii with a contact angle of 30°

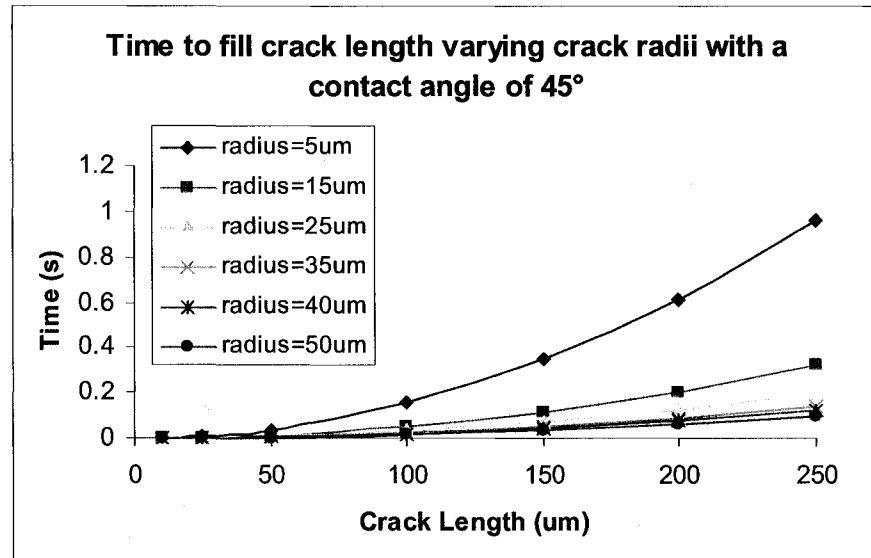


Figure C-2: Plot of time required to fill various crack lengths and crack radii with a contact angle of 45°

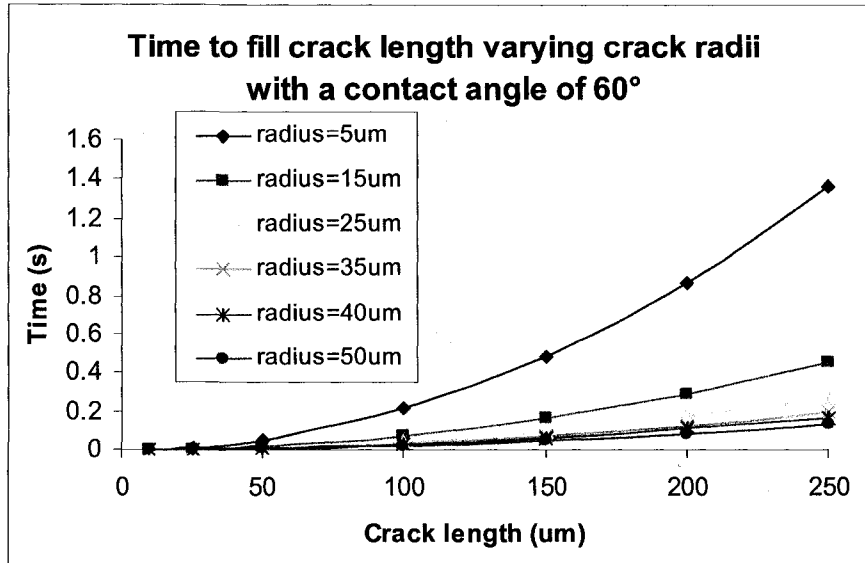


Figure C-3: Plot of time required to fill various crack lengths and crack radii with a contact angle of 60°

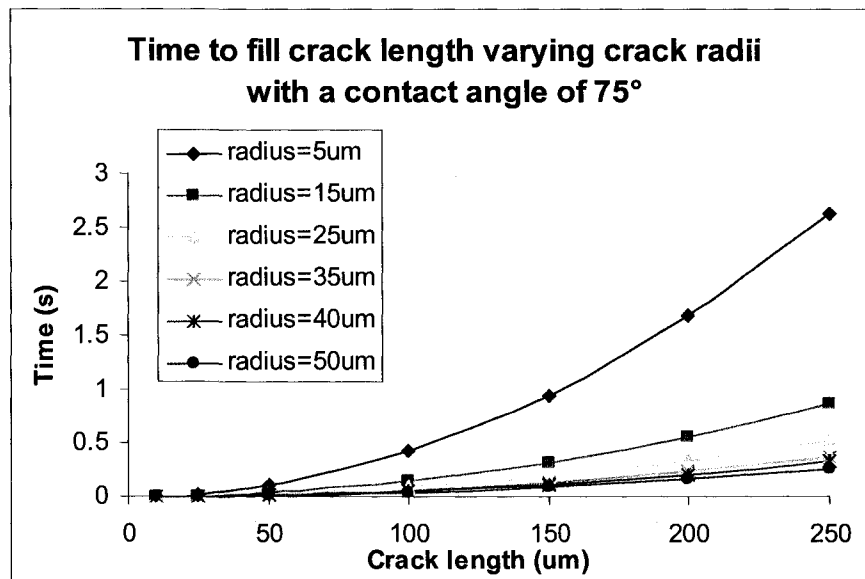


Figure C-4: Plot of time required to fill various crack lengths and crack radii with a contact angle of 75°

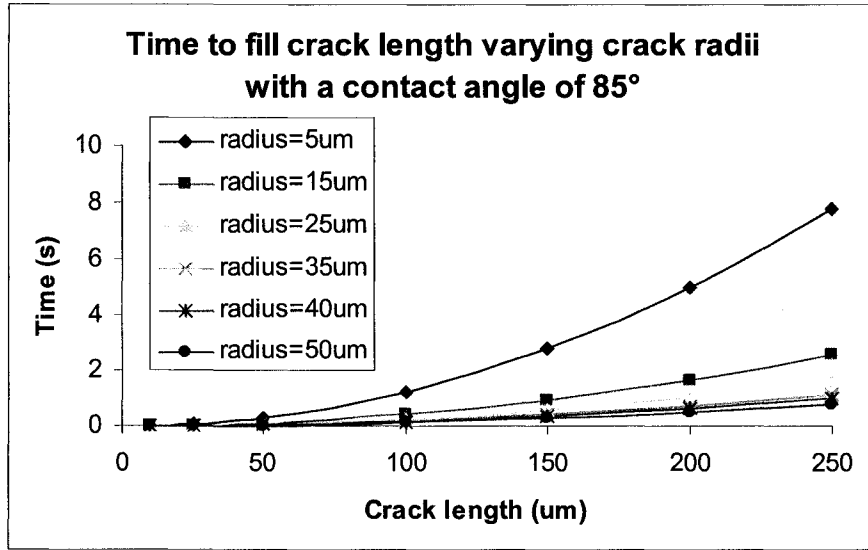


Figure C-5: Plot of time required to fill various crack lengths and crack radii with a contact angle of 85°

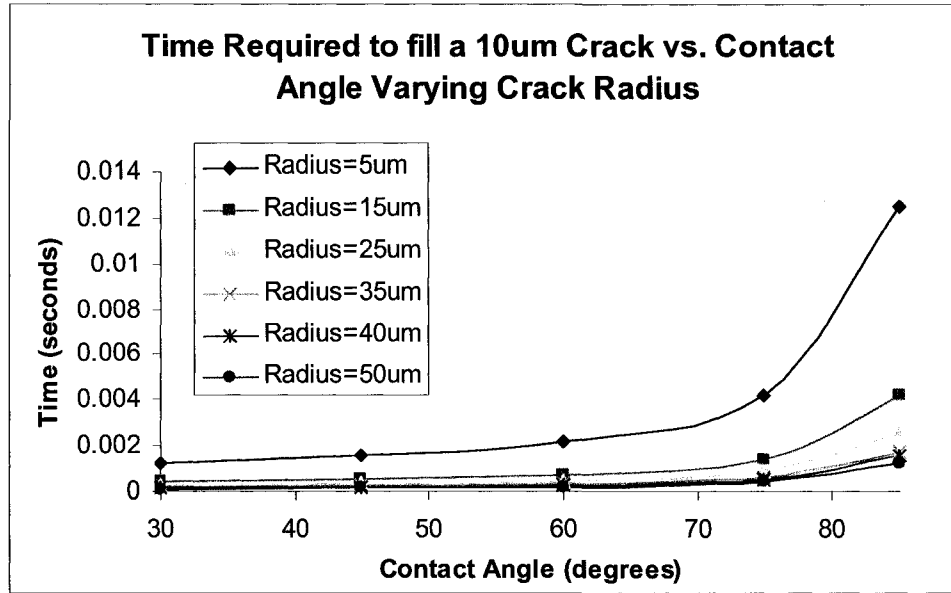


Figure C-6: Plot of time required to fill a 10um crack varying crack radii and contact angles.

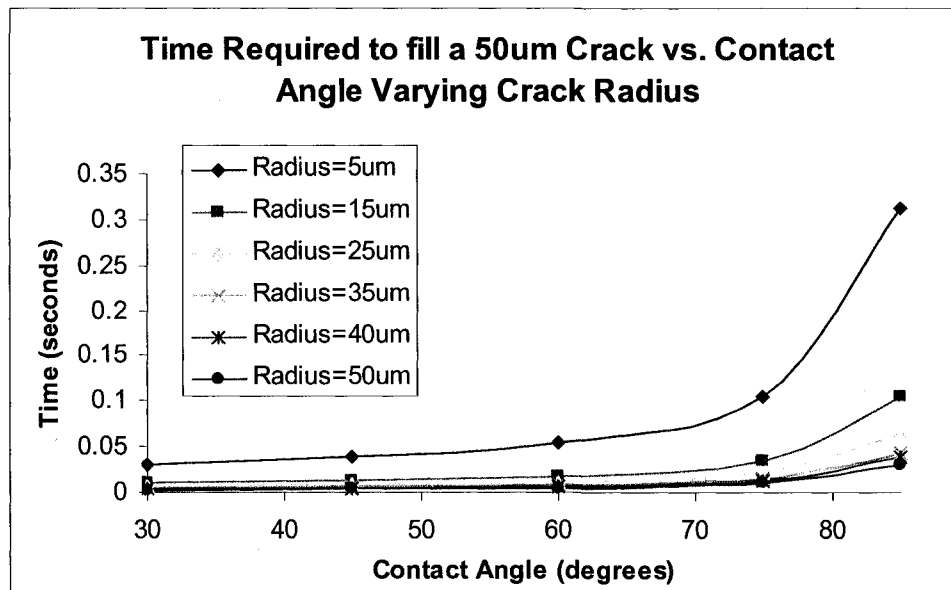


Figure C-7: Plot of time required to fill a 50um crack varying crack radii and contact angles.

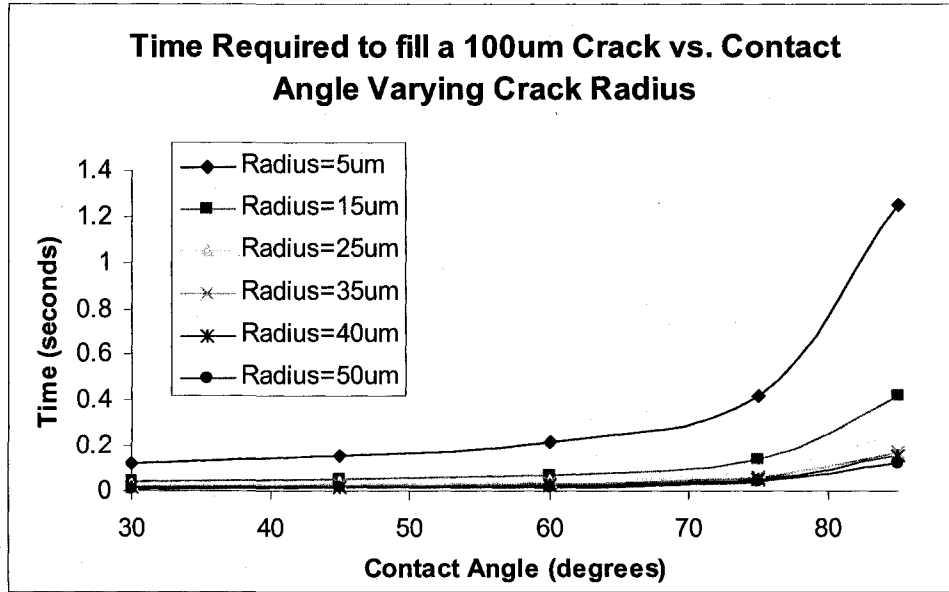


Figure C-8: Plot of time required to fill a 100um crack varying crack radii and contact angles.

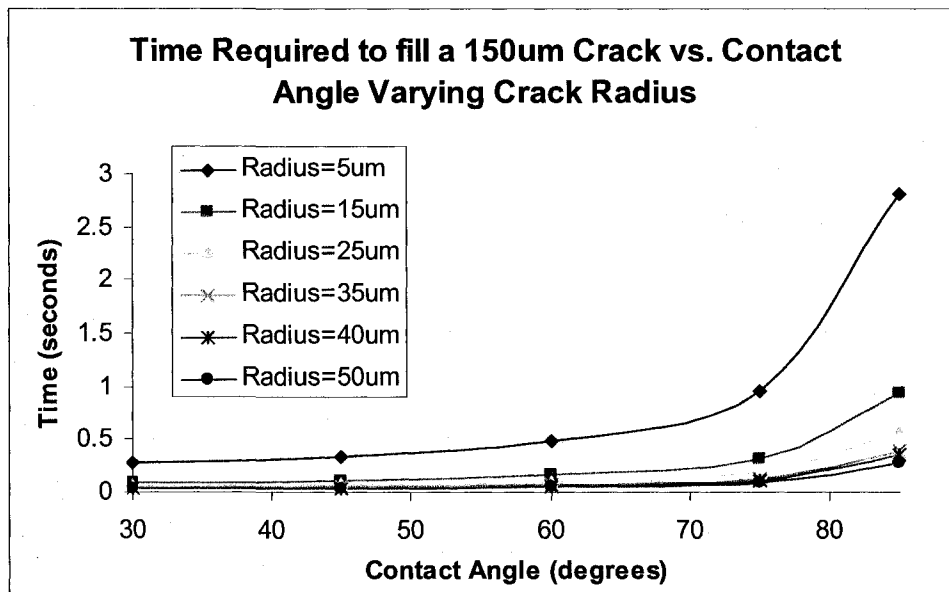


Figure C-9: Plot of time required to fill a 150um crack varying crack radii and contact angles.

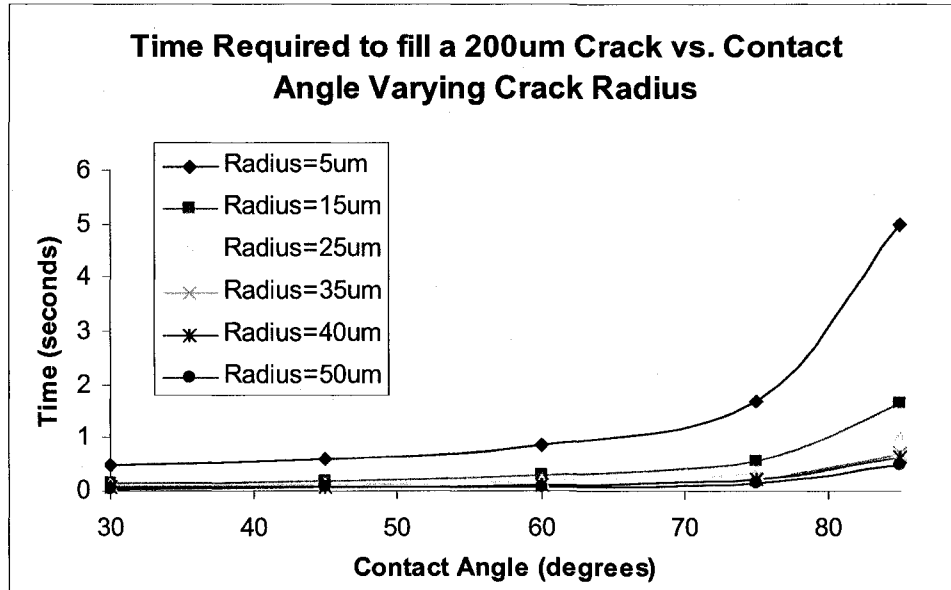


Figure C-10: Plot of time required to fill a 200um crack varying crack radii and contact angles.

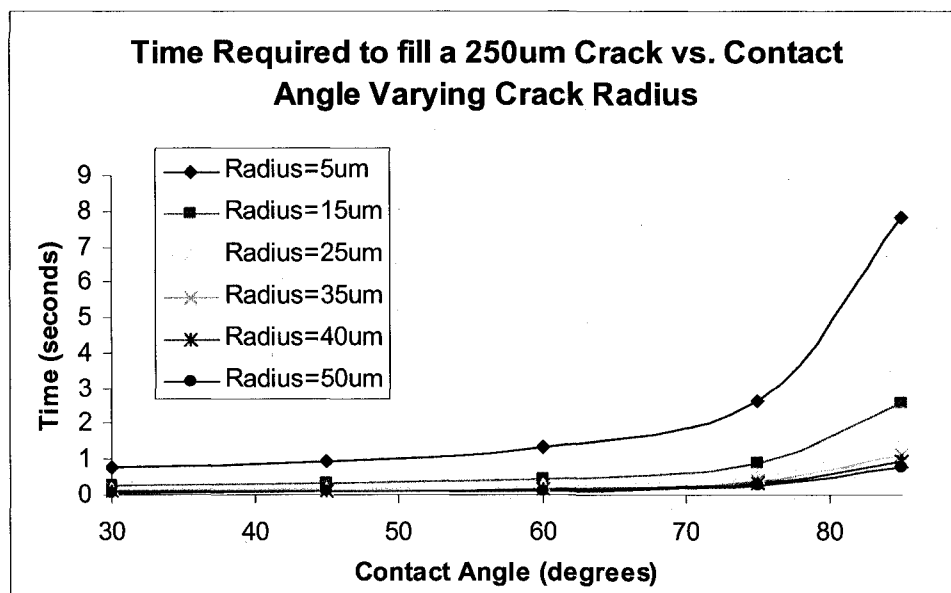


Figure C-11: Plot of time required to fill a 250um crack varying crack radii and contact angles.

Amine Adduct:

The surface tension and viscosity values of amine adduct are taken as 44 dynes/cm²⁵ and 220.4 poise respectively.

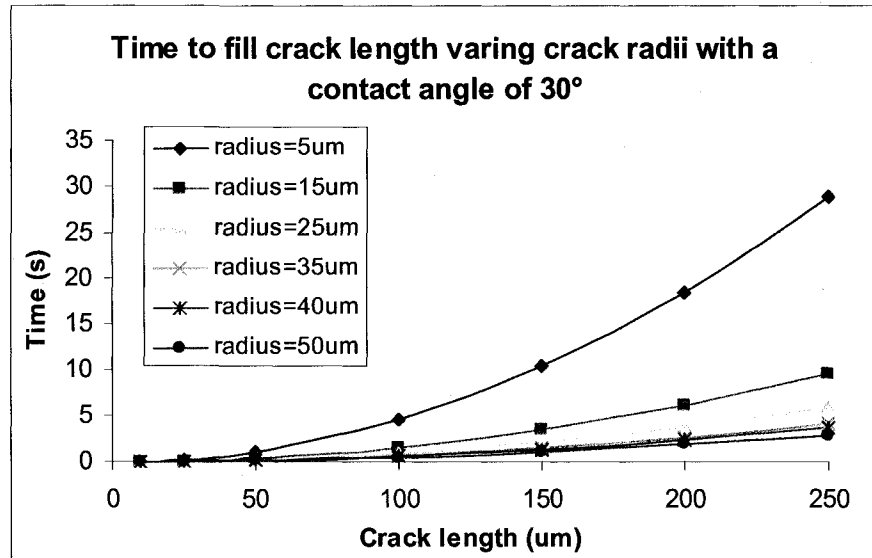


Figure C-12: Plot of time required to fill various crack lengths and crack radii with a contact angle of 30°

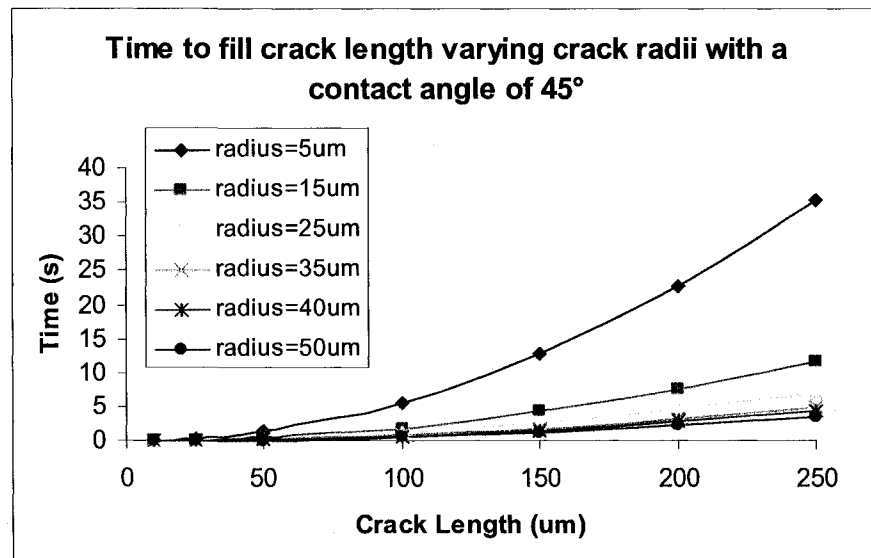


Figure C-13: Plot of time required to fill various crack lengths and crack radii with a contact angle of 45°

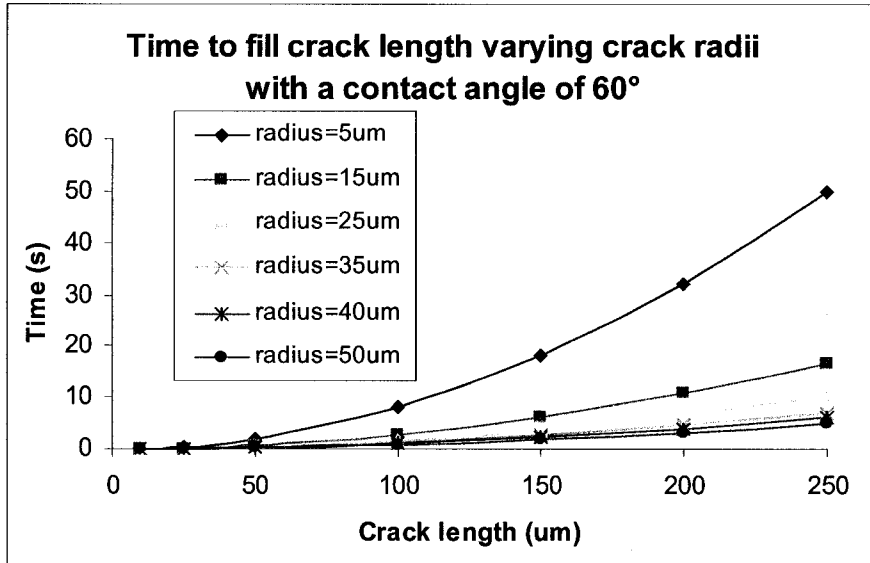


Figure C-14: Plot of time required to fill various crack lengths and crack radii with a contact angle of 60°

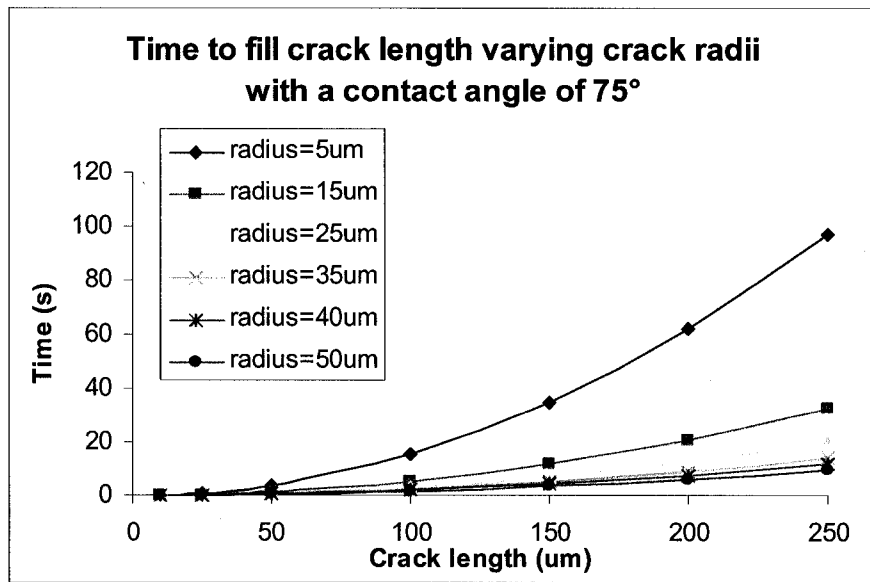


Figure C-15: Plot of time required to fill various crack lengths and crack radii with a contact angle of 75°

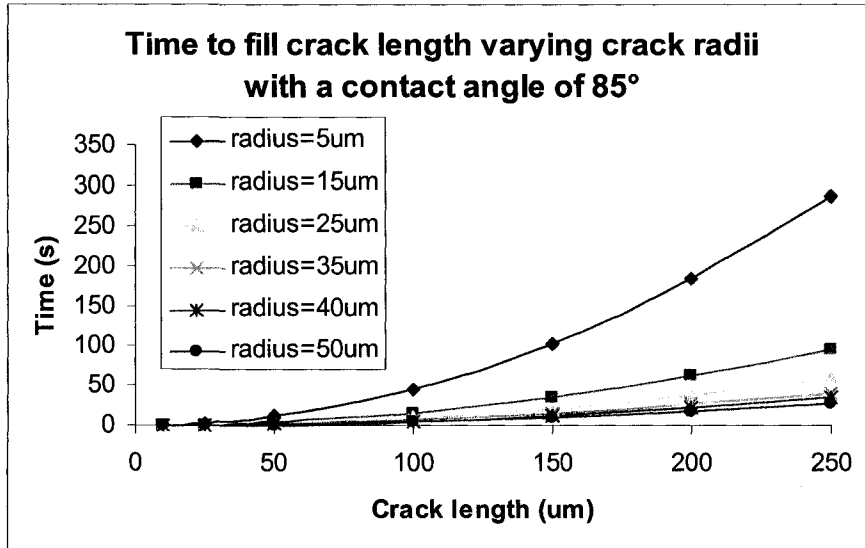


Figure C-16: Plot of time required to fill various crack lengths and crack radii with a contact angle of 85°

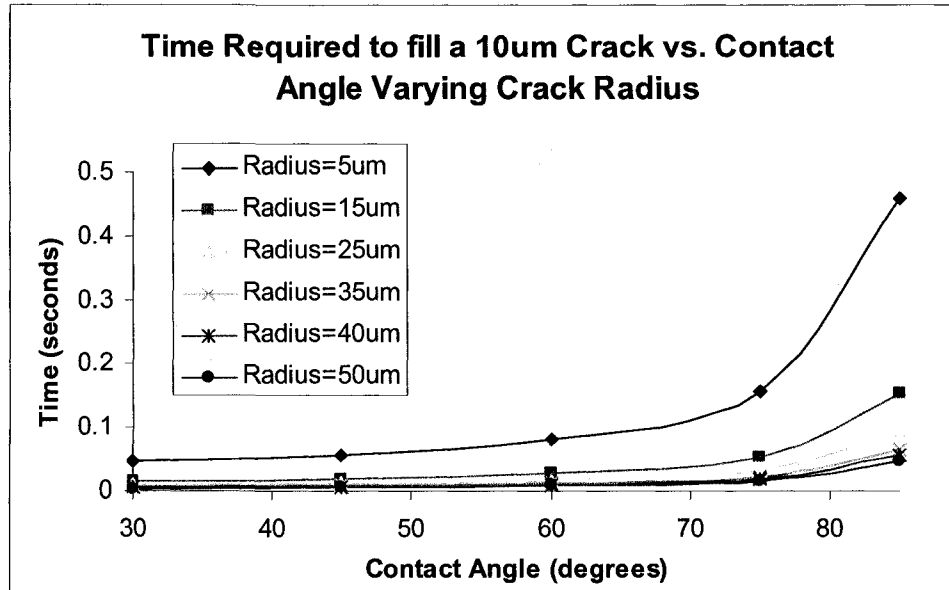


Figure C-17: Plot of time required to fill a 10um crack varying crack radii and contact angles.

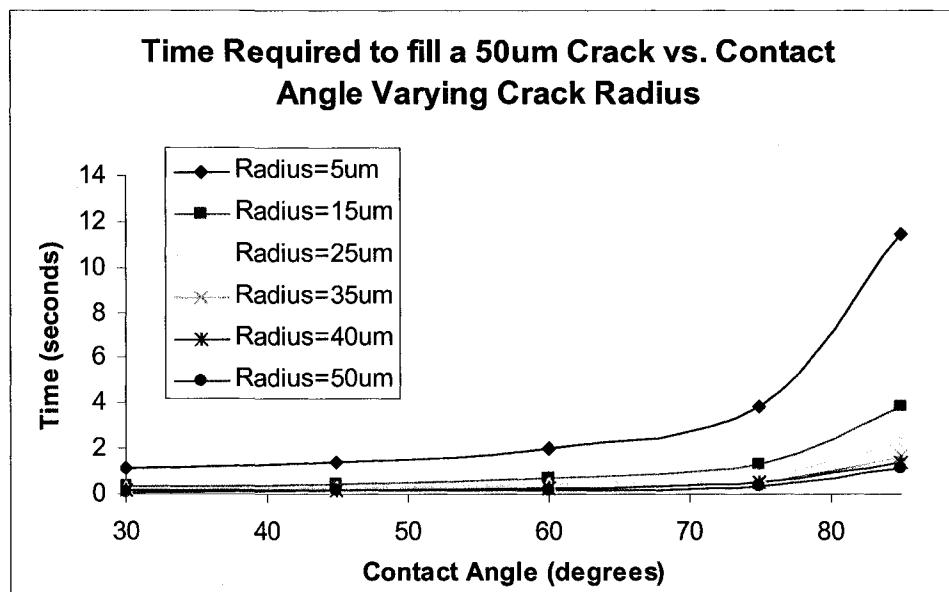


Figure C-18: Plot of time required to fill a 50um crack varying crack radii and contact angles.

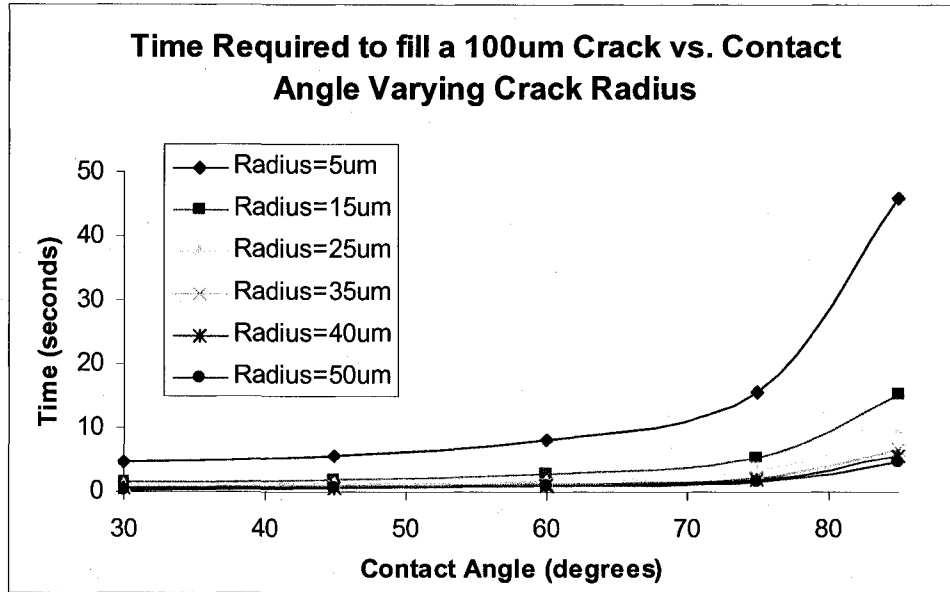


Figure C-19: Plot of time required to fill a 100um crack varying crack radii and contact angles.

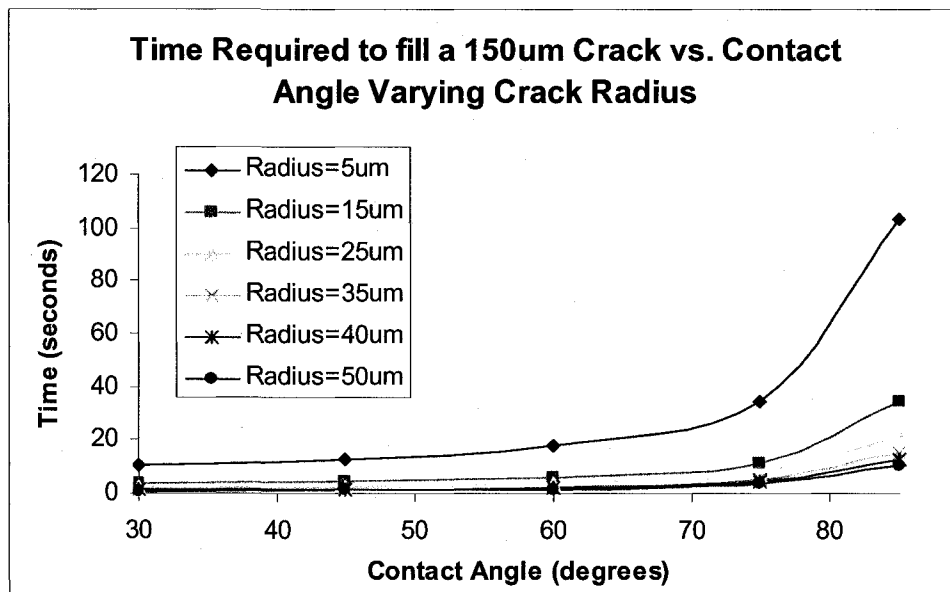


Figure C-20: Plot of time required to fill a 150um crack varying crack radii and contact angles.

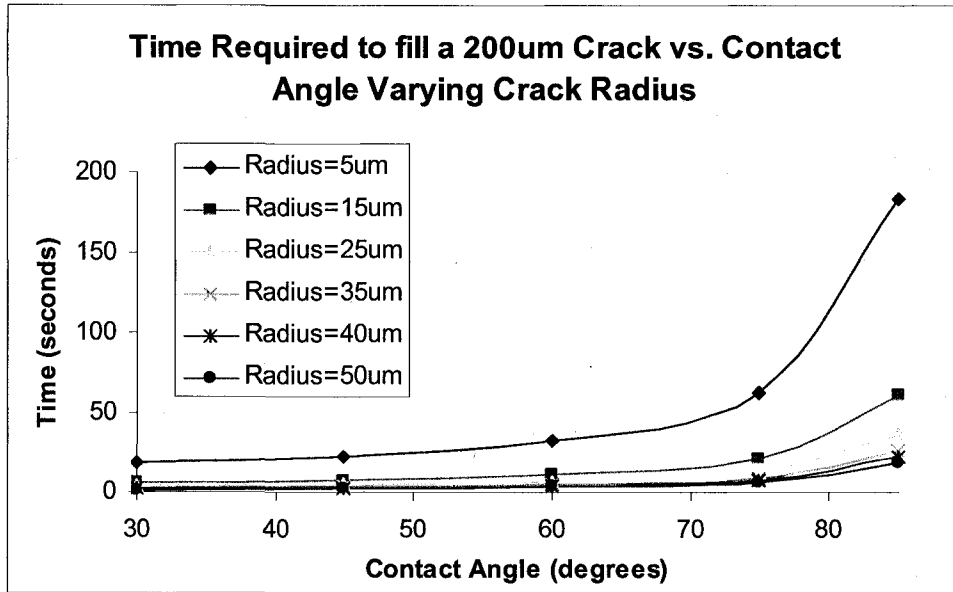


Figure C-21: Plot of time required to fill a 200um crack varying crack radii and contact angles.

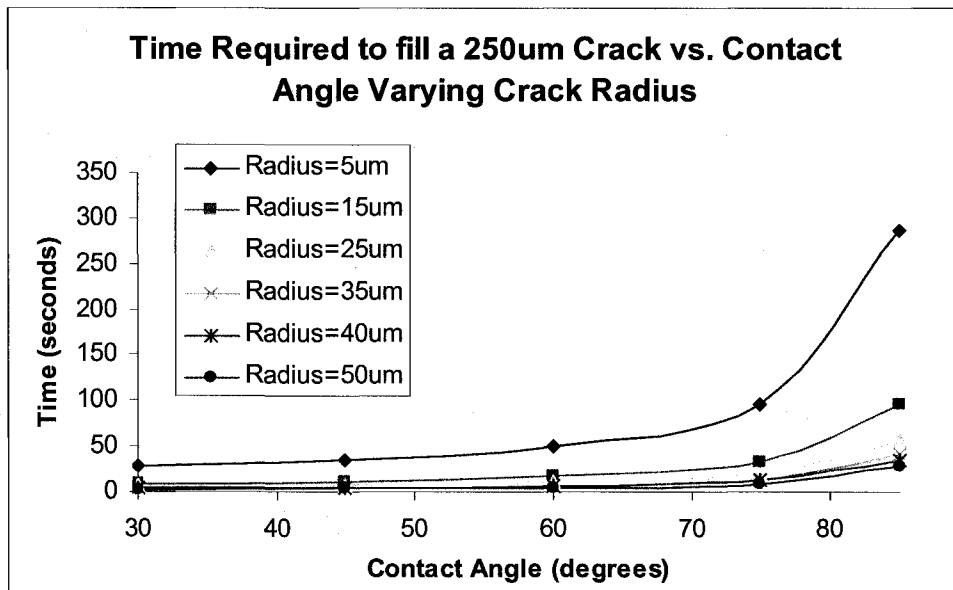


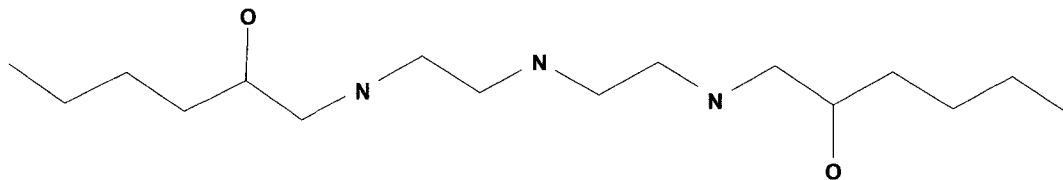
Figure C-22: Plot of time required to fill a 250um crack varying crack radii and contact angles.

Appendix D

Amine Adducts

Adduct 1:

1 mol DETA + 2 mol 1,2-Epoxyoctane



*note shown as DETA with epoxyhexane

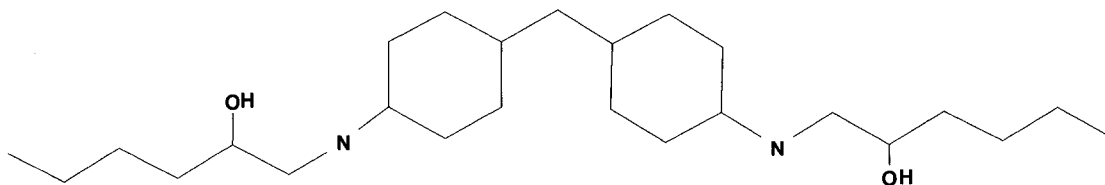
Log P = -1.4

Log P (without OH) = 0.18

Log P (without OH and middle N) = 2.1

Adduct 2:

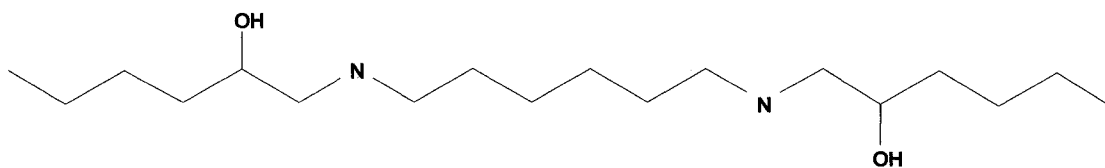
1 mol 4,4 Diaminodicyclohexylmethane + 2 mol 1,2 Epoxyhexane



Log P = 1.02

Adduct 3:

1 mol 1,6 Diaminohexane + 2 mol 1,2 Epoxyhexane

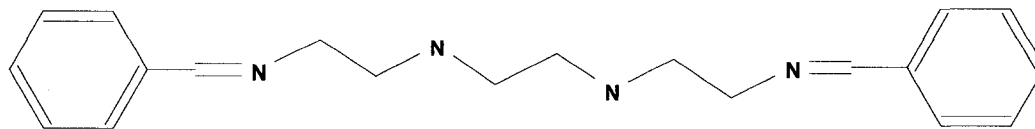


Log P = -0.26 (with OH)

Log P = 1.82 (without OH)

Adduct 4:

1 mol TETA + 2mol Benzaldehyde



Log P = 0.04

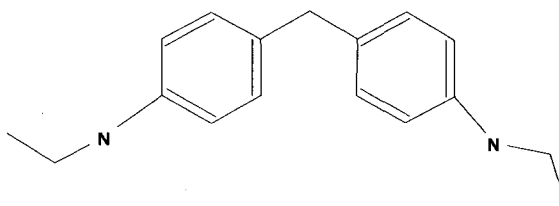
Log P (if nitrogen changed to carbon) = 4.56

Log P (if added a methyl group to each benzene ring) = 1.68

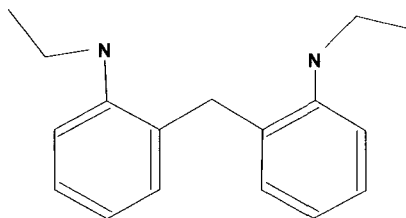
Log P (if added a ethyl group to each benzene ring) = 1.9

Adduct 5:

MDI + H₂O and alkylation of amines (with methyl/ethyl bromide)



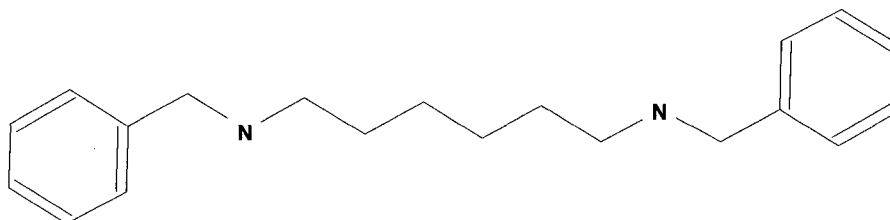
And (mixture)



Log P = unknown

Adduct 6:

1, 6 diaminohexane + benzaldehyde + catalyst



Log P = -0.07

Log P (with nitrogen changed to C) = 5.47

Log P (with nitrogen changed to C-OH) = 3.14

Appendix E

NMR Data of IDEO Adduct and Starting Components

1,2-Epoxyoctane:

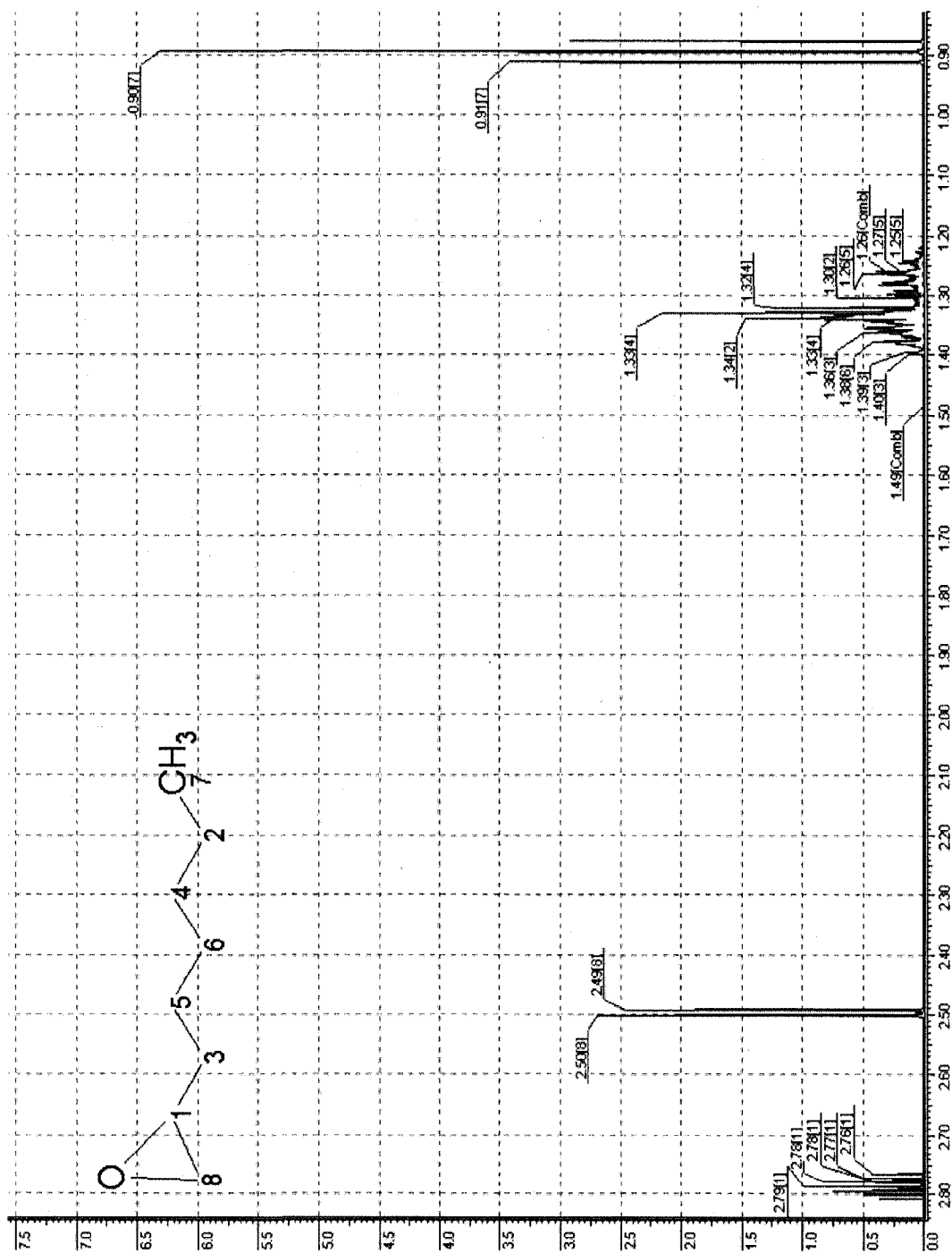


Figure E-1: Predicted Proton NMR Spectra of 1,2-Epoxyoctane.

VVPR0013058-500-bb-H
 Epoxyoctane pure (white)
 quantitative proton di=30 seconds
 Data Collected on:
 01/25/90
 File directory:
 Ar/export/home/Sundberg/vmrsys/data
 Sample directory:
 File: PROTON
 Pulse Sequence: s2pul

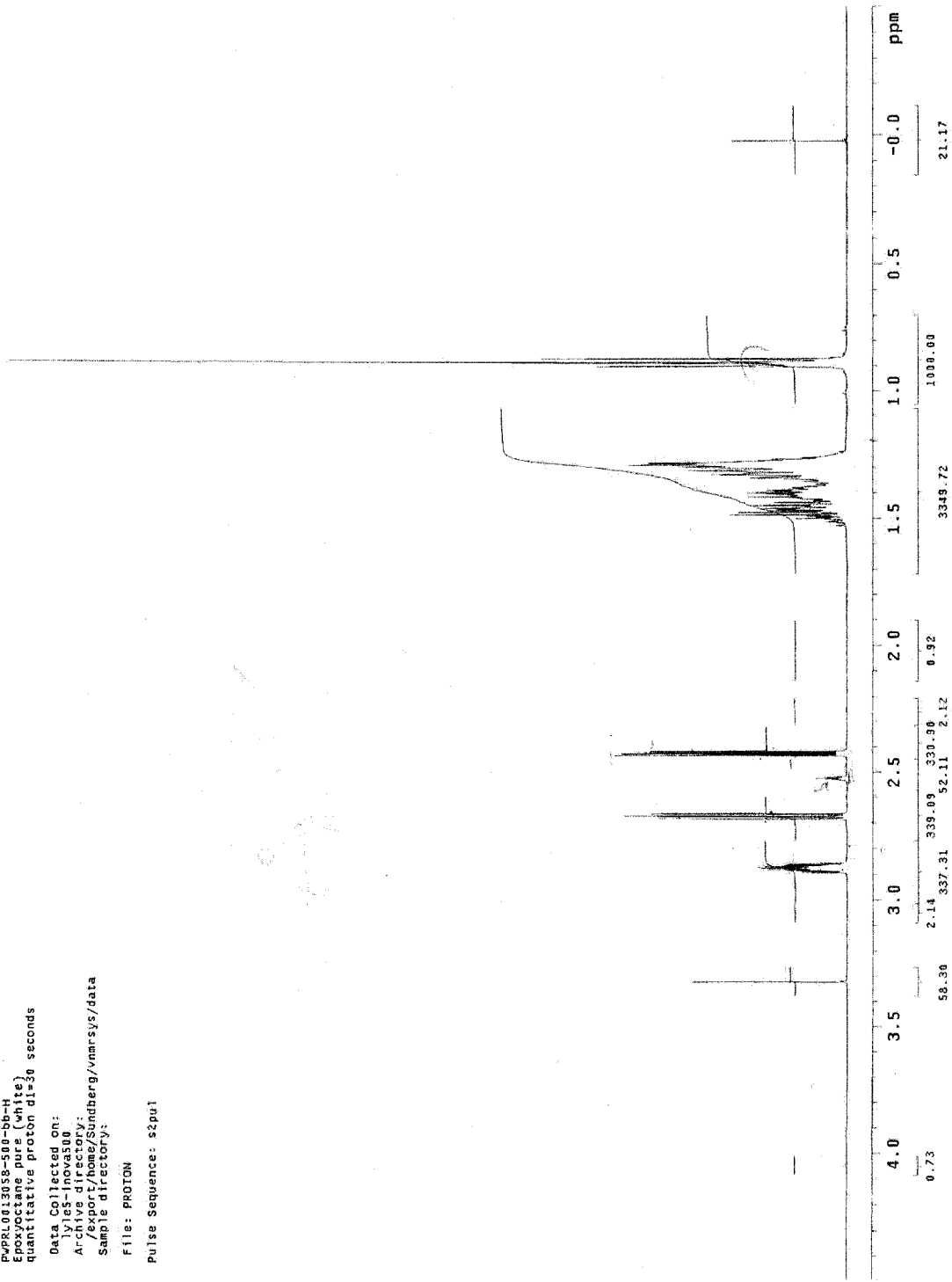


Figure E-2: Proton NMR Spectra of 1,2-Epoxyoctane.

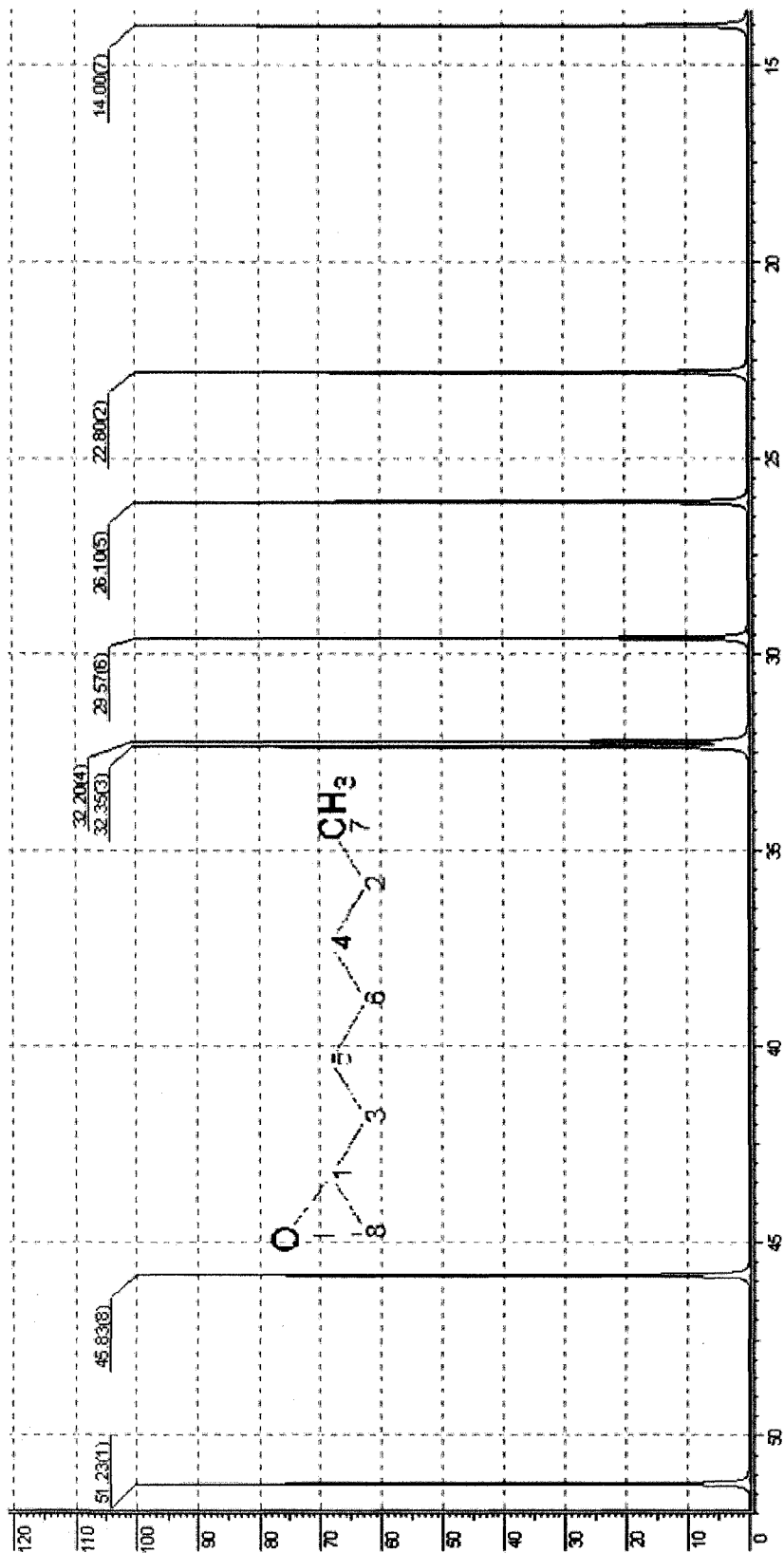


Figure E-3: Predicted Carbon NMR Spectra of 1,2-Epoxyoctane.

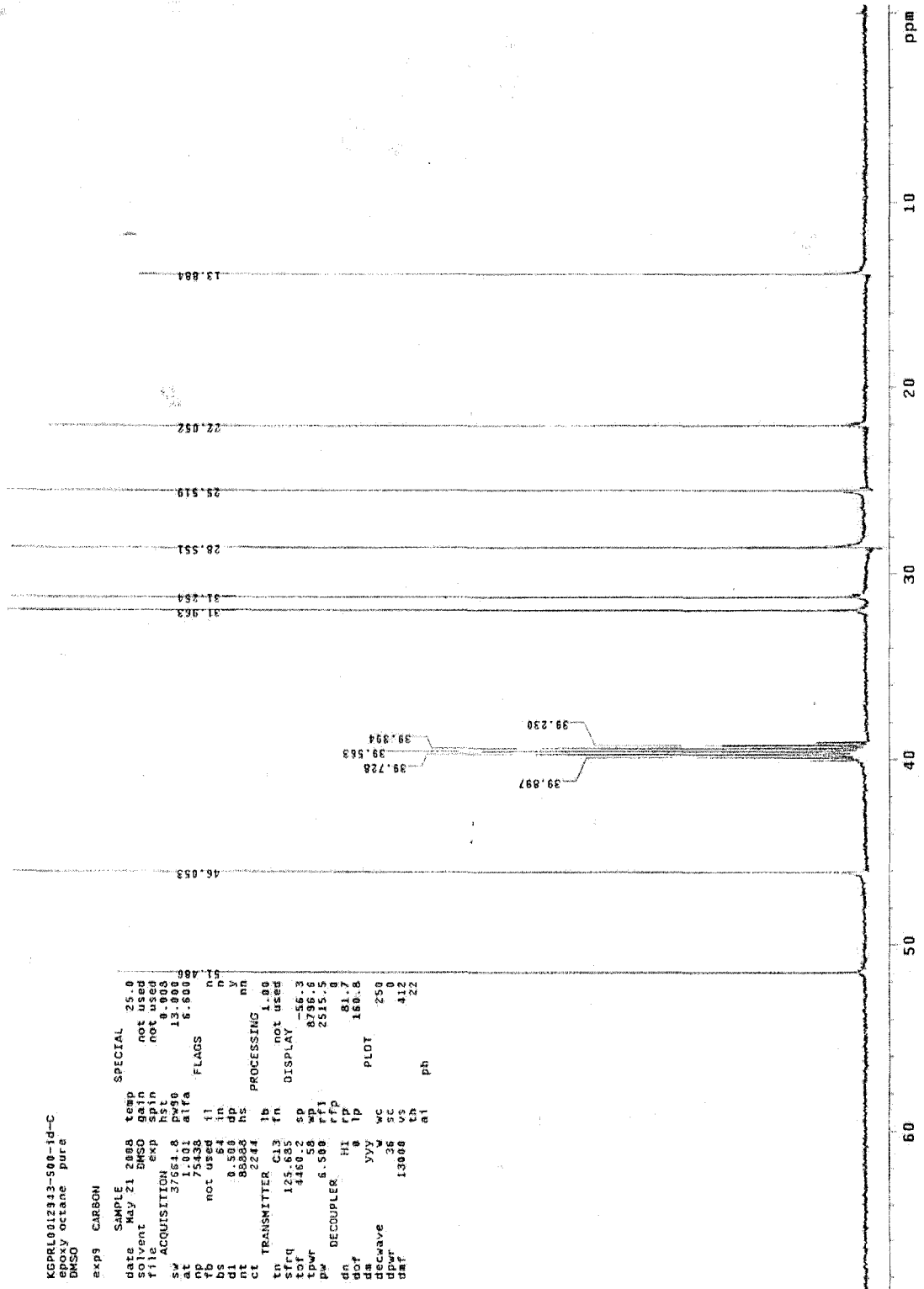


Figure E-4: Carbon NMR Spectra of 1,2-Epoxyoctane

Isophorone Diamine:

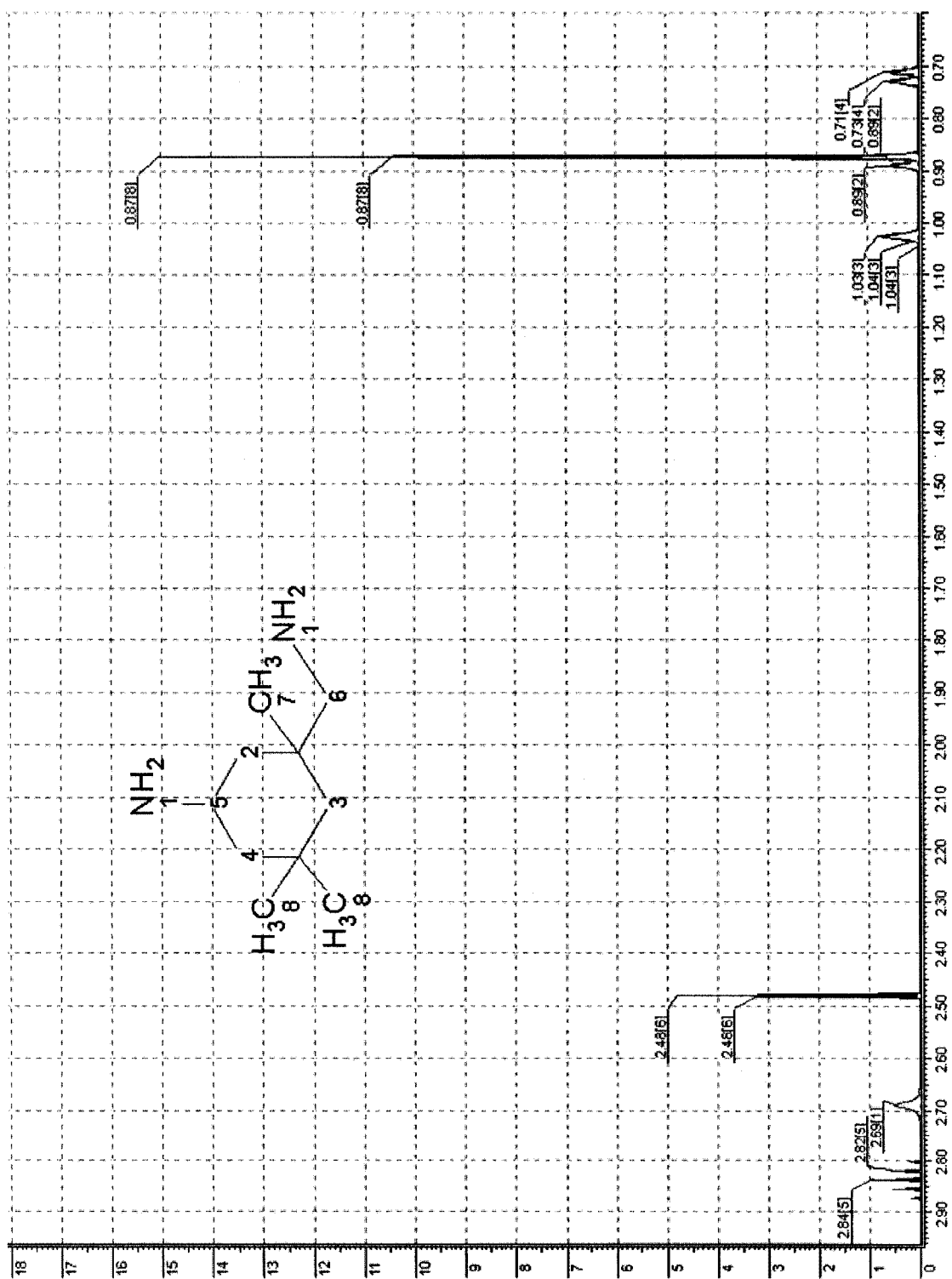


Figure E-5: Predicted Proton NMR Spectra of Isophorone Diamine

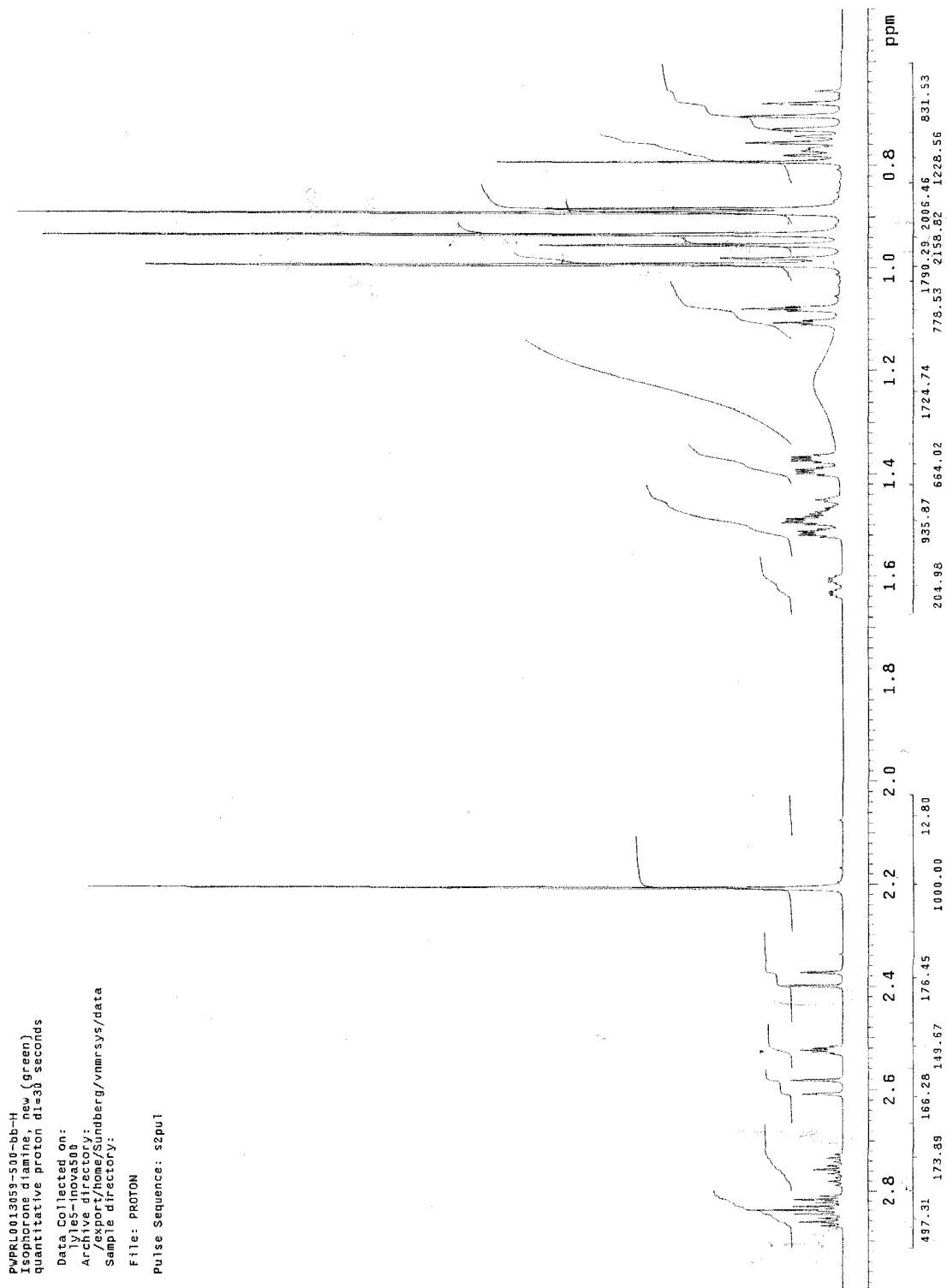


Figure E-6: Proton NMR Spectra of Isophorone Diamine

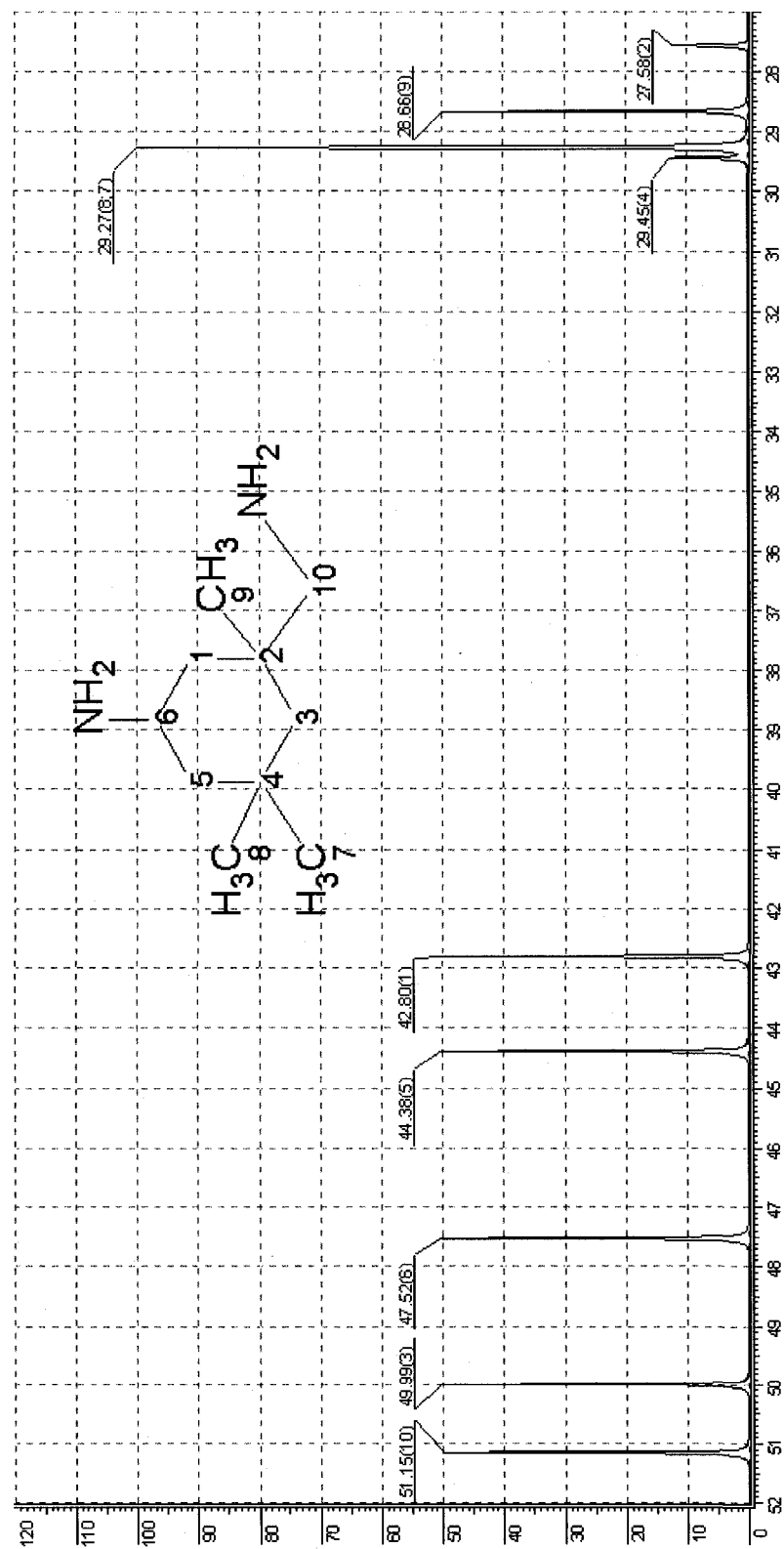


Figure E-7: Predicted Carbon NMR Spectra of Isophorone Diamine

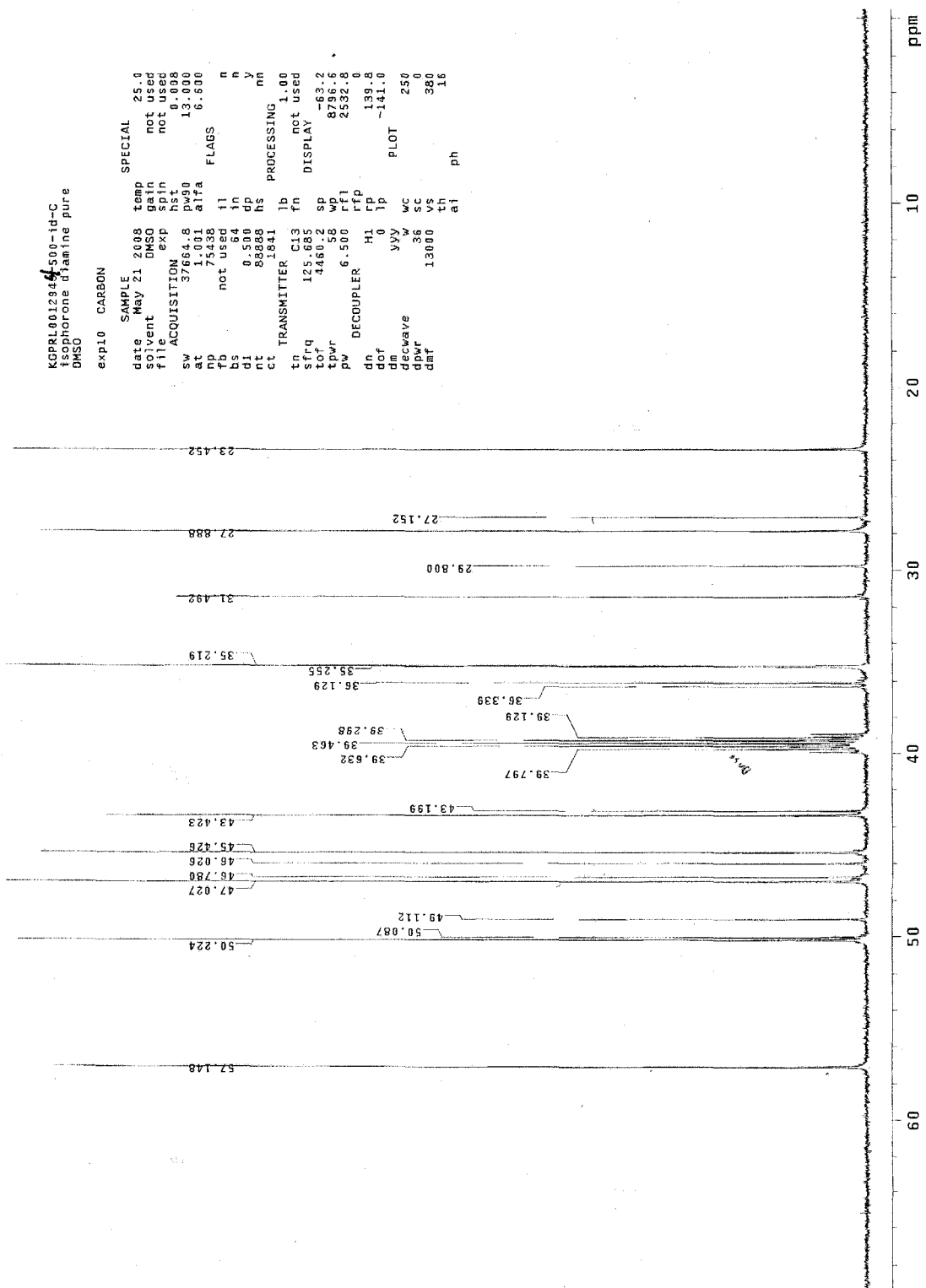


Figure E-8: Carbon NMR Spectra of Isophorone Diamine

IDEO Adduct:

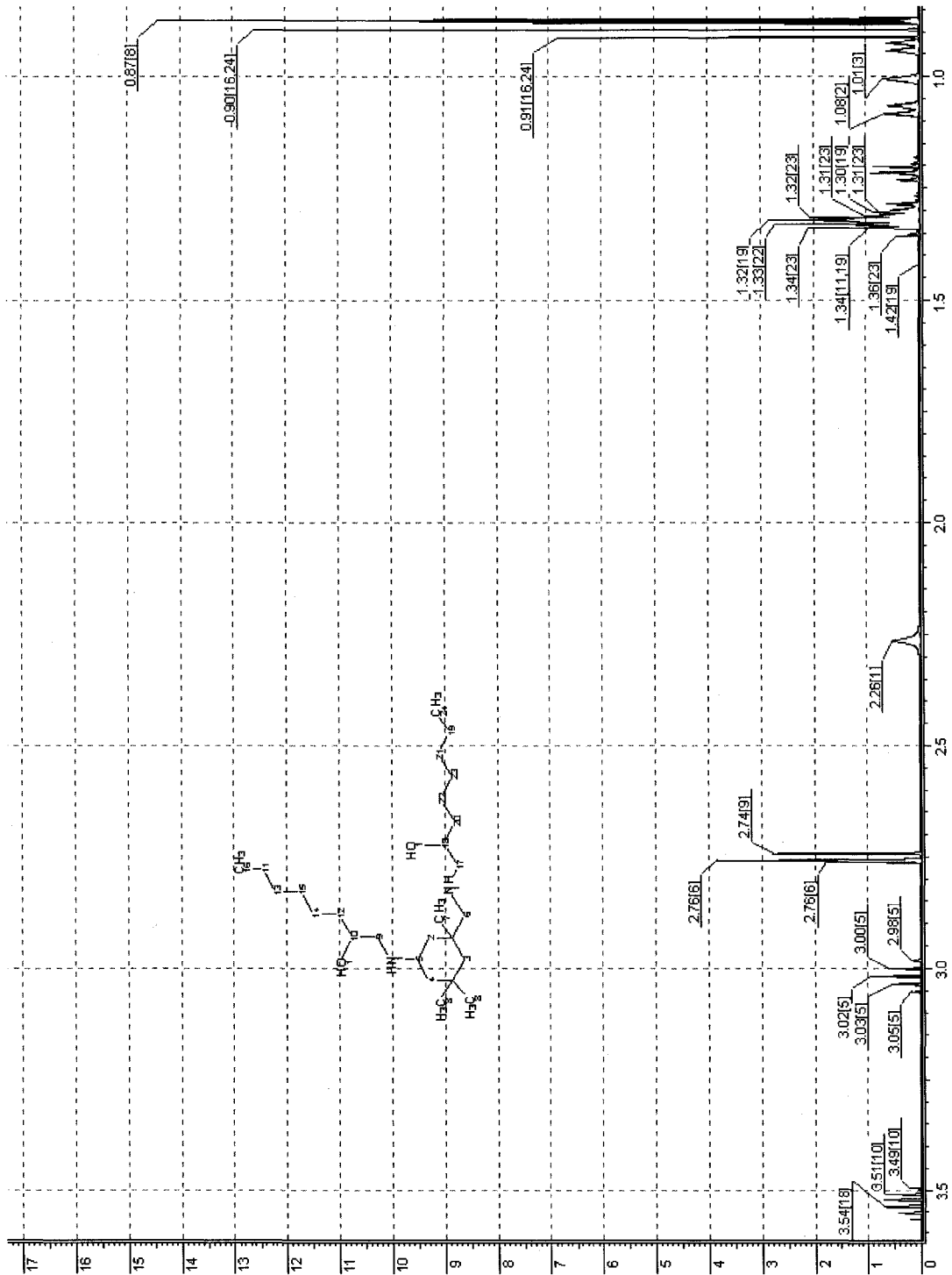


Figure E-9: Predicted Proton NMR Spectra of Di-functionalized Isophorone Diamine Adduct

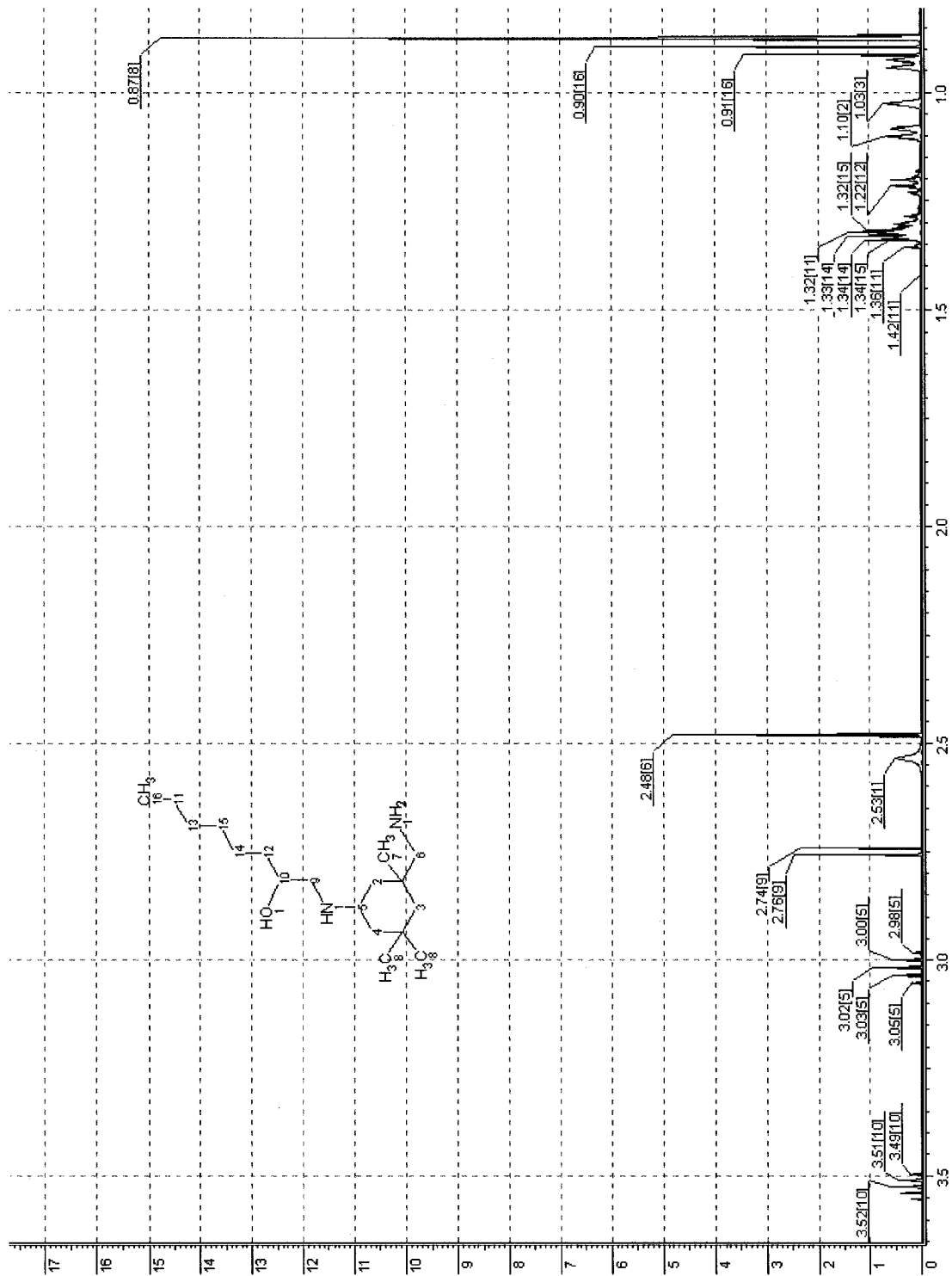


Figure E-10: Predicted Proton NMR Spectra of a Mono-functionalized (top) Isophorone Diamine Adduct

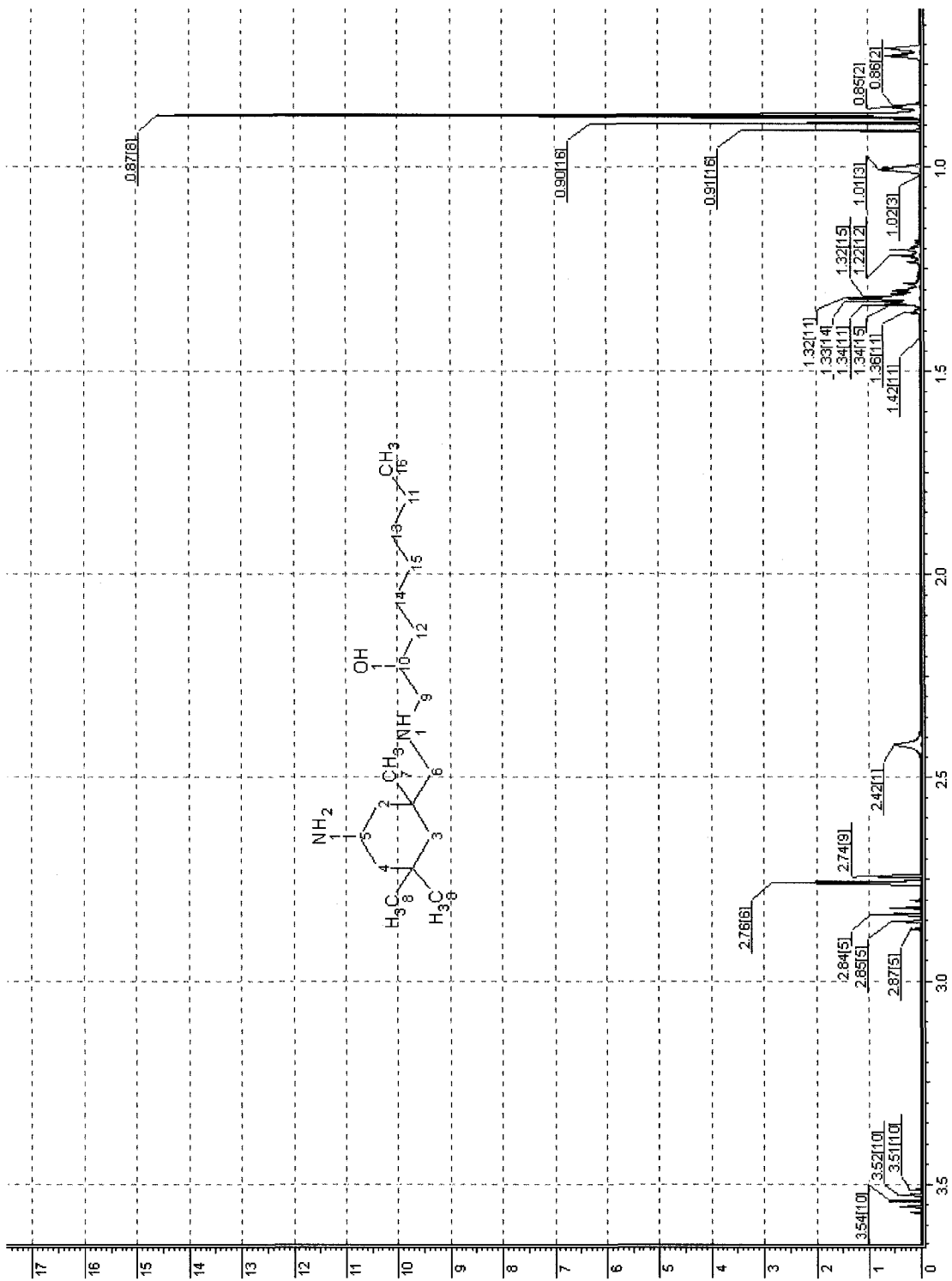


Figure E-11: Predicted Proton NMR Spectra of a Mono-functionalized (top) Isophorone Diamine Adduct

PWRLE013060-500-bb-H
 13pmr-1e4 diamine adduct_new
 quantitative proton d1=30 seconds

 Data Collected on:
 lyles-inova500
 Archive directory:
 /export/home/Sundberg/vmrsys/data
 Sample directory:

 File: PROTON
 Pulse Sequence: s2pu1

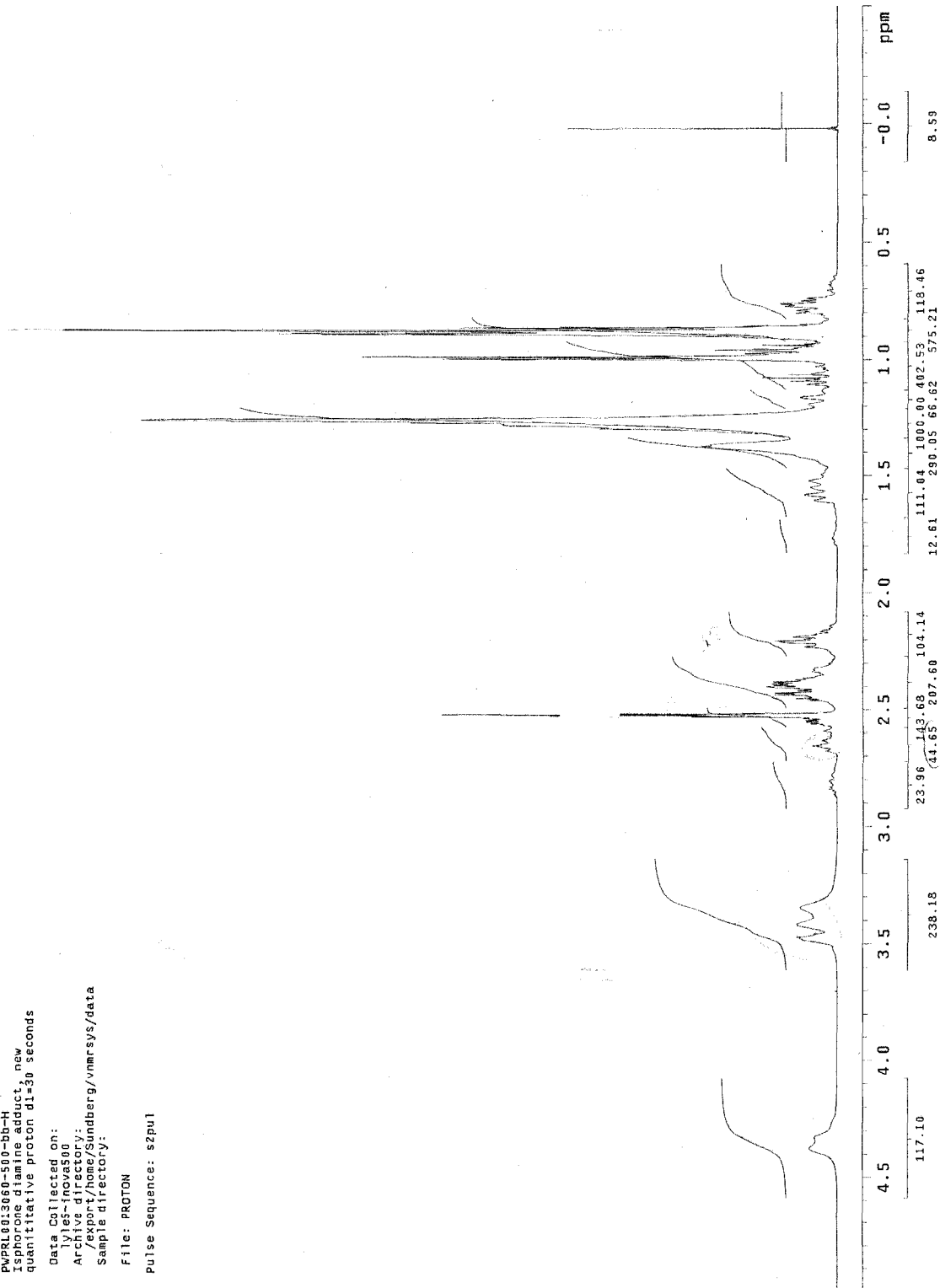


Figure E-12: Proton NMR Spectra of Isophorone Diamine Adduct

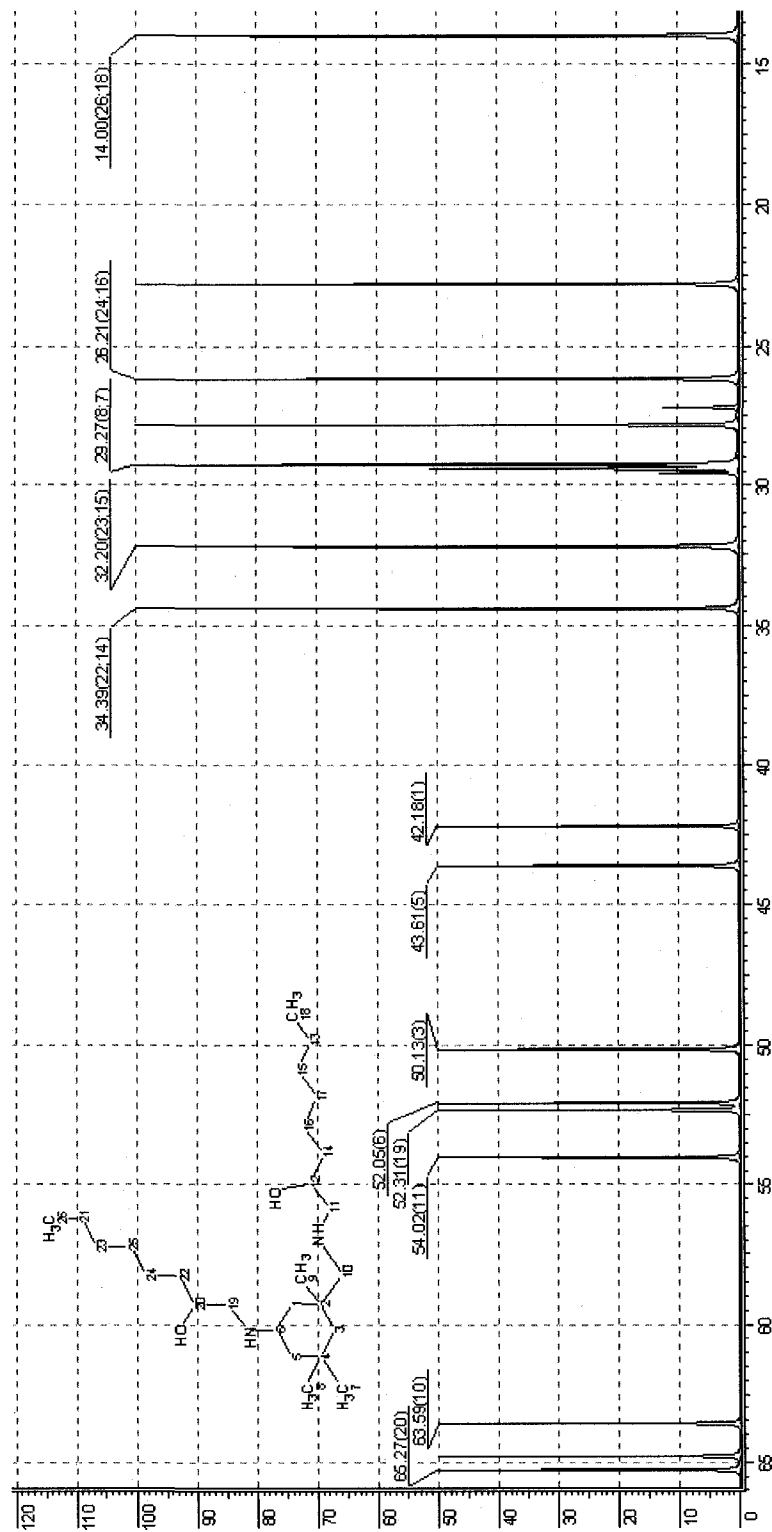


Figure E-13: Predicted Carbon NMR Spectra of a Di-functionalized Isophorone Diamine Adduct

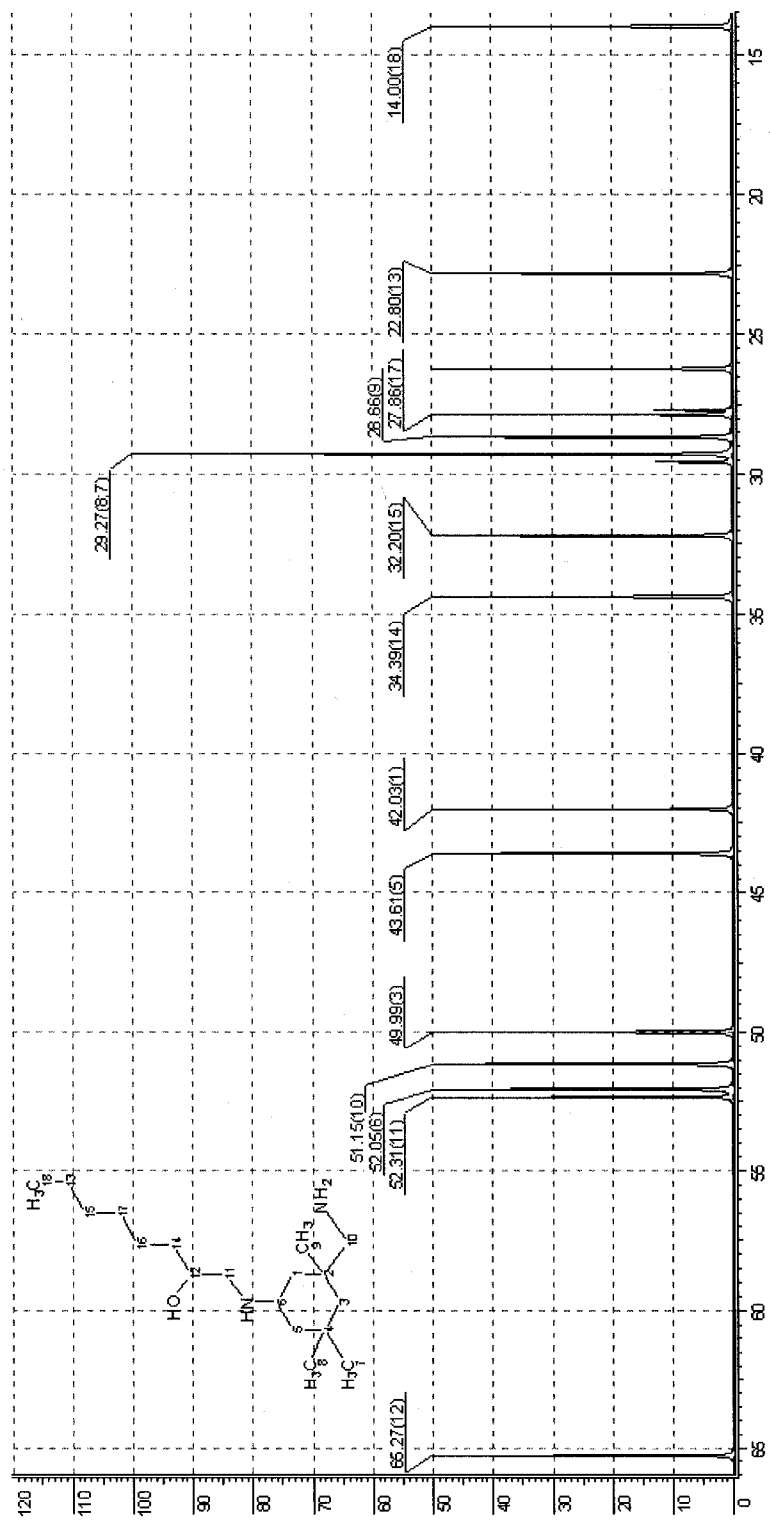


Figure E-14: Predicted Carbon NMR Spectra of a Mono-functionalized (top) Isophorone Diamine Adduct

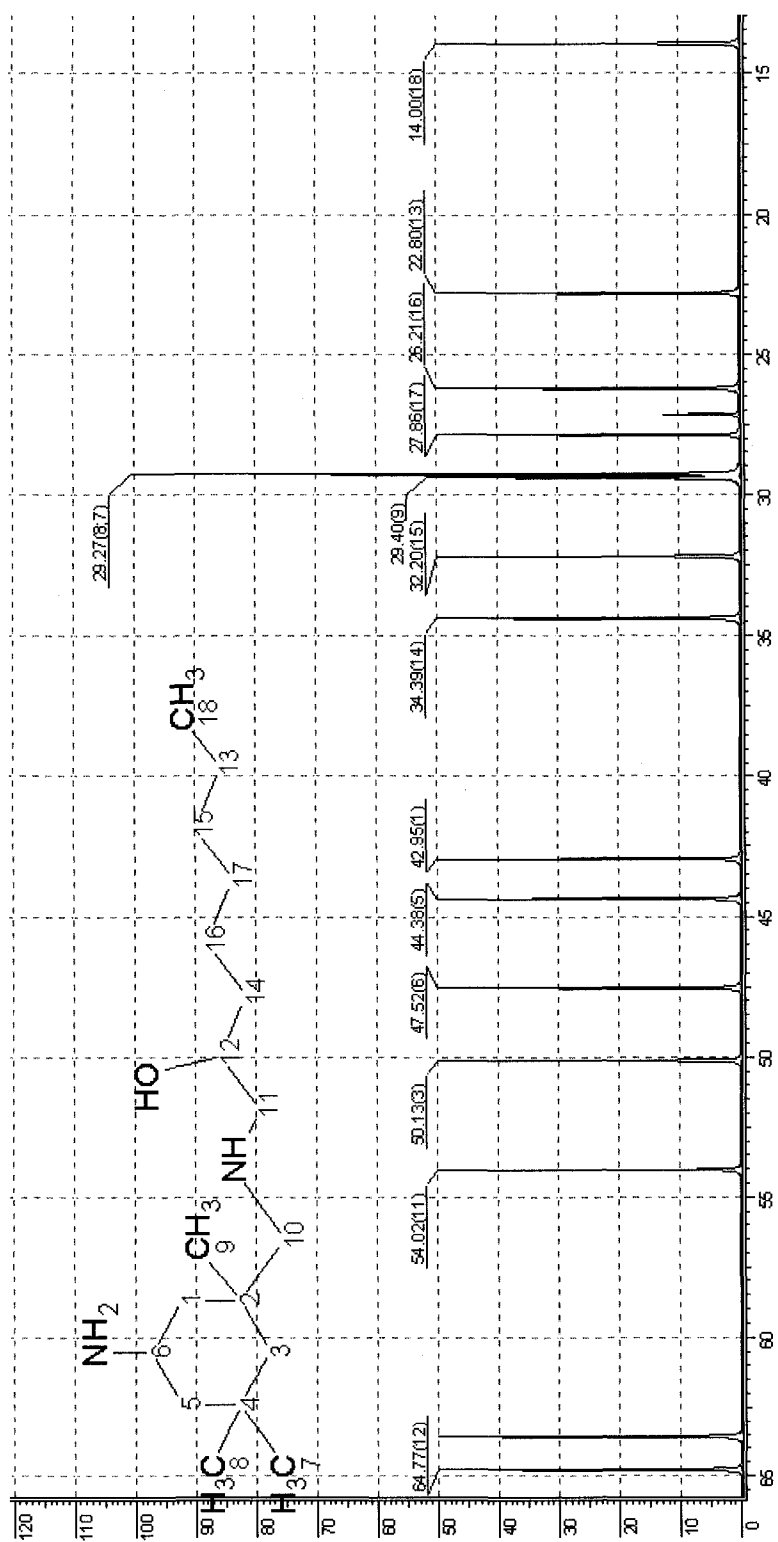


Figure E-15: Predicted Carbon NMR Spectra of a Mono-functionalized (bottom) Isophorone Diamine Adduct

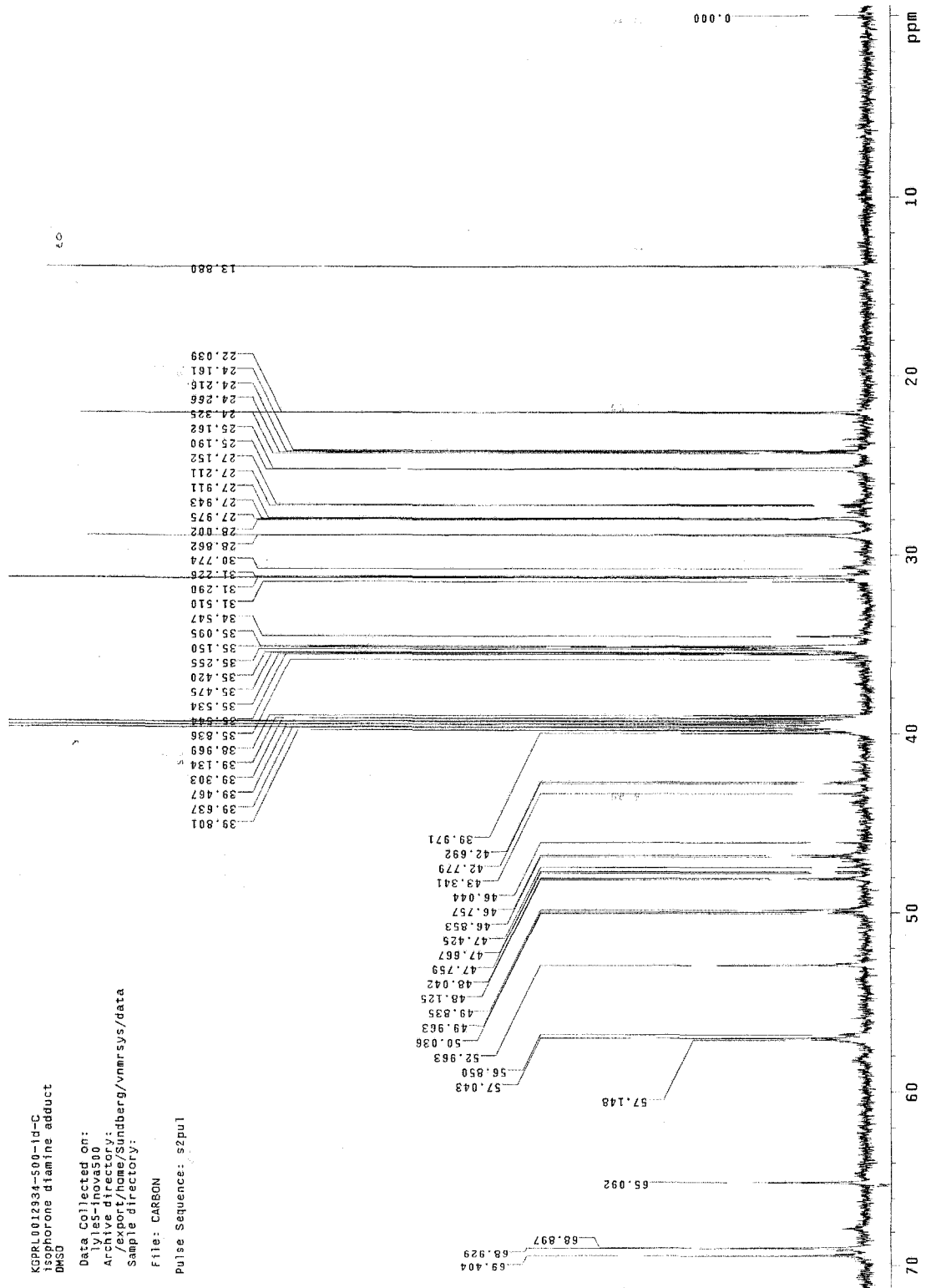


Figure E-16: Carbon NMR Spectra of Isophorone Diamine Adduct

APPENDIX F

Calculation of the Extent of Reaction vs. Time from DSC Analysis

To determine extent of reaction vs. time for the EPON815C and the IDEO Adduct, an isothermal experiment with the DSC was performed at 25°C for 12 hours, and then isothermal at 90°C for two hours. The first part of the analysis (25°C for 12 hours) was performed to obtain data used to determine the kinetics of the IDEO adduct and EPON resin reaction (plot of extent of reaction vs. time). The second part of the analysis (90°C for two hours) is raised to a much higher temperature to ensure full cure and obtain data on the total energy to calculate the extent of reaction. Figure F-1 is plot of Heat Flow vs. Time obtained from the DSC equipment.

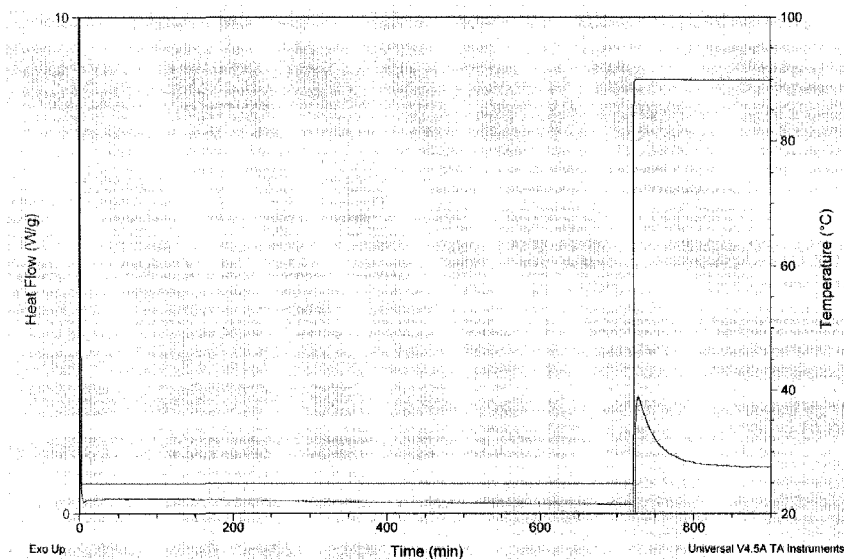


Figure F-1: DSC trace of Heat Flow vs. Time of a run reacting at 25°C for 12 hours then heated to 90°C for 2 hours

The plot in Figure F-1 must be split into two different plots and have the baselines adjusted accordingly in order to integrate the overall curing energy and determine the extent of reaction. Figures H-2 and H-3 are separated, where one was performed isothermally at 25°C (0-720 minutes) and the other at 90°C (721-840 minutes).

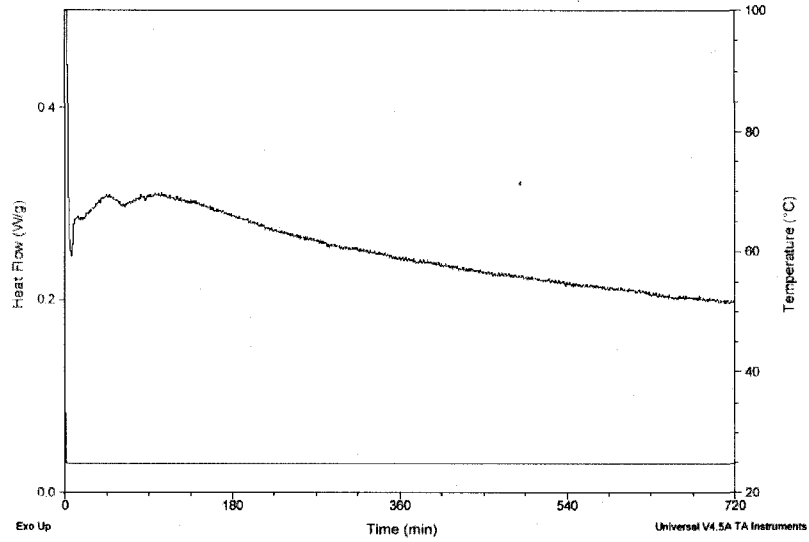


Figure F-2: Heat Flow vs. Time curve from 0 to 720 minutes Isothermal at 25°C

The above plot has a base line above zero on the y axis. Readjusting the baseline to zero is required prior to integrating under the curve to obtain the overall energy (J/g) of the curing reaction between 0 to 720 minutes. Integration for this particular experiment yielded a value of 6.57×10^6 J/g.

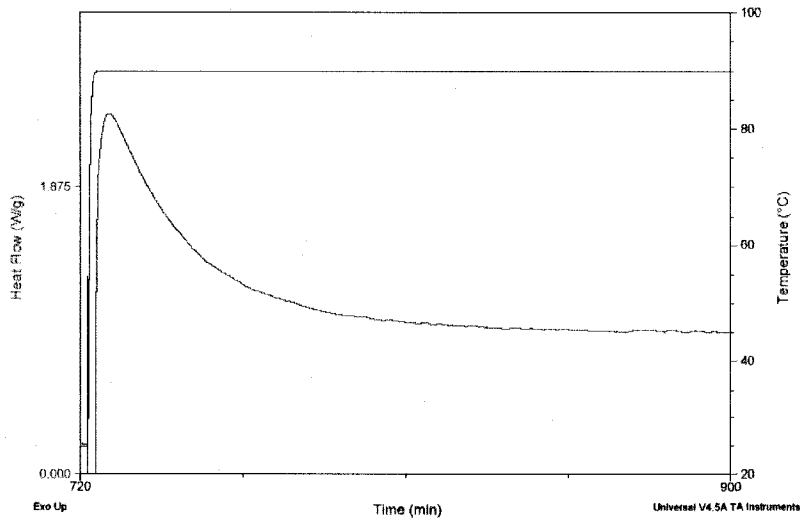


Figure F-3: Heat Flow vs. Time curve from 720 to 840 minutes Isothermal at 90°C

Similar to Figure F-2, the base line must be shifted prior to integration in Figure H-3. Integration of the curve yielded a value of 2.99×10^6 J/g. With the two plots individually integrated the two energy values are summed together to obtain the total energy required to fully cure the EPON 815C/IDEO adduct epoxy. The total energy of reaction is 9.55×10^6 J/g.

To obtain the extent of reaction at time t , one must integrate from 0 to t and then divide that value by the total energy (obtained from fully integrating Figure F-2-and F-3). With the extent of reaction calculated, one can generate a plot of Extent of reaction vs. Time shown in Figure F-4 below.

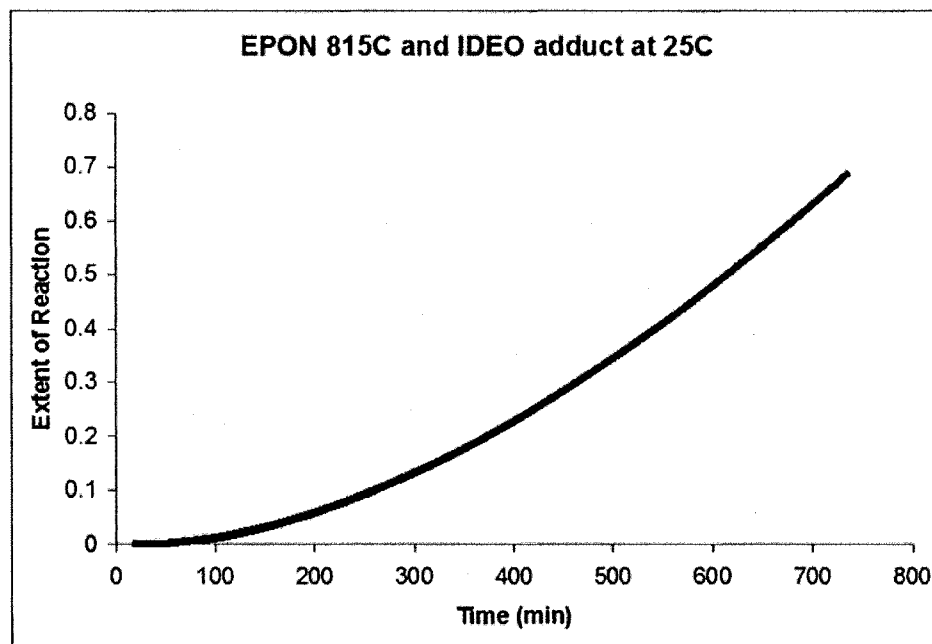


Figure F-4: Extent of Reaction vs. Time plot for EPON 815C and IDEO adduct at 25°C

APPENDIX G

Characterization of PMMA/PBMA Copolymer from IDEO Amine Adduct

DSC Analysis:

The DSC was performed to determine if a PMMA/PBMA copolymer would be plasticized by the IDEO adduct and if so to what extent. Figure G-1 is a plot of reversible heat capacity vs. temperature and the derivative of reversible heat capacity vs. temperature.

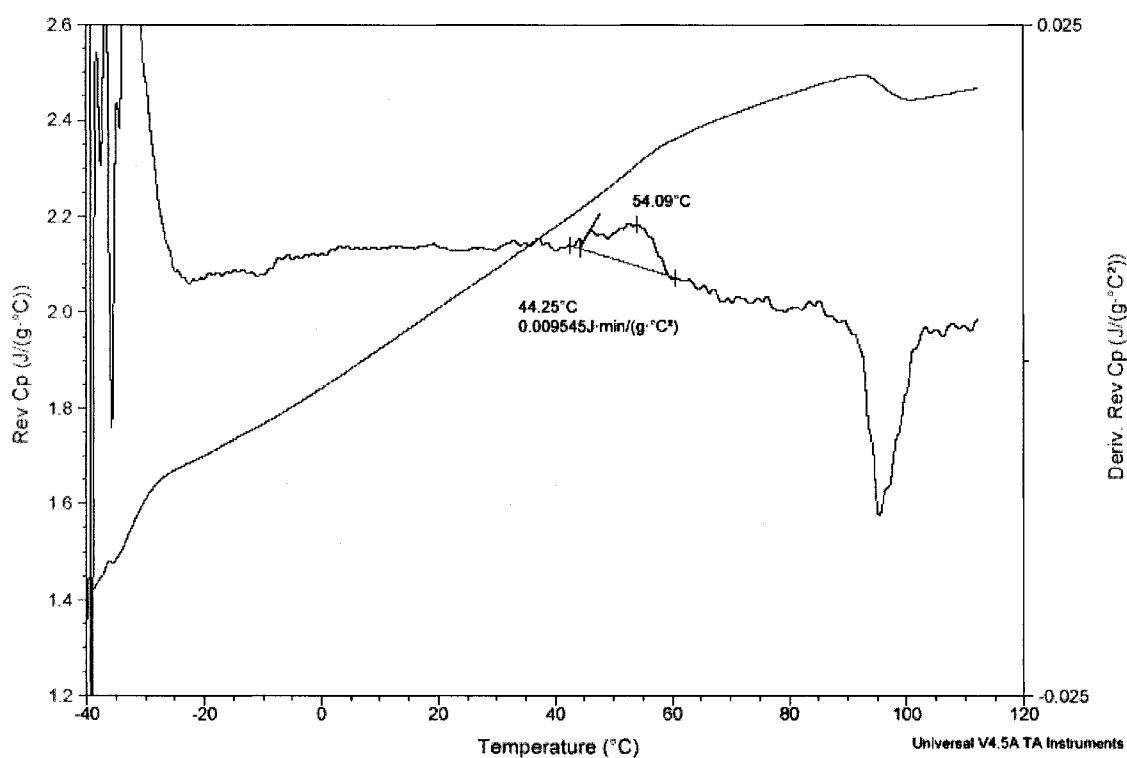


Figure G-1: DSC Trace of JN5-29 MMA/BMA/IDEO adduct solution polymerization.

Integration of the peak between the temperatures of 40°C and 60°C (typical polymer T_g 's span across 20°) on the derivative of reversible heat capacity curve, resulted in a T_g of approximately 54°C. This is lower than the calculated T_g by the Fox-Flory equation shown below for a copolymer composed of 60% MMA and 40% BMA.

$$\frac{1}{T_g} = \frac{W_1}{T_{g1}} + \frac{W_2}{T_{g2}} \quad (\text{G.1})$$

where W_1 is the weight fraction of homopolymer 1 (0.6 MMA), W_2 is the weight fraction of homopolymer 2 (0.4 BMA). T_{g1} and T_{g2} are the glass transition temperatures for the corresponding homopolymers (119°C and 35°C, respectively). A sample calculation of the T_g is written out below.

$$\frac{1}{T_g} = \frac{0.6}{393.15K} + \frac{0.4}{308.15K} \quad (\text{G.2})$$

$$T_g = 354.08K = 80.9^\circ C \quad (\text{G.3})$$

With the T_g of the PMMA/PBMA/IDEO adduct mixture lower than that of the calculated T_g , there may be some plasticization of the polymer. Plasticization can either be caused by the IDEO adduct or from the residual monomer, even though there was an attempt to remove it.

APPENDIX H

IDEO Amine Adduct Encapsulation Experiments

Table H-1: Experiments replicating JN4-72

Experiment	Recip Type (G)	PAP (G)	Stannifer (G)	(MMA) (G)	(BMA) (G)	(ECMA) (G)	Hexametha (G)	(% 85/15)	DEO solvent (G)	Temp C	Mixing	Homogenization	Time	Results
JN4-72	128	5.12	0.0892	6.4	4.26	0	0.106	0.106	10.66	66	Stirplate (yellow stipitate setting) 11 during homogenization then 7 afterwards	2	15 min + time to heat water bath (Ca. 340 min)	Second crop present. Capsules in 80-50um range
JN4-73	128	5.12	0.0892	6.4	4.26	0	0.106	0.106	10.66	66	11 during homogenization then 7 afterwards	2	15 min + time to heat water bath (Ca. 340 min)	Second crop present. Large agglomerates formed
JN4-87	128	5.12	0.0892	6.4	4.26	0	0.106	0.106	10.66	66	11	2	15 min + time to heat water bath (Ca. 340 min)	Second crop present. Large agglomerates formed
JN4-88	128	5.12	0.0892	6.4	4.26	0	0.106	0.106	10.66	66	11	2	15 min + time to heat water bath (Ca. 340 min)	Second crop present. Large agglomerates formed. Low yield
JN4-90	128	5.12	0.0892	6.4	4.26	0	0.106	0.106	10.66	66	11	2	15 min + time to heat water bath (Ca. 340 min)	Second crop present. Large agglomerates formed
JN5-12	192	19.2	0.0892	6.4	4.26	0	0.106	0.106	10.66	66	11 during homogenization then 7 afterwards	2	15 min + time to heat water bath (Ca. 340 min)	Second crop present. Large agglomerates formed
JN5-13	128	5.12	0.0892	6.4	4.26	0	0.106	0.106	10.66	66	11 during homogenization then 10 afterwards	2	15 min + time to heat water bath (Ca. 340 min)	Second crop present. Large agglomerates formed
JN5-14	128	5.12	0.0892	6.4	4.26	0	0.106	0.106	10.66	66	11 during homogenization then 7 afterwards	2	15 min + time to heat water bath (Ca. 340 min)	Second crop present. Large agglomerates formed
JN5-15	128	5.12	0.0892	6.4	4.26	0	0.106	0.106	10.66	66	11	2	15 min + time to heat water bath (Ca. 340 min)	Second crop present. Large agglomerates formed
JN5-16	128	5.12	0.0892	6.4	4.26	0	0	0.106	10.66	66	11	2	15 min + time to heat water bath (Ca. 340 min)	Second crop present. Large agglomerates formed

Table H-2: Encapsulation Attempts Using Mechanical Stirring

Experiment	Recipe H2O (g)	PVP (g)	Scavenger (g)	(MMA) (g)	(BMA) (g)	(ECDDMA) (g)	Headacams (g)	(μ 45) (g)	IDEO adduct (g)	Temp. C	Stirring Mechanical (RPM)	Homogenization Sealing	Time	Results
JN482	128	5.12	0.0882	8.4	4.26	0	0.108	0.108	10.86	65	200	2	15 min + time to heat water bath (Ca=45min)	Second crop present. Capsules in the range of 800um
JN493	128	5.12	0.0882	8.4	4.26	0	0.108	0.108	10.86	65	200	2	15 min + time to heat water bath (Ca=45min)	Second crop present. Large agglomerates formed
JN494	128	5.12	0.0882	8.4	4.26	0	0.108	0.108	10.86	65	200	2	15 min + time to heat water bath (Ca=45min)	Second crop present. Capsules in the range of 800um
JN495	128	5.12	0.0882	8.4	4.26	0	0.108	0.108	10.86	65	180	2	15 min + time to heat water bath (Ca=45min)	Second crop present. Capsules in the range of 800um
JN496	128	5.12	0.0448	3.2	2.13	0	0.053	0.053	5.33	65	200	2	15 min + time to heat water bath (Ca=45min)	Second crop present. Large agglomerates formed
JN497	102	7.68	0.1318	8.9	8.4	0	0.159	0.159	15.04	65	200	2	15 min + time to heat water bath (Ca=45min)	Second crop present. Capsules in the range of 800um
JN498	102	7.68	0.0882	8.4	4.26	0	0.108	0.108	10.86	65	275	2	15 min + time to heat water bath (Ca=45min)	Second crop present. Capsules in the range of 800um
JN499	102	11.52	0.0882	8.4	4.26	0	0.108	0.108	10.86	65	275	2	15 min + time to heat water bath (Ca=45min)	Second crop present. Capsules in the range of 800um
JN4100	102	15.36	0.0882	8.4	4.26	0	0.108	0.108	10.86	65	300	2	15 min + time to heat water bath (Ca=45min)	Second crop present. Capsules in the range of 800um
JN501	102	15.36	0.0882	8.4	4.26	0	0.108	0.108	10.86	65	275	2	15 min + time to heat water bath (Ca=45min) 20 minutes	Second crop present. Capsules in the range of 800um
JN502	102	15.36	0.0882	8.4	4.26	0	0.108	0.108	10.86	65	275	3	15 min + time to heat water bath (Ca=45min)	Second crop present. Capsules in the range of 800um
JN503	102	15.36	0.0882	8.4	4.26	0	0.108	0.108	10.86	65	375	3	15 min + time to heat water bath (Ca=45min)	Second crop present. Capsules in the range of 800um
JN504	102	19.2	0.0882	8.4	4.26	0	0.108	0.108	10.86	65	250	3	15 min + time to heat water bath (Ca=45min)	Second crop present. Capsules in the range of 800um
JN505	102	19.2	0.0882	8.4	4.26	0	0.108	0.108	10.86	65	275	3	15 min + time to heat water bath (Ca=45min)	Second crop present. Capsules in the range of 800um
JN508	102	19.2	0.0448	3.2	2.13	0	0.053	0.053	10.86	65	275	3	15 min + time to heat water bath (Ca=45min)	No encapsulation
JN509	102	19.2	0.0882	8.4	4.26	0	0.108	0.108	10.86	65	300	2	15 min + time to heat water bath (Ca=45min)	Second crop present. Capsules in the range of 800um
JN510	102	19.2	0.0882	8.4	4.26	0	0.108	0.108	10.86	65	300	2.5	15 min + time to heat water bath (Ca=45min)	Second crop present. Capsules in the range of 800um